University of Silesia
Faculty of Science and Technology
August Chełkowski Institute of Physics

Magdalena Kordiaczyńska

In quest of doubly charged Higgs bosons at low and high energies

PhD Thesis

PhD Supervisor:
prof. dr hab. Janusz Gluza
co-Supervisor:
dr Bartosz Dziewit

UNIVERSITY OF SILESIA
IN KATOWICE

Katowice 2023

słowa kluczowe: mechanizm Higgsa, Model Standardowy, triplet pól skalarnych, podwójnie naładowane bozony skalarne, LHC, przyszłe zderzacze cząstek

key words: Higgs mechanism, Standard Model, scalar triplets, doubly charged scalar bosons, LHC, future colliders

Oświadczenie autora pracy

Ja, niżej podpisana: Magdalena Kordiaczyńska, autorka pracy doktorskiej pt. '*In quest of doubly charged Higgs bosons at low and high energies*'.

Oświadczam, że ww. praca doktorska:

- została przygotowana przeze mnie samodzielnie,
- nie narusza praw autorskich w rozumieniu ustawy z dnia 4 lutego 1994 r. o prawie autorskim i prawach pokrewnych (tekst jednolity Dz. U. z 2006 r. Nr 90, poz. 631, z późn. zm.) oraz dóbr osobistych chronionych prawem cywilnym,
- nie zawiera danych i informacji, które uzyskałam w sposób niedozwolony, nie była podstawą nadania stopnia doktora nauk, dyplomu wyższej uczelni lub tytułu zawodowego ani mnie, ani innej osobie.

Oświadczam również, że treść pracy doktorskiej zapisanej na przekazanym przeze mnie jednocześnie nośniku elektronicznym jest identyczna z treścią zawartą w wydrukowanej wersji pracy.

Jestem świadoma odpowiedzialności karnej za złożenie fałszywego oświadczenia.

....

Miejscowość, data Podpis autora pracy

Acknowledgments

This work was supported by the Polish National Science Center (NCN): Preludium grant 2015/17/N/ST2/040672, grants 2017/25/B/ST2/01987, 2020/37/B/ST2/02371, and by the COST (European Cooperation in Science and Technology) Action CA16201 PARTICLEFACE.

Abstract

The primary hypothesis on which the Thesis relies is the existence of additional scalar particles other than the Higgs boson discovered in 2012 at LHC. Finding other scalar particles would have a conspicuous effect on the future development of particle physics.

I consider the Higgs Triplet Model (`HTM`) not restricted by the custodial symmetry and the Minimal Left-Right Symmetric Model (`MLRSM`). The models include scalar triplets with different complexity of scalar potentials and, due to experimental restrictions, completely different scales of non-standard triplet vacuum expectation values. In both models, a doubly charged Higgs boson $H^{\pm\pm}$ can acquire a mass of hundreds of gigaelectronvolts, which can be probed at HL-LHC, future e^+e^-, and hadron colliders. Notably, $H^{\pm\pm}$ particles are connected with different neutrino mass generation mechanisms, seesaw type-I in case of `MLRSM`, and seesaw type-II in case of `HTM`. Thus, collider's $H^{\pm\pm}$ discovery signals can help to understand neutrinos' properties.

I consider $H^{\pm\pm}$ production and decay in e^+e^- and pp colliders, including possible clean four charged lepton signals without missing energy in the final state. The signals are compared with the Standard Model background predictions. In signal estimates, I take into account a comprehensive set of constraints on the parameters of both models coming from neutrino oscillations, LHC, e^+e^- and low-energy lepton flavour violating data.

I show that the discovery of the $H^{\pm\pm}$ leptonic signals over the SM background in two models is possible and for which parameters there is a chance to discriminate between the models when four leptons are identified in the final state.

Streszczenie

Podstawową hipotezą na której opiera się niniejsza rozprawa doktorska jest istnienie dodatkowych cząstek skalarnych, innych niż bozon Higgsa odkryty w 2012 roku w eksperymencie LHC w CERN-ie. Znalezienie dodatkowych cząstek skalarnych nadałoby duży impet rozwojowi fizyki wykraczającej poza Model Standardowy.

W pracy rozważam model z trypletem pól Higgsa (`HTM`) który nie jest ograniczony przez tzw. symetrię opiekuńczą oraz minimalny model symetryczny lewo-prawo (`MLRSM`). Modele te zawierają skalarne tryplety o różnej złożoności potencjałów skalarnych oraz, ze względu na ograniczenia eksperymentalne, zupełnie różne skale niestandardowych wartości oczekiwanych stałych próżniowych trypletów. W obu modelach podwójnie naładowany bozon Higgsa $H^{\pm\pm}$ może uzyskać masę setek gigaelektronowoltów, cząstki takie można badać w HL-LHC, przyszłych zderzaczach e^+e^- i zderzaczach hadronowych. Warto zauważyć, że cząstki $H^{\pm\pm}$ są powiązane z różnymi mechanizmami generowania mas neutrin, huśtawki typu-I w przypadku `MLRSM` i huśtawki typu-II w przypadku `HTM`. Zatem odkrycie cząstek $H^{\pm\pm}$ w zderzaczach może doprowadzić do lepszego zrozumienia własności neutrin.

W rozprawie skupiam się na przypadku produkcji podwójnie naładowanych bozonów Higgsa $H^{\pm\pm}$ w zderzaczach e^+e^- i pp z ich późniejszym rozpadem na cztery naładowane leptony. Sygnał ten jest porównany z tłem w ramach Modelu Standardowego. Przy oszacowaniu sygnału uwzględniam szerokie spektrum istniejących ograniczeń dotyczących parametrów obu modeli pochodzących z oscylacji neutrin, eksperymentów LHC, e^+e^- i niskoenergetycznych danych łamiących zapachowe liczby leptonowe.

W rozprawie pokazuję, że odkrycie sygnałów leptonowych pochodzących od bozonów skalarnych $H^{\pm\pm}$ ponad standardowe tło w obu modelach jest możliwe i oba modele mogą być rozróżnione przy identyfikacji czterech leptonów w stanie końcowym dla określonego zakresu parametrów modeli.

List of papers

This thesis is based on the following papers and conference contributions:

1. G. Bambhaniya, J. Chakrabortty, J. Gluza, M. Kordiaczyńska, R. Szafron, *'Left-Right Symmetry and the Charged Higgs Bosons at the LHC'*, JHEP 05 (2014) 033, doi:10.1007/JHEP05(2014)033.

2. G. Bambhaniya, J. Chakrabortty, J. Gluza, T. Jeliński, M. Kordiaczynska, *'Lowest limits on the doubly charged Higgs boson masses in the minimal left-right symmetric model'*, Phys. Rev. D 90 (2014), 9, 095003 doi:10.1103/PhysRevD.90.095003.

3. T. Jeliński, M. Kordiaczyńska, *'Heavy Neutrino Masses and Mixings at the LHC'*, Acta Phys. Polon.B 46 (2015) 11, 2193, doi:10.5506/APhysPolB.46.2193.

4. J. Gluza, M. Kordiaczyńska, T. Srivastava, *'Doubly Charged Higgs Bosons and Spontaneous Symmetry Breaking at eV and TeV Scales'*, Symmetry 12 (2020) 1, doi:10.3390/sym12010153

5. J. Gluza, M. Kordiaczynska, T. Srivastava, *'Discriminating the HTM and MLRSM models in collider studies via doubly charged Higgs boson pair production and the subsequent leptonic decays'*, Chin. Phys. C 45 (2021) 7, 073113, doi:10.1088/1674-1137/abfe51

6. B. Dziewit, M. Kordiaczyńska, T. Srivastava, *'Production of the Doubly Charged Higgs Boson in Association with the SM Gauge Bosons and/or Other HTM Scalars at Hadron Colliders'*, Symmetry 13 (2021) 7, 1240 doi:10.3390/sym13071240

Contents

1 Introduction

1.1 Meaning of the Higgs boson in particle physics

In general, the name *boson* describes integer spin objects that follow the Bose-Einstein statistics, as opposed to half-integer spin *fermions*, which obey the Fermi–Dirac statistics crucial for atoms formation (Pauli exclusion principle). The boson might be an elementary particle or a composite one. Even a bound state of two fermions might behave like an integer spin particle, as in the case of superconductivity, when two electrons are combined into a bound state called Cooper pairs.

Depending on the value of the spin and parity behavior under the Lorentz transformation, we distinguish vector bosons (for example gauge bosons with spin equal to 1), scalars (for example the Higgs boson, spin 0, even parity), and pseudoscalars (for example π mesons, spin 0, odd parity). Among the elementary particles within the Standard Model (SM), we classify force carriers vector bosons, which intermediate the fundamental interactions: photon γ (electromagnetism) , Z, $W^{\pm}$ (weak interactions), and gluons (strong interactions). These non-zero spin carriers of fundamental interactions are completed by one extraordinary spin-zero particle, the Higgs boson. With gathered statistics and its decay rate to $\gamma\gamma$ [1,2], we know already that the spin-parity of the Higgs boson discovered in 2012 (throughout the thesis we will call it H^0) is dominantly CP-even $J^P = 0^+$ [3–7]. Establishing spin of H^0 is non-trivial, it is summarized in Fig. 1 [8].

The present Particle Data Group H^0 mass is [9]

$$m_{H^0} = 125.25 \pm 0.17 \text{ GeV}. \tag{1.1}$$

It is the second among heaviest SM elementary particles[1], heavier is the top quark ($m_t \simeq 173.2$ GeV), lighter are gauge bosons: $m_{W^{\pm}} \simeq 80.385$ GeV, $m_{Z^0} \simeq 91.1876$ GeV [11].

[1]Interestingly, as noticed in [10], taken masses of the heaviest particles of spin zero, half, and one,

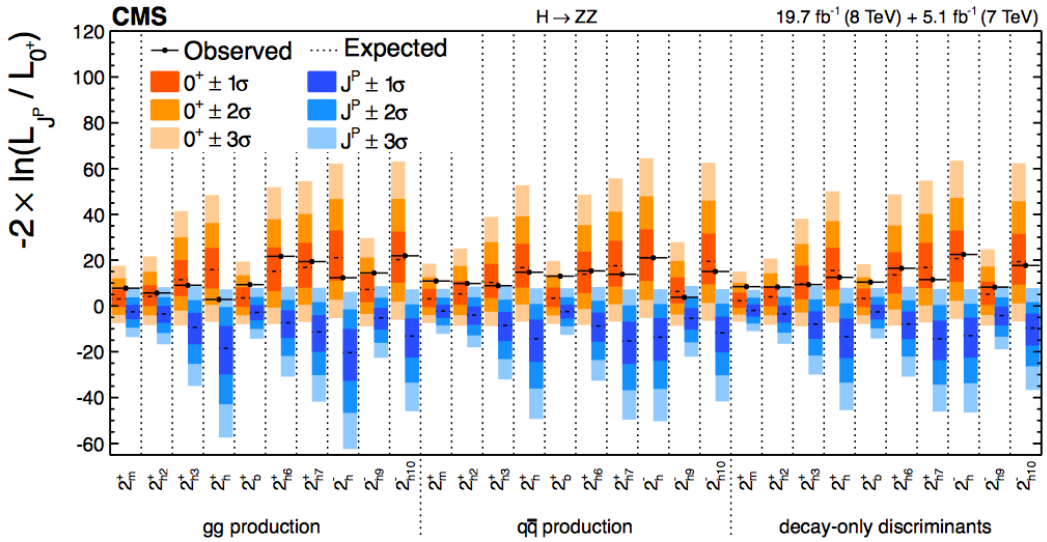

Figure 1: Tests of spin-parity hypotheses for the Higgs boson. Scenarios favour strongly the 0^+ assignment expected in the SM. Figure taken from [8].

Discovered in 2012 Higgs boson is responsible for a basic mass generation mechanism of fermions and gauge bosons[2]. It was the last missing element of the Standard Model, and the scalar boson discovery at the LHC [13–15] confirmed the role it plays in particles mass generation through spontaneous symmetry breaking (SSB). Observed decays of the Higgs boson to gauge boson particles W^+W^- and ZZ [3, 4, 16] fits beautifully into this picture. Similarly, determination of $t\bar{t}H^0$ couplings in gluon fusion [17–19] and $t\bar{t}H^0$ production [20] confirm Higgs boson role in fermion mass generation. I will extend this subject in the section 1.2. The status of H^0 after its discovery is described nicely in reviews [21–23].

---

we get

$$\rho_t = \frac{m_{Z^0} m_t}{m^2_{H^0}}, \tag{1.2}$$

$$\rho_t^{(exp)} = 1.0022 \pm 0.007 \pm 0.009. \tag{1.3}$$

Does it mean that some symmetry is hidden behind the relation (1.2)?

[2]It has begun a standard calling the SM scalar spin-zero boson the Brout-Englert-Higgs (BEH) boson [12].

The Higgs boson is connected with the mechanism of spontaneous symmetry breaking which brings the situation when the original system's Lagrangian obeys a symmetry which is not held anymore for lower-energy solutions. The mechanism of SSB is known in many contexts, in particle physics within the electroweak theory or chiral symmetry breaking in quantum chromodynamics (QCD), another example is the Ginzburg-Landau's theory in superconductivity[3]. Superconductivity in low temperatures is described by the Bardeen–Cooper–Schrieffer (BCS) theory [24], which postulates that two electrons with opposite spin directions create a bounded state - a Cooper pair. The Ginzburg-Landau theory describes this process from the phenomenological perspective using the SSB mechanism in a form as we use in the SM, see V_{SM} in Eq. (1.4), where the symmetry breaking parameter is the temperature, changing the sign of the μ^2 in Eq. (1.4).

In the case of QCD, the Lagrangian for the first generation of quarks has a chiral symmetry under the $SU(2)_L \times SU(2)_R$, which is broken when quark-gluon plasma formed hadrons. It is worth noticing that the chiral symmetry in the fermion sector of QCD is only approximate due to the non-zero quark masses. That is why the Goldstone bosons will also be massive and called *pseudo*-Goldstone bosons. After the SSB $SU(2)_L \times SU(2)_R \to SU(2)_{\mathrm{Y}}$, where by Y I mean isospin, three pions appear as pseudo-Goldstone bosons. The same approach can be used after adding the charm quark to the theory and considering the $SU(3)_L \times SU(3)_R$ symmetry breaking. In this case, apart from the pions, the whole mesons octet plays the role of massive pseudo-Goldstone bosons, and even the SSB mechanism can be used for describing the baryon octet and decouplet. More details can be found in [25].

For this thesis, the most important case of SSB is the mass generation mechanism in the SM and its extensions, which introduce the theory of massive vector bosons and other scalar particles. The power of the Higgs mechanism comes from its simplicity[4],

[3]Other symmetry breaking examples are discussed in [23].

[4]Actually, it was to large extent the collective effort by Englert, Kibble, Guralnik, Brout, Englert

expressed by the SM scalar potential

$$V_{SM} \quad = \quad -\mu^2\Phi^\dagger\Phi + \lambda(\Phi^\dagger\Phi)^2. \tag{1.4}$$

This potential is invariant under the SM SU(2)×U(1) symmetry. Φ is the Higgs complex doublet of four real fields, μ is the bare mass term of the potential and λ is the self-interacting scalars coupling.

An important feature of V_{SM} is that its origin is unstable, and is surrounded by a valley where $\langle H\rangle \equiv v \simeq 246$ GeV, the electroweak vacuum, see Fig.2 which can be generated in Gnuplot [32] using the following commands:

```
set xzeroaxis
set yzeroaxis
set isosamples 50
set hidden3d
set parametric
set contour both
splot [0:230][0:2*pi] u*cos(v), u*sin(v), μ^2*u**2 +  λ*(u**2)**2
```

By μ^2 and λ I mean the potential parameters from Eq. (1.4), so the mass term parameter and the Higgs self-coupling constant. They are connected with the vacuum expectation value (`VEV`) v ot the potential by relation: $v^2 = -\frac{\mu^2}{\lambda}$, and with the SM Higgs particle's mass by relation: $\mu^2 = -\frac{m_{H^0}^2}{2}$.

Considering fluctuations of the Φ field $\frac{1}{\sqrt{2}}(v+\eta)e^{i\frac{\xi}{v}}$ around the minimum of the potential at $v^2 = -\frac{\mu^2}{\lambda}$, the `SSB` mechanism emerges, which brings mass terms to fermions (originating from the Yukawa Lagrangian) and gauge bosons $W^\pm$, Z (originating from the kinetic Lagrangian), after subtle absorption of the Goldstone fields ξ of the complete $SU(2) \times U(1)$ gauge group. This SM mechanism has been described in my master's thesis [33].

and Higgs [26–31] of whom the two last received the 2013 Nobel Prize for Physics.

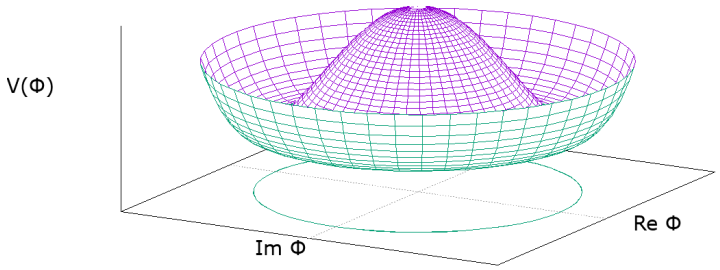

Figure 2: The shape of the SM scalar potential $V(\Phi)$ as a function of the complex field Φ for parameters $\mu^2 = \frac{m_{H^0}^2}{2}$ and $\lambda = -\frac{\mu^2}{v^2}$. The minimum of the potential is marked by a green circle. Points of the circle fulfil condition $\Phi^\dagger\Phi = \frac{1}{2}v$.

The SM theory combines electromagnetic, weak, and strong interactions to implement the gauge boson and their masses and finally introduces the scalar Higgs boson. In the next chapter, the scalar sector of the SM and its history is presented.

1.2 The Standard Model and hunting for the Higgs boson

As described in [34], for the first time, the mechanism of mass generation was associated with vacuum fluctuations of another field in 1957 in work by Julian Schwinger [35], followed by the work of Murray Gell-Mann with Maurice Lévy [36]. The σ-model was considered. Schwinger has shown how to give masses to nucleons. The model contains four scalar particles with the $O(4)$ symmetry with local left and right chiral symmetries of vector fields, $O(4) = SU(2)_L \times SU(2)_R$.

In 1962 Jeffrey Goldstone, Abdus Salam, and Steven Weinberg showed that the SSB in field theory leads to the existence of other massless and spinless particles, commonly called 'Goldstone bosons' [37]. Another important paper was written in 1962 by Philip Anderson [38]. Anderson studied superconductivity and the Meissner effect but showed

how the Goldstone boson could become massive due to an interaction with a gauge field and raised the possibility of using the SSB mechanism in particle physics. The idea to use a scalar field and the SSB mechanism to enable the mass generation in the SM was an extension of those works. It appeared in 1964 in the famous papers by Peter Higgs [27, 28], François Englert, Robert Brout [26] and Gerald Guralnik, Carl Richard Hagen, Tom Kibble [29]. In those papers, local symmetry is broken, but the Goldstone field is connected with the third polarisation of a vector gauge particle, which became massive. Living authors of those crucial papers (François Englert and Peter W. Higgs) were awarded the Nobel prize in 2013.

The Higgs mechanism and prediction of the existence of a massive scalar particle was a landmark moment. However, it was still not completing the SM theory, which bases on the symmetry-breaking mechanism. Among essential papers, it is worth mentioning the seminal work firstly by Sheldon Glashow [39], where the author extended Schwinger's studies and predicted the existence of the neutral Z vector boson. In 1964 Abdus Salam and John Ward wrote a paper based on a similar idea and predicted a massless photon and three gauge bosons [40]. In 1967 Tom Kibble extended those studies to non-abelian gauge symmetries and implemented the SSB mechanism [31]. Then Weinberg proposed the unified theory of electromagnetic and weak interactions [41] based on the $SU(2) \times U(1)$ gauge group, known since then as the *Standard Model*. The only thing left was to prove that the theory is renormalizable, which was done in 1971 by Gerard 't Hooft [42]. The Standard Model is now also called the Glashow-Weinberg-Salam model. Those three physicists were awarded the Nobel prize in 1979. The $SU(2) \times U(1)$ SM was completed when the quantum chromodynamics (QCD) sector with quarks and gluons was based on the $SU(3)$ gauge symmetry exhibiting notions of asymptotic freedom, discovered in 1973 by David Gross and Frank Wilczek [43, 44], and independently by David Politzer [45] in the same year. For this work, all three authors shared the 2004 Nobel Prize in Physics. I should add that the so-called eigth-fold quark model (based on the $SU(3)$ groups of colors and flavors) was suggested independently in 1964 by Murray Gell-Mann [46] and George Zweig [47].

Hand in hand, experimentalists tested the theory and provided the foundations for the upcoming theoretical work. Until the fifties, only a few elementary particles were known, such as photons, electrons, and muons. Electron [48] and muon neutrinos' existence were predicted theoretically. The electron neutrino was observed in 1956 by Clyde Cowan, and Frederick Reines [49]. Muon neutrino was discovered a few years later, in 1962 [50]. The famous experiment by Wu [51], crucial for the SM studies, took place within that time, confirming the hypothesis formulated by Tsung-Dao Lee and Chen-Ning Yang, that parity is not conserved in weak interactions [52]. The neutral current predicted by the electroweak theory (evidence of the Z boson existence) was observed for the first time in 1973 at CERN [53, 54]. One year later, the τ lepton was observed at Stanford Linear Accelerator Center (SLAC) and Lawrence Berkeley National Laboratory [55], but for the discovery of the tau neutrino physicists had to wait till 2000, when the DONUT experiment confirmed its existence [56]. The evidence of gluons was established by the PLUTO detector at DESY in 1978 [57] and the quarks were registered for the first time in 1968 in the electron-proton collision at SLAC [58, 59]. Due to the hadronisation, there is not possible to observe an unbound gluon or quark. However, it is possible to detect them indirectly. Deep inelastic e^--p scattering at SLAC proved that the proton is not an elementary particle and was the first experimental evidence of quarks' existence. The observation of the proton inner structure at SLAC with gluons was observed at PLUTO as a narrow resonance in e^+e^- annihilation with quarkonium decay: $e^+e^- \to q^+q^- \to 3g \to 3j$. Experimental completion of the SM quark sector came with the discovery of the heaviest of them. The top quark was observed in 1995 at Tevatron [60, 61].

So till 2000, when the tau neutrino was observed, almost every particle predicted by the SM was confirmed experimentally, except the scalar boson - Higgs particle.

Searches for the Higgs boson started in the nineties of the last century at Large Electron–Positron Collider (LEP) at CERN. There are two main ways to produce the Higgs boson in electron-positron collision [62]: Higgsstrahlung $e^+e^- \to HZ$ and vector boson fusion $e^+e^- \to e^+He^-/\nu_e H\tilde{\nu}_e$. LEP has reached the energy of 209 GeV, so it

potentially could produce a single Higgs particle. LEP has found a 3σ excess around the 114 GeV [63] but has not observed the Higgs boson directly. LEP was shut down in 2000, establishing the lower bound on its mass at 114.4 GeV with 95% confidence level [64]. Searches were also conducted at the proton-antiproton collider Tevatron. Also, in Tevatron, a slight excess (around 1.5 σ) of data events over the background estimation was observed between the mass range from 115 GeV to 140 GeV in the $b\bar{b}$ decay channel [65], excluding a wide range of Standard Model scalar boson masses. Tevatron was shut down in 2011, but Large Hadron Collider (LHC) had started its first run with the energy of 7 TeV one year earlier. Now comes the successful story of the H^0 discovery at LHC.

1.3 H^0 at LHC: the discovery, current status and HL-LHC

The following figures show the SM Higgs boson H^0 decay and production modes, prior to the H^0 discovery when the SM Higgs boson mass was a free parameter.

In Fig. 3 branching ratios for the SM Higgs decay are shown alongside with Feynman diagrams which dominates at the tree level the H^0 production process.

Discovery of the 125 GeV H^0 massive scalar at LHC confirmed the theoretical predictions for branching ratios which are dominated by the heavy flavor fermion decays $(b\bar{b}, \tau\tau)$, see the upper left plot in Fig. 3. The production process is dominated by the gluon fusion process (ggF), see Tab. 1 for present precision and accuracy (taken from PDG 2022 [67]). The corresponding ggF Feynman diagram is given in Fig.3(a). Other leading production diagrams given in the figure contributing to the Higgs boson production are the following; VBF: vector-boson fusion (b); WH: Higgs-strahlung (c); ZH: ssociated production with a gauge-boson (d); associated production with a pair of top quarks (e); $t\bar{t}H$: production in association with a single top quark (f) and (g).

Concerning the branching ratios alone, the first clear H^0 signals were connected with the H^0 decay to four leptons (muons) but not b-quarks which we could expect from the branching ratios at $m_{H^0} = 125$ GeV. This is due to a tricky background. A clear

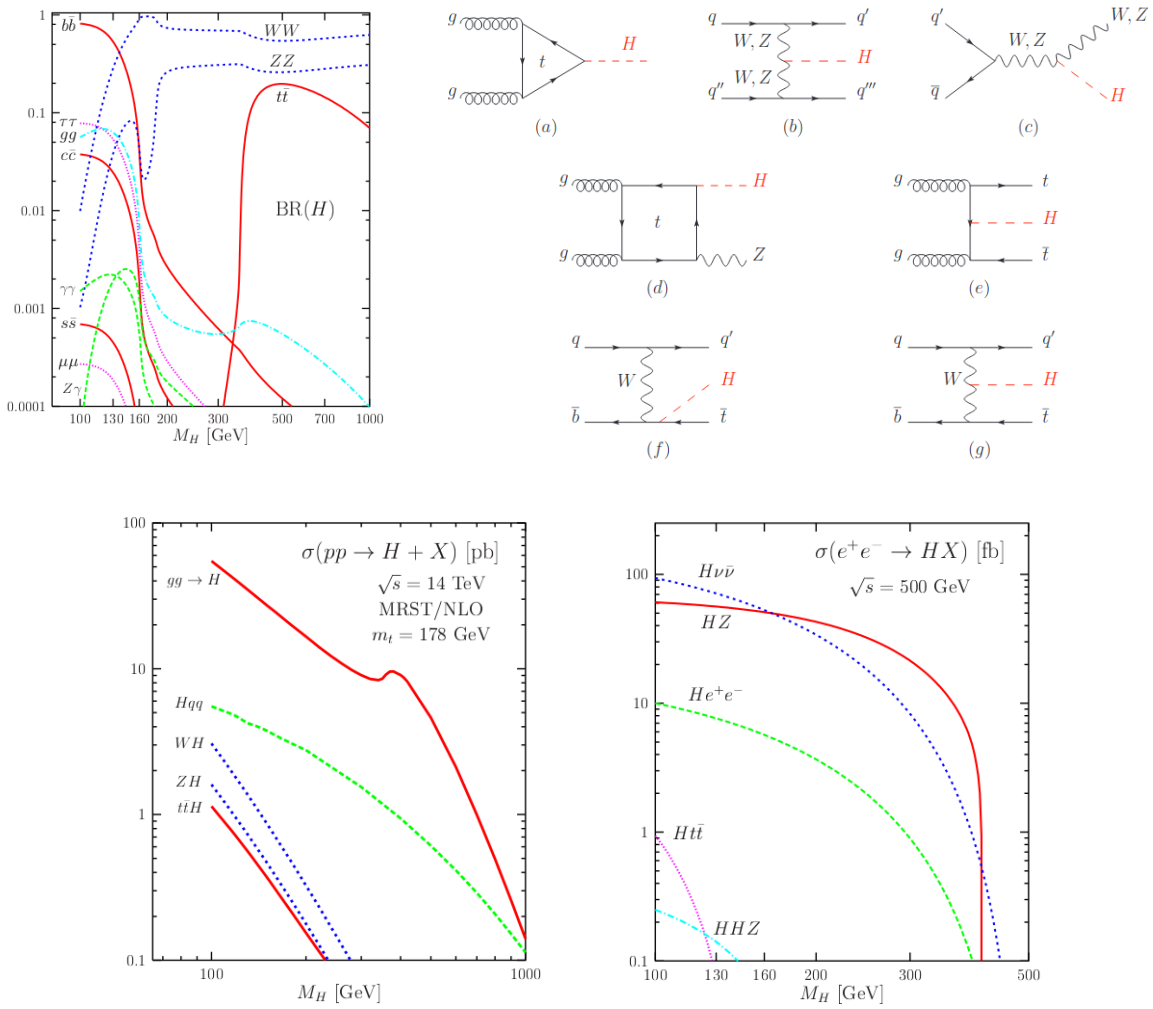

Figure 3: The decay branching ratios of the Standard Model Higgs boson (top left plot) and the Standard Model Higgs boson production cross sections (bottom plots) in the main channels at the $\sqrt{s} = 14$ TeV pp and $\sqrt{s} = 500$ GeV e^+e^- colliders. Feynman diagrams (a)-(g) are explained in the main text. Plots taken from the arxiv.org distribution in [66].

discovery that the Higgs boson decays to the third generation of fermions is spectacular, namely to the pairs of τ leptons and b-quarks. Especially determination of the Yukawa Higgs boson coupling to b-quarks is difficult, as though this channel amounts to about 60% of Higgs boson decays, the QCD b-quark background is overwhelming [68].

In 2011 LHC observed some significant excesses in W^+W^-, ZZ, $\gamma\gamma$, $b\bar{b}$ and $\tau^+\tau^-$ decay channels [62]. Finally, on the 4 July 2012 two LHC experiments, ATLAS and CMS, announced the discovery of the SM-like scalar particle [69, 70].

$\sqrt{s}$ (TeV)	Production cross section (in pb) for $m_H = 125\,\text{GeV}$					
	ggF	VBF	WH	ZH	$t\bar{t}H$	total
1.96	$0.95^{+17\%}_{-17\%}$	$0.065^{+8\%}_{-7\%}$	$0.13^{+8\%}_{-8\%}$	$0.079^{+8\%}_{-8\%}$	$0.004^{+10\%}_{-10\%}$	1.23
7	$16.9^{+5.5\%}_{-7.6\%}$	$1.24^{+2.2\%}_{-2.2\%}$	$0.58^{+2.2\%}_{-2.3\%}$	$0.34^{+3.1\%}_{-3.0\%}$	$0.09^{+5.6\%}_{-10.2\%}$	19.1
8	$21.4^{+5.4\%}_{-7.6\%}$	$1.60^{+2.1\%}_{-2.1\%}$	$0.70^{+2.1\%}_{-2.2\%}$	$0.42^{+3.4\%}_{-2.9\%}$	$0.13^{+5.9\%}_{-10.1\%}$	24.2
13	$48.6^{+5.6\%}_{-7.4\%}$	$3.78^{+2.1\%}_{-2.1\%}$	$1.37^{+2.0\%}_{-2.0\%}$	$0.88^{+4.1\%}_{-3.5\%}$	$0.50^{+6.8\%}_{-9.9\%}$	55.1
14	$54.7^{+5.6\%}_{-7.4\%}$	$4.28^{+2.1\%}_{-2.1\%}$	$1.51^{+1.8\%}_{-1.9\%}$	$0.99^{+4.1\%}_{-3.7\%}$	$0.61^{+6.9\%}_{-9.8\%}$	62.1

Table 1: The present, state-of-the-art production accuracy of the H^0 production at LHC, which include higher order radiative corrections, details and references can be found in the PDG Higgs review *Status of Higgs Boson Physics* [67].

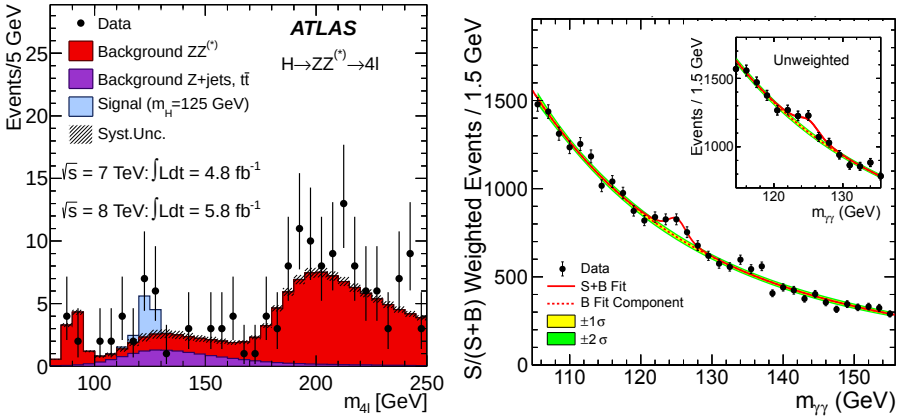

Figure 4: On left the H^0 discovery result by the ATLAS collaboration for the observed four-lepton invariant mass, compared to expected backgrounds [13]. On right the H^0 discovery result by the CMS collaboration for the observed diphoton invariant mass distribution [71].

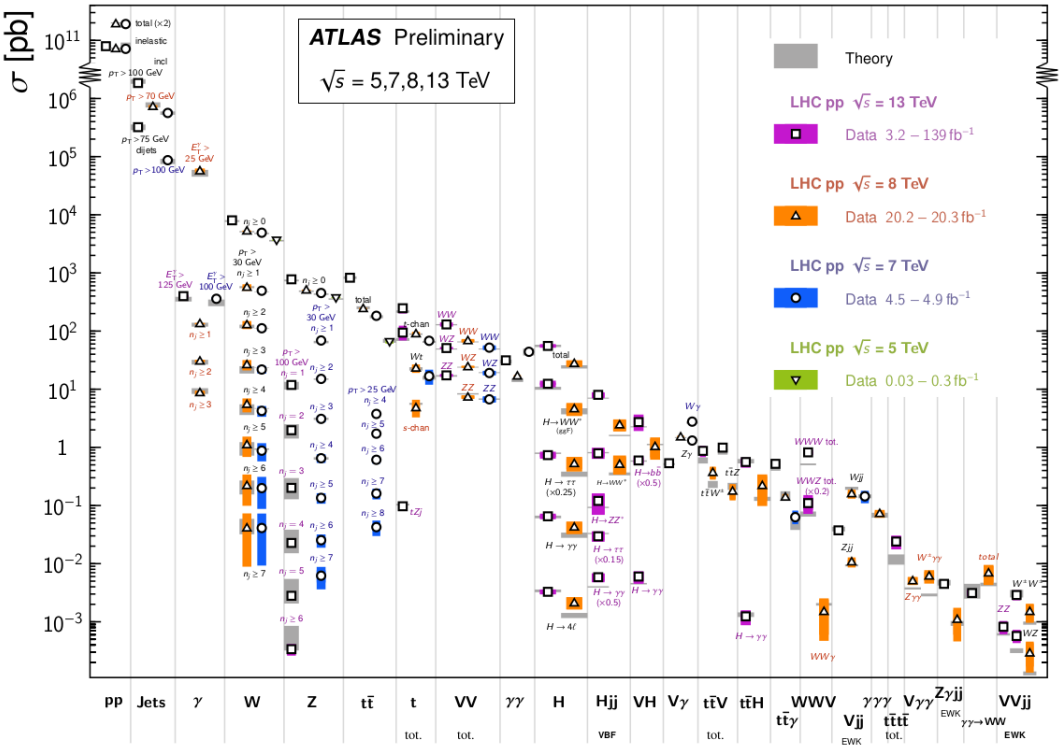

Figure 5: Summary of experimental results and theoretical recent predictions for a wide spectrum of processes studied at LHC. Figure taken from the Corfu 2022 talk [73].

Fig. 4 shows the first H^0 discovery plots at LHC for $\sqrt{s} = 7$ and 8 TeV. At the moment, ten years after the H^0 discovery in 2012, with gathered 139 fb^{-1}, *7.7 million of Higgs bosons has been identified* [5] [72]. The LHC story continues with the Run-3 update [72, 73]. The next step will be the High-Luminosity LHC (HL-LHC) which will operate at least till the end of the next decade [74] (i.e. $\sim$ 2038 year, see the scheme in the next section, Fig. 7). The goal for HL-LHC is to deliver about $L = 0.25\ ab^{-1} = 250\ fb^{-1}$ per year with the aim of integrated total luminosity in the range of 3 to 4.5 ab^{-1} by the late 2030s [75].

In Fig. 5 I present the summary for recent theory developments and computations

[5] In this section, I will refer to several recent talks which have been given in September 2022 at the Corfu SM and Beyond conference. They summarize the present status of some of the most important presently run and planned colliders.

for a broad array of processes considered at LHC. These impressive results show a very good agreement and confirmation for the SM theory predictions (electroweak and QCD) in hadron collissions, at the percentage level and better.

2 Higgs searches for future high-intensity and energy frontiers

In the thesis I will focus mainly on aspects of searching for new Higgs bosons, namely doubly charged Higgs scalars $H^{\pm\pm}$. These scalar BSM particles give a chance of finding clear lepton flavour violating effects (LFV) at future colliders. I focus on future e^+e^- high energy colliders signals and pp high energy collisions, including planned hadron colliders and HL-LHC. I will study mainly the leptonic signals, shortly mentioning gauge boson decays. Some recent detailed works exploring the doubly charged scalars production at the LHC, with subsequent decay into gauge bosons, can be found in [76, 77]. As we will see, LFV signals are naturally connected with Majorana neutrinos in model building. So in estimation of detection signals we profit also from present and foreseen constraints connected with low energy, so-called intensity frontier experiments, such as nuclear μ to e conversion or $(\beta\beta)_{0\nu}$ experiments, see e.g. [78–80]. In one specific model which we will consider (i.e. HTM model), also neutrino oscillation data will be relevant.

The scheme in Fig. 6 and Table 2 show some processes along with experiments which are discussed for improving limits on LFV signals in intensity frontier studies. More on that will be discussed in section 4.3.

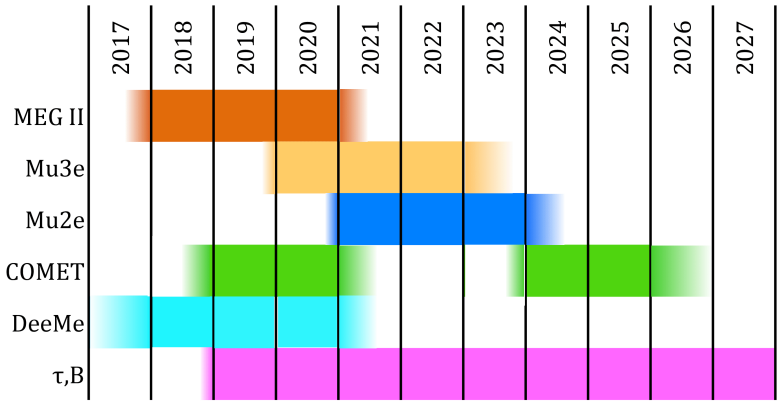

Figure 6: Estimated duration of individual experiments looking for processes violating the principle of preserving the lepton number [81].

Process	Present limits	Expected limits	References	Experiment
$\mu^+ \to e^+\gamma$	$< 4.2 \times 10^{-13}$	5×10^{-14}	[82]	MEG II
$\mu^+ \to e^+e^-e^+$	$< 1.0 \times 10^{-12}$	10^{-16}	[83]	Mu3e
$\mu^-\mathrm{Al} \to e^-\mathrm{Al}$	$< 6.1 \times 10^{-13}$	10^{-17}	[84]	Mu2e, COMET
$\mu^-\mathrm{Si/C} \to e^-\mathrm{Si/C}$	–	5×10^{-14}	[85]	DeeMe
$\tau \to e\gamma$	$< 3.3 \times 10^{-8}$	5×10^{-9}	[86]	Belle II
$\tau \to \mu\gamma$	$< 4.4 \times 10^{-8}$	10^{-9}	[86]	Belle II
$\tau \to eee$	$< 2.7 \times 10^{-8}$	5×10^{-10}	[86]	Belle II
$\tau \to \mu\mu\mu$	$< 2.1 \times 10^{-8}$	5×10^{-10}	[86]	Belle II
$\tau \to e$ had	$< 1.8 \times 10^{-8}$	3×10^{-10}	[86]	Belle II
$\tau \to \mu$ had	$< 1.2 \times 10^{-8}$	3×10^{-10}	[86]	Belle II
had $\to \mu e$	$< 4.7 \times 10^{-12}$	10^{-12}	[87]	NA62
$H^0 \to e\mu$	$< 3.5 \times 10^{-4}$	3×10^{-5}	[88]	HL-LHC
$H^0 \to \tau\mu$	$< 2.5 \times 10^{-3}$	3×10^{-4}	[88]	HL-LHC
$H^0 \to \tau e$	$< 6.1 \times 10^{-3}$	3×10^{-4}	[88]	HL-LHC

Table 2: Current and future experimental limitations for selected lepton number breaking processes, based on [81].

Aiming at sub-percent precision for Higgs boson decays, quantitative tests of the

SM for Higgs boson parameters (the mass, decay branching ratios, couplings) need further scrutinizing studies at HL-LHC and future Higgs factories. These also include the investigation of the Higgs boson self-coupling [89] and BSM effects in extended Higgs sector.

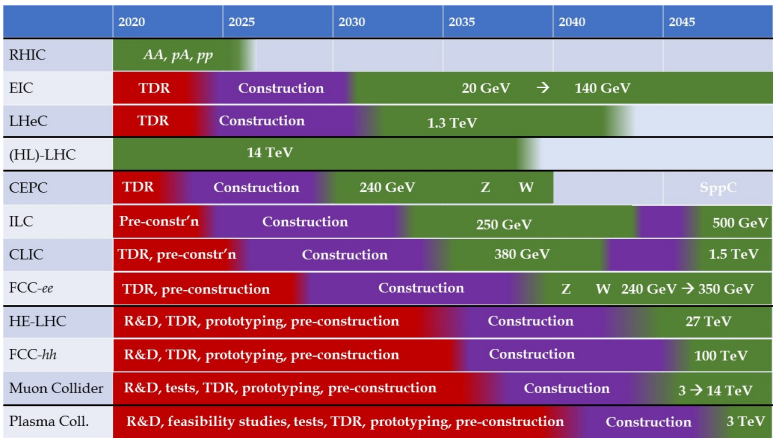

Figure 7: Rough timelines of future large colliding beam facilities, the chart taken from [90].

There are several proposals towards so-called Higgs factories where the first focus is on study of the Higgs sector of the theory. Fig. 7 gathers the main projects. Some of them are already operating (RHIC, LHC) accepted for extension (HL-LHC) or are under construction (Electron-Ion Collider, EIC [91]). The rest is under hot debate, some features of them will be outlined now. Let me start from several general remarks. First, each of these project is extremely complicated in terms of physics studies preparations but in particular in terms of technological and infrastructure planning. As an example, in Fig. 8 the scheme of action for HL-LHC is shown. Preparation of such undertakings takes years and decades.

Second, there is a permanent progress in R&D (Research and Development) concerning particles collisions. In Fig. 9 solid and dashed lines indicate a kind of ten-fold increase per decade for hadron (circles) and lepton (triangles) colliders achievements in terms of collision energies and luminosities.

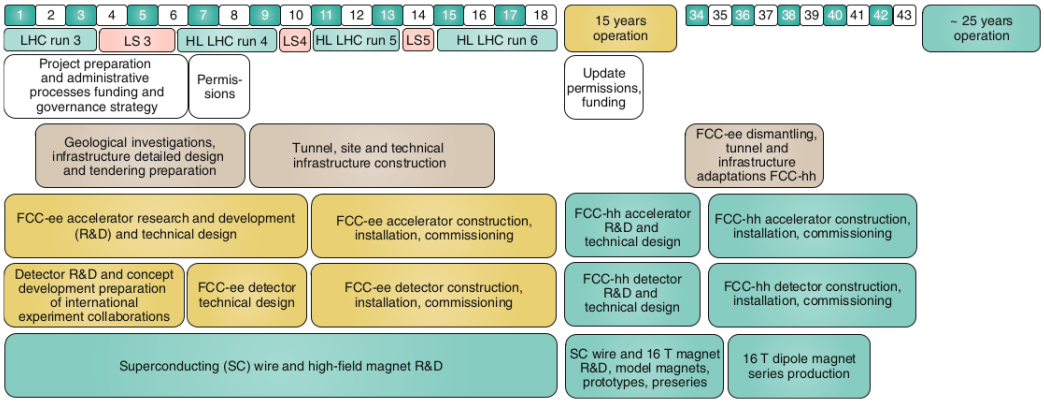

Figure 8: HL-LHC operation stages, the chart taken from [92].

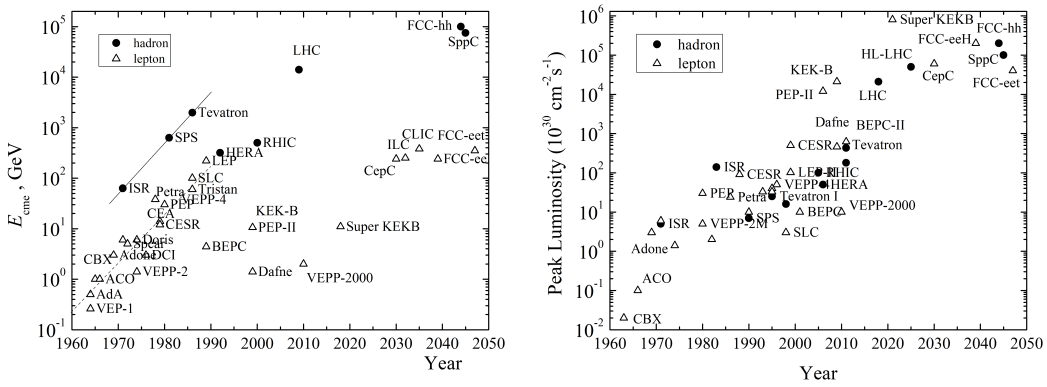

Figure 9: Center of mass energy reach of particle colliders vs their start of operation (on left). Luminosity of particle colliders (on right). Triangles are lepton colliders and full circles are hadron colliders. Plots taken from the arxiv.org distribution in [90].

There are a few plans regarding future particle colliders. First, as already written, the High Luminosity LHC (HL-LHC) will start operating in early 2028 according to the plans [93]. While the proton-proton LHC reached the integrated luminosity 189.3 fb^{-1} for ALICE and CMS experiment [94], the HL-LHC is intended to increase that value to around 3000 fb^{-1} within 14 years of activity [74].

Another collider planned to be built at CERN is the Future Circular Collider (FCC) [95]. That project would be located in a new, 100 km tunnel near Geneva. The FCC is planned to operate in several stages. At the moment, the first stage covers the

electron-positron collider FCC-ee with center-of-mass energies between 88 and 365 GeV. FCC-ee would be the SM factory for W, Z, the top quark, and H particles, but also it would cover the flavor physics beyond the current low energy projects, e.g., BES-III or Belle [96]. The second stage covers the hadron (pp) collider FCC-hh with the center of energy goal of the order of 100 TeV, so around seven times higher than the LHC.

FCC would continue the LHC mission at energy frontiers and also provide the ions and electron-hadron options for collision (FCC-eh). FCC-hh, defined by the target of 100 TeV proton-proton collisions within 25 years of activity, will be able to reach a total integrated luminosity of 20-30 ab^{-1} [97]. In total, the FCC-integrated project will cover seven decades of analysis, the latest estimates can be found in the talk [98]. The first stage, FCC-ee, is planned[6] for years 2040-2055, second, FCC-hh, for years 2060-2070.

The research program of FCC is very broad. Just two examples. In Fig. 10 taken from [99], it is shown how much precision of SM parameters' determination will improve with FCC-ee (here W and top quark masses). Typically, the improvements for electroweak observables are at the level of one to two orders of magnitude [100]. This sensitivity of course opens the way for studying indirect BSM effects in specific models or within effective theories [11, 101].

Fig. 11 shows the ultimate sensitivity and reach that the FCC-ee project can achieve: measurement of the electron Yukawa coupling; in other words measurement of the Higgs boson coupling to electrons (which is, as predicted by the SM Higgs mechanism smaller than the muon-Higgs coupling by the electron to muon mass ratio).

Continuing the list of considered future colliders, another idea is to run the high energy LHC (HE-LHC), which could reach the energy of 27 GeV and luminosity around 3 times higher than HL-LHC, giving the integrated luminosity exceeding 10 ab^{-1} during

[6] As still nothing is established for good, estimations are changing all the time. In addition, economic and even political situations influence the plans, which is especially clear after the 24^{th} February 2022 Russian invasion of Ukraine. This remark refers to all future projects.

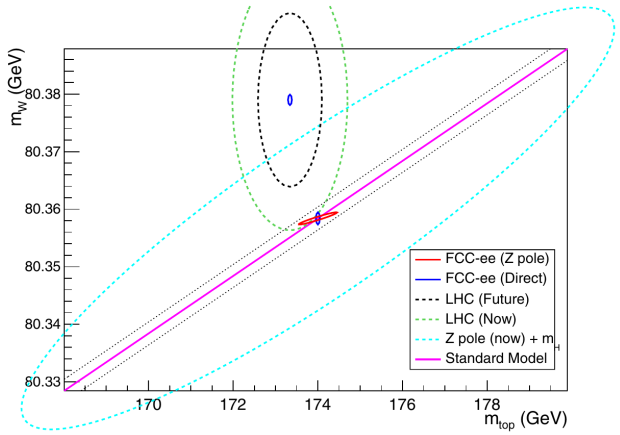

Figure 10: Contours of 68% confidence level from fits of the SM to the electroweak precision measurements at FCC-ee. The fit is compared to the direct m_W and m_t measurements at the W^+W^- and $t\bar{t}$ thresholds. For details see [99] from where the plot has been taken.

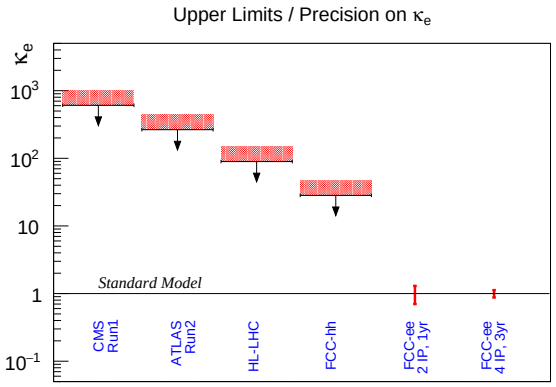

Figure 11: The so-called κ_e Higgs boson coupling modifier to electrons at present and future LHC and FCC experiments as defined in [102] and discussed in [103] shows how much precision of the $H^0 - e^- - e^+$ coupling will improve in future collider experiments. Plot taken from [104].

20 years of operation [105]. That could produce particles up to 12 TeV at a significant scale and, for example, measure the Higgs self-coupling [106]. Both those machines would use the existing LHC infrastructure, including its 27 km long tunnel. By the

way, there was also an idea to use the same tunnel and install there again an electron-positron collider, LEP3 [107]. However, this idea seems rather changed into the FCC-ee option.

China has its own idea of a future collider, but similar in concept to FCC-ee, namely a 100 km collider called the Circular Electron Positron Collider (CEPC), with maximum energy of 240 GeV [108]. At this threshold it will operate as a Higgs factory for 7 years reaching integrated luminosity of 5.6 ab^{-1} [109]. Later, in the same tunnel, the collider could be upgraded to Super Proton-Proton Collider (SPPC) [110] with centre-of-mass energy in the range of 75-125 TeV. In Table 4 the comparison of future hadron colliders capabilities is presented.

	LHC	HL-LHC	HE-LHC	FCC-hh	SPPC
Centre-of-mass energy:	8-14 TeV	14 TeV	27 TeV	100 TeV	75-150 TeV
Length:	27 km	27 km	27 km	100 km	100 km
Luminosity per year*:	55 fb^{-1}	250 fb^{-1}	730 fb^{-1}	>1000 fb^{-1}	3000 fb^{-1}
Integrated luminosity:	$\sim$ 190 fb^{-1}	3000 fb^{-1}	>10 ab^{-1}	>25 ab^{-1}	30 ab^{-1}

Table 3: Comparison of basic features of future hadron colliders. In the first row, we present the planned maximum energy. Luminosity per year was calculated assuming 160 days of activity annually [105, 110].

Regarding the lepton colliders, a few plans are considered. First, there are mentioned earlier circular e^+e^- colliders, LEP3 [107], FCC-ee [111], both planned location at CERN, and CEPC in China. Apart from that, two linear lepton colliders are also considered: Compact Linear Collider (CLIC) and International Linear Collider (ILC). CLIC would be built at CERN near Geneva and could reach energy up to 3 TeV [112]. Regarding the ILC, a few potential locations are discussed, and the accelerator itself will operate with energies up to 1 TeV [113]. Those accelerators aim to discover new physics effects but would also test the SM parameters with unprecedented precision, like Z, W, top, and Higgs couplings, see Figs. 10 and 11 for the FCC-ee case. The colliders would work at a few stages with different energies corresponding to masses of

desired particles. Integrated luminosity would depend strongly on energies and activity time, but generally, it will reach the level of ab^{-1}. Fig. 12 summarizes the luminosity goals for future e^+e^- colliders.

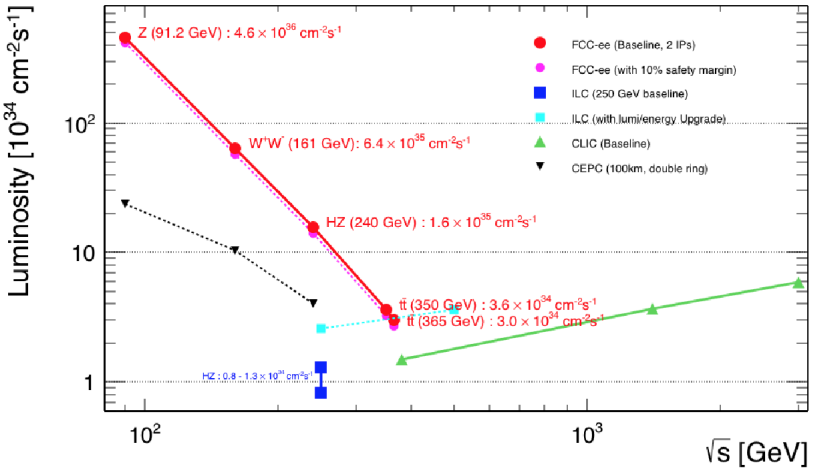

Figure 12: Baseline luminosities expected to be delivered (summed overall interaction points) as a function of the centre-of-mass energy $\sqrt{s}$, at each of the four worldwide e^+e^- collider projects: ILC (blue square), CLIC (green upward triangles), CEPC (black downward triangles), and FCC-ee (red dots). The plot taken from [95].

In Table 4 the comparison of future lepton colliders capabilities is presented.

	LEP3	ILC	CLIC	FCC-ee	CEPC
Centre-of-mass energy:	240 GeV	250 - 500 GeV	380-1500 GeV	88-365 GeV	88-240 GeV
Length:	27 km	30-50 km	up to 50 km	100 km	100 km
Type:	circular	linear	linear	circular	circular
Activity in years:	5-10	20	>10	15	10

Table 4: Comparison of basic features of future e^+e^- colliders.

Finally, coming back to Fig. 7, there are also plans for the muon collider[7] [117].

[7]The list of ideas for future colliders can be easily extended, e.g., towards e.g. photon colliders [114] or recent plan for the C^3 collider in the US [115]. And maybe extreme energies, in the end, will become

For this work, we will consider just high-energy electron-positron and proton-proton collisions. For example, the lepton-hadron collision with doubly charged scalars was discussed in [118].

Setting the scenery for future intensity frontier and high energy experiments, the BSM Higgs theories of interest will be introduced in the next chapter, which includes doubly charged Higgs scalars.

possible in Plasma Wakefield Linear Colliders [116].

3 Higgs bosons beyond the Standard Model: Theory

Going beyond the SM, crucial questions concerning the scalar sector are: what is the representation for the scalar multiplets and what is the shape of the scalar potential of the fundamental theory in particle physics? Are the fundamental forces unified, and if so, then how? So far, we do not have any particular answer to these queries and acquiring knowledge on the Higgs sector and scalar potential is essential. For instance, in the SM the electroweak vacuum is unstable, in principle, with a possible quantum tunnelling effects, matter of theoretical studies in cosmology [119]. Examples of improving vacuum stability are supersymmetry [120] or extra dimensions [121]. However, it is argued in [122] that the SM is stable in cosmological time up to the Planck scale.

3.1 Extentions of the SM - why triplets?

So far, the experiment confirms the Standard Model predictions with great accuracy. The scalar boson, discovered in 2012 at CERN, also seems to fulfil SM requirements, and it completes the list of elementary particles predicted by the Standard Model. However, although the SM answers many questions, a few problems remain unsolved. The SM does not include gravity since translating gravity to an effective field theory leads to unremovable nonrenormalizability of the theory. But apart from the quantization of gravity, there are other problems too.

One of the main weaknesses of the SM lies in the fact that it does not provide the dark matter candidate. A priori, among many exotic scenarios, neutrinos are excellent candidates for contributing to the dark matter density: They do exist and are massive. To be a WIMP (Weakly Interacting Massive Particle) dark matter candidate, a particle should be massive and interact with the forces not stronger than weak interactions. For neutrinos DM constructions including beyond WIMPs scenarios, see e.g. [123] and recent [124]. Regarding neutrinos, the classic version of the Standard

Model does not include neutrino masses. The neutrino masses can be easily added to the model by introducing to the theory right-handed fields, like in the seesaw type-I mechanism. Another solution is to add a scalar triplet to the model (seesaw type-II) or a lepton triplet (seesaw type-III). In this work, I will concentrate on the first two options, that means seesaw type I and II mechanisms realized within the Left-Right Symmetric Model (chapter 3.3.2) and the Higgs Triplet Model (3.3.1).
Both those models have extended scalar sectors with one or two scalar triplets, but the first one contains right-handed heavy neutrinos and has an extended gauge group too. Non-standard models with triplet extensions are exciting since, depending on the triplet hypercharge, they might contain singly and doubly charged scalar particles. Doubly charged scalars are the main object of this thesis. For that purpose, we need to add to the theory triplets with hypercharge $Y = 1$ or $Y = 2$, depending on the convention. For $Y = 1$, the electric charge of the field is given by the sum of its third isospin component, and the hypercharge $Q = T_3 + Y$ is used. For $Y = 2$, the electric charge is given by the formula

$$Q = T_3 + \frac{Y}{2}. \tag{3.1}$$

I will follow the second convention. Of course, it is possible to add the scalar triplet with the hypercharge $Y = 0$, but from Eq. (3.1), it is clear that in that case, it is not possible to get a doubly charged particle in the model spectrum.

However, adding triplet scalar fields to the model also creates potential problems. In the next section I will discuss them in detail.

3.2 Imprints of models with triplet fields

BSM models include new particles, which usually couple with SM particles, even if very weakly. Thus, even if their detection is beyond present experimental sensitivity, they may leave their imprints in modifications of the SM parameters and observables. One of the key parameters of this kind is the ρ-parameter and when the scalar sector

is extended, the ρ-parameter should remain close to one at the tree level [125–127] as

$$\rho = \frac{J_{NC}}{J_{CC}} \tag{3.2}$$

$$= \frac{M_W^2}{M_Z^2 \cos^2\theta_W}, \tag{3.3}$$

and $\rho_{\rm SM}^{\rm tree} = 1$. The relation (3.2) defines ρ as a ratio of neutral J_{NC} to charged J_{CC} currents.

The SM tree level ρ-parameter in (3.3) gets modifications due to radiative corrections which changes M_W, M_Z and $s_W^2 \equiv \sin^2\theta_W$

$$s_W^2 = \left(1 - \frac{M_W^2}{M_Z^2}\right)_{\rm tree} + \delta s_W^2 \tag{3.4}$$

$$= 1 - \frac{M_W^2}{M_Z^2} + c_W^2 \left(\frac{\Pi_{WW}(M_W^2)}{M_W^2} - \frac{\Pi_{ZZ}(M_Z^2)}{M_Z^2}\right) = 1 - \frac{M_W^2}{M_Z^2} + c_W^2 \Delta\rho, \tag{3.5}$$

so $\Delta\rho$ is defined by the difference between mass corrections to W and Z boson masses, $M_V^2 \to M_V^2 - \Pi_{VV}(M_V^2)$ where Π_{VV} is the real part of the transverse component of the self–energy of V at the scale M_V, $V = W, Z$.

In SM, this correction due to the top-quark is substantial (at the percentage level) while correction due to H^0 is moderate (logarithmic behaviour, screening theorem [128])

$$\Delta\rho = 3\frac{G_\mu m_t^2}{8\sqrt{2}\pi^2}\left[1 + \Delta\rho^{\rm t} + \Delta\rho^{\rm H} + \ldots\right], \tag{3.6}$$

$$\Delta\rho^t = \frac{3\sqrt{2} m_t^2 G_\mu}{16\pi^2}, \tag{3.7}$$

$$\Delta\rho^{\rm H} \sim -\frac{3G_\mu M_W^2}{8\sqrt{2}\pi^2}\,\frac{s_W^2}{c_W^2}\log\frac{M_H^2}{M_W^2} \quad \text{for } M_H \gg M_W. \tag{3.8}$$

$\Delta\rho$ is one of the key parameters considered in the precision physics calculations. It is one of the so-called oblique corrections [129] (self-energy corrections) which is also used to parametrize BSM radiative contributions through S, T, U parameters, which are defined as follows [129]

$$\alpha S = 4s_W^2 c_W^2 \left[\Pi_{ZZ}(0) - (c_W^2 - s_W^2)/(s_W c_W)\Pi'_{Z\gamma}(0) - \Pi'_{\gamma\gamma}(0)\right], \tag{3.9}$$

$$\alpha T = \Pi_{WW}(0)/M_W^2 - \Pi_{ZZ}(0)/M_Z^2, \tag{3.10}$$

$$\alpha U = 4s_W^2 \left[\Pi'_{WW}(0) - c_W^2\Pi'_{ZZ}(0) - 2s_W c_W \Pi'_{Z\gamma}(0) - s_W^2\Pi'_{\gamma\gamma}(0)\right]. \tag{3.11}$$

The variable αT is just the shift of the ρ-parameter due to BSM effects, $\alpha T = 1 - \rho - \Delta\rho|_{\rm SM}$. The primes in the above equations state for the derivative of self-energies over momenta squared.

Later we will consider this so-called T-parameter in the framework of considered BSM models. Electroweak corrections and S, T, U parameters for models with triplets can be found in [130, 131] and for `MLRSM` in [132] and [133].

In general, the ρ-parameter will depend on the scalar sector and will restrict the additional multiplets VEVs. This is due to masses in Eq. (3.2) and the SSB mechanism, and we get

$$\rho = \frac{\sum_i \left[T_i(T_i+1) - (T_{3i})^2\right] v_i^2}{2\sum_i T_{3i}^2 v_i^2}. \tag{3.12}$$

For the SM Higgs doublet with the hypercharge $Y = 1$ and weak isospin $T = \frac{1}{2}$ (as well as for multi-doublets and singlets), the ρ-parameter is naturally equal to 1. In this case the model has a custodial $SU(2)$ global symmetry [34]. In the SM, this symmetry is broken at the loop level when fermions of the same doublets have different masses [134] and by the hypercharge group. E.g., by adding multiplets under the $SU(2)_L$ group with the hypercharge $Y = 2$, it is needed to keep in mind that the ρ-parameter will be modified[8]

$$\rho = \frac{1 + 2\frac{v_\Delta^2}{v_\phi^2}}{1 + 4\frac{v_\Delta^2}{v_\phi^2}}, \tag{3.13}$$

[8] In [127] it has been noticed that $\rho = 1$ in general can be sustained in the case when a Higgs multiplet H fulfills the condition $T^H(T^H+1) = 3(T_3^H)^2$, which has nontrivial solutions in (T^H, T_3^H), e.g. when $(1/2, \pm 1/2)$ or $(3, \pm 2)$.

where v_ϕ corresponds to the Standard Model Higgs doublet's VEV and v_Δ denotes the additional triplet's VEV. Since the final value depends on the multiplet's VEV, we have obtained the first bound on non-standard triplets' parameters.

As we can see from (3.13), addition of triplets changes ρ to be smaller than 1. In the limit $v_\Delta \to \infty$, $\rho = 1/2$ (triplets only). For $v_\Delta \to 0$, $\rho = 1$ (doublets only). So in general (at tree level), $1/2 \leq \rho \leq 1$.

The exact values of ρ with inclusion of radiative corrections depend on renormalization schemes, for instance, in the on-shell scheme $s_W^2 = 1 - M_W^2/M_Z^2$ to all orders in perturbation theory by definition, so $\rho = 1$, in the $\overline{\text{MS}}$ scheme, $\rho = 1.01013 \pm 0.00005$, see J. Erler and A. Freitas 'Electroweak Model and Constraints on New Physics' in [9]. Anyway, in any renormalization scheme, the final value of ρ is very close to one. *That means that, if exist, triplets addition to the SM theory is very small, within experimental errors.* Typically, v_Δ is restricted to 1-2 GeV level, at best, see for instance our estimate in [135]. As we will see, other low experimental data are also important, decreasing the scale of v_Δ in an unambiguous way to the (sub)electronvolt level for the SM model with $Y = 2$ triplet.

Let us note that in some triplet extended models the ρ-parameter can be protected by the custodial symmetry, for example in the Georgi-Machacek Model [136]. The pay for not considering special constructions or symmetries like in [137, 138] is that, as we will see, $v_\Delta \ll v_\phi$, which makes experiments more challenging to detect its traces.

Another theoretical restrictions on extended scalar sectors with triplets comes from the unitarity and vacuum stability. Vacuum stability means that a scalar potential should be bounded from below [139, 140]. Perturbative unitarity protects masses and couplings to the level in which the scattering amplitudes do not blow up at high energy regime [141, 142]. Those issues in the context of the Higgs Triplet Model (see section 3.3.1) were discussed in [143–147], and in the context of the Left Right Symmetric Models (section 3.3.2) were mentioned for example in [143, 148–150]. Unitarity and vacuum stability impose some relations on the scalar potential parameters, so scalar

particle masses, since they are expressed as functions of those parameters. I will cover that subject in section 4.

3.3 GUT models with triplets

The SM theory is based on 19 free parameters [9]. Among those parameters are $SU(3)_C$, $SU(2)_L$, and $U(1)_Y$ gauge couplings g_S, g, and g'. Further, charged fermion masses (9 parameters for leptons and quarks) and four parameters for mixing angles and the CP phase in the CKM matrix. The remaining three parameters are QCD angle θ_{QCD}, scalar doublet VEV v_ϕ, and Higgs quartic coupling λ. It is also necessary to add the neutrino parameters (3 neutrino masses and six mixing angles for Majorana neutrinos). The experimental data fix all those parameters, but understanding their origin would be a milestone. Many attempts were undertaken to create the so-called Grand Unification Theory (GUT). That theory is supposed to answer the above questions about the nature of coupling constants and unify the SM interactions. The GUT models assume that a larger gauge symmetry enfolds the SM gauge group before the symmetry breaking at high energies, for example, by the $SO(10)$ group. One example of the GUT model is the Minimal Left-Right Symmetric Model (`MLRSM`), which is introduced in section 3.3.2.

For the aim of this thesis, the most interesting part is the extension of the scalar sector. There are two ways to create a model with a more complex scalar sector, indirectly, by extending the gauge group, which will enforce further extension of the scalar sector to break the symmetry, or simply by introducing more scalar multiplets to the theory "by hand". Below, I will introduce two models that present those two approaches, `MLRSM` (section 3.3.2) with an extended gauge group and `HTM` (section 3.3.1), based on the `SM` gauge group.

3.3.1 The Higgs Triplet Model (HTM)

The Higgs Triplet Model (HTM) is one of the less complicated extensions of the SM. It is created just by adding a triplet (like in Eq. (3.15 below) to the scalar sector, which affects neutrino masses without introducing right-handed neutrino fields (so the model realizes the type-II seesaw mechanism). The gauge group remains the same as in SM. The scalar sector is built from the SM-like doublet Φ and the triplet Δ with the desired hypercharge. I chose a model with the hypercharge $Y = 2$ and followed the convention where the electric charge is given by the relation $Q = T_3 + \frac{1}{2}Y$, and the following notation for scalar triplet and doublet fields

$$\Phi = \frac{1}{\sqrt{2}} \begin{pmatrix} \Phi^+ \\ \Phi^0 \end{pmatrix} = \frac{1}{\sqrt{2}} \begin{pmatrix} \sqrt{2} w_\Phi^+ \\ v_\Phi + h_\Phi + i z_\Phi \end{pmatrix} \quad , \tag{3.14}$$

$$\Delta = \frac{1}{\sqrt{2}} \begin{pmatrix} \Delta^+ & \sqrt{2}\Delta^{++} \\ \sqrt{2}\Delta^0 & \Delta^+ \end{pmatrix} = \frac{1}{\sqrt{2}} \begin{pmatrix} w_\Delta^+ & \sqrt{2}\delta^{++} \\ v_\Delta + h_\Delta + i z_\Delta & -w_\Delta^+ \end{pmatrix}. \tag{3.15}$$

The VEVs of the doublet Φ and the triplet Δ fulfil the condition

$$v = \sqrt{v_\Phi^2 + 2v_\Delta^2} \simeq 246 \text{ GeV}, \tag{3.16}$$

The most general form of the scalar potential for a model with SM-like doublet Φ and an additional scalar triplet Δ is presented, for example, in [146]

$$\begin{aligned} V \;=\; & -m_\Phi^2 \left(\Phi^\dagger \Phi\right) + \tfrac{\lambda}{4} \left(\Phi^\dagger \Phi\right)^2 + M_\Delta^2 \mathrm{Tr}\left(\Delta^\dagger \Delta\right) + \left[\mu \left(\Phi^T i\sigma_2 \Delta^\dagger \Phi\right) + \text{h.c.}\right] + \\ & + \lambda_1 \left(\Phi^\dagger \Phi\right) \mathrm{Tr}\left(\Delta^\dagger \Delta\right) + \lambda_2 \left[\mathrm{Tr}\left(\Delta^\dagger \Delta\right)\right]^2 + \lambda_3 \mathrm{Tr}\left[\left(\Delta^\dagger \Delta\right)^2\right] + \lambda_4 \Phi^\dagger \Delta \Delta^\dagger \Phi \,, \end{aligned} \tag{3.17}$$

where m_Φ and m_Δ are functions of scalar potential's parameters and triplet Δ and doublet Φ vacuum expectation values

$$m_\Phi^2 = \frac{\lambda}{4} v_\Phi^2 + \frac{(\lambda_1+\lambda_4)}{2} v_\Delta^2 - \sqrt{2}\mu\, v_\Delta\,, \tag{3.18a}$$

$$m_\Delta^2 = -(\lambda_2+\lambda_3)\, v_\Delta^2 - \frac{(\lambda_1+\lambda_4)}{2} v_\Phi^2 + \frac{\mu}{\sqrt{2}} \frac{v_\Phi^2}{v_\Delta}\,. \tag{3.18b}$$

The physical particles are described as superpositions of the above fields. The H^0 particle is interpreted as the SM-like Higgs boson

$$H^{\pm\pm} = \delta^{\pm\pm}, \tag{3.19a}$$

$$\begin{pmatrix} G_0 \\ A \end{pmatrix} = \begin{pmatrix} \cos\beta' & \sin\beta' \\ -\sin\beta' & \cos\beta' \end{pmatrix} \begin{pmatrix} z_\Phi \\ z_\Delta \end{pmatrix} \quad , \qquad \tan\beta' = \frac{2v_\Delta}{v_\Phi}\,, \tag{3.19b}$$

$$\begin{pmatrix} G^\pm \\ H^\pm \end{pmatrix} = \begin{pmatrix} \cos\beta & \sin\beta \\ -\sin\beta & \cos\beta \end{pmatrix} \begin{pmatrix} w_\Phi^\pm \\ w_\Delta^\pm \end{pmatrix} \quad , \qquad \tan\beta = \frac{\sqrt{2}v_\Delta}{v_\Phi}\,, \tag{3.19c}$$

$$\begin{pmatrix} h \\ H^0 \end{pmatrix} = \begin{pmatrix} \cos\alpha & \sin\alpha \\ -\sin\alpha & \cos\alpha \end{pmatrix} \begin{pmatrix} h_\Phi \\ h_\Delta \end{pmatrix} \quad , \qquad \tan 2\alpha = \frac{2B_S}{C_S - A_S}\,, \tag{3.19d}$$

where the coefficients A_S, B_S and C_S are

$$A_S = \frac{\lambda v_\Phi^2}{2}\,, \tag{3.20a}$$

$$B_S = \sqrt{2}\mu v_\Phi - (\lambda_1+\lambda_4) v_\Delta v_\Phi\,, \tag{3.20b}$$

$$C_S = \frac{\mu v_\Phi^2}{\sqrt{2}v_\Delta} + 2(\lambda_2+\lambda_3) v_\Delta^2\,. \tag{3.20c}$$

So for an additional triplet Δ with a hypercharge $Y = 2$, we obtained the following scalar particles spectrum: two Goldstone particles G^0, G^+, one SM-like neutral scalar H^0, one charged and one doubly charged scalars: $H^\pm$ and $H^{\pm\pm}$.

Since the model provides neutrino masses, the Yukawa part of the Lagrangian has to be added. Firstly, as in the Standard Model, neutral and charged leptons are grouped in doublets under the $SU(2)_L$ transformation

$$L_\ell = \begin{pmatrix} \nu_\ell \\ \ell \end{pmatrix}_L , \quad [\ell = e, \mu, \tau] . \tag{3.21}$$

The Yukawa Lagrangian, in that case, is presented below, C is the charge conjugation operator (it can be written using the Dirac matrices in the form $C = i\gamma^2\gamma^0$) and $\mathcal{Y}_{\ell\ell'}$ is the symmetric Yukawa matrix

$$\mathcal{L}_Y^\Delta = \frac{1}{2}\mathcal{Y}_{\ell\ell'} L_\ell^T C^{-1} i\sigma_2 \Delta L_{\ell'} + \text{h.c.} \tag{3.22}$$

The σ_2 denotes the second Pauli matrix. The above formula includes the neutrino mass term

$$\mathcal{L}_\nu = \frac{1}{2}\,\bar{\nu}_\ell\,\frac{v_\Delta}{\sqrt{2}}\,\mathcal{Y}_{\ell\ell'}\,\nu_{\ell'}. \tag{3.23}$$

As mentioned, this neutrino mass generation mechanism using additional Higgs fields is called seesaw type-II. Apart from providing massive neutrinos, the Lagrangian $\mathcal{L}_Y^\Delta$ also describes the interaction between triplet fields and leptons, particularly the $H^{\pm\pm} - l^\mp - l'^\mp$ and $H^\pm - l^\mp - \nu_{l'}$ vertices. *Those vertices break the lepton number and can be a part of not observed so far processes* like $\mu \to e\gamma$, as well as contribute to the muon anomalous magnetic moment $(g-2)_\mu$. Those processes put bounds on the Yukawa coupling $\mathcal{Y}_{\ell\ell'}$. I will present those bounds in section 4.3. To find the exact form of the Yukawa coupling, it is necessary to diagonalize the Yukawa term, usually using a biunitary transformation, and keep an eye on the Yukawa term that leads to the neutrino masses too. Finally, the physical coupling is given by a formula [151]

$$\mathcal{Y}_{\ell\ell'}^{\text{HTM}} = \frac{1}{\sqrt{2}v_\Delta}\, V_{PMNS}^*\, \text{diag}\{m_{\nu_e}, m_{\nu_\mu}, m_{\mu_\tau}\}\, V_{PMNS}^\dagger, \tag{3.24}$$

where m_{ν_e}, m_{ν_μ} and m_{μ_τ} denote the neutrino masses.

3.3.2 The Minimal Left-Right Symmetric Model (MLRSM)

The Left-Right Symmetric Model was created in the seventies of the last century by Rabindra Nath Mohapatra, Jogesh Pati, Abdus Salam, and Goran Senjanović [152–154]. That model is based on an extended gauge group with an additional $SU(2)_R$ term in the product, underlined below. The simplest gauge group which implements the left-right symmetry is

$$SU(3)_C \times \underline{SU(2)_R} \times SU(2)_L \times U(1)_{B-L}. \tag{3.25}$$

Another exciting thing in the above equation is that the $U(1)$ group generator is interpreted as a subtraction of the baryon and lepton numbers ($Y = B - L$) [155].

As mentioned earlier, the seesaw type-I mechanism is realized in this model. That means that the model predicts the existence of right-handed neutrino fields, which transform under the $SU(2)_R$ group with the right-handed charged lepton fields. So in the Left-Right Symmetric model, both leptons and quarks form doublets. I follow the notation of [156]

$$L_{iL}=\begin{pmatrix} \nu'_i \\ l'_i \end{pmatrix}_L , \; Q_{iL}=\begin{pmatrix} u'_i \\ d'_i \end{pmatrix}_L , \tag{3.26}$$

$$L_{iR}=\begin{pmatrix} \nu'_i \\ l'_i \end{pmatrix}_R , \; Q_{iR}=\begin{pmatrix} u'_i \\ d'_i \end{pmatrix}_R . \tag{3.27}$$

Since left- and right-handed fermions undergo the transformation under $SU(2)_{L,R}$ groups, it is needed to introduce another gauge coupling, so there are two independent $SU(2)$ couplings, g_L and g_R

$$\begin{aligned} \psi_L &\rightarrow \left[e^{-i\, g' \frac{Y}{2}\, \Theta(x)\, -i\, g_L \frac{1}{2}\, \vec{\sigma}\, \cdot\, \vec{\Theta}(x)}\right]\psi_L, \\ \psi_R &\rightarrow \left[e^{-i\, g' \frac{Y}{2}\, \Theta(x)\, -i\, g_R \frac{1}{2}\, \vec{\sigma}\, \cdot\, \vec{\Theta}(x)}\right]\psi_R. \end{aligned} \tag{3.28}$$

In this thesis, I will consider the so-called *"manifest"* version of the Left-Right Symmetric Model, where the explicit P symmetry is assumed. That implicates equal gauge

coupling $g_L = g_R$, as well as the hermitian Yukawa coupling matrices [3]. So I will use the "MLRSM" abbreviation since I mean that particular version of the model.

Returning to Eq. (3.28), since the gauge transformation is more complex, also the covariant derivatives need to contain extra gauge fields

$$\begin{aligned} D_\mu \psi_L &= \left(\partial_\mu - ig' \tfrac{Y}{2} B_\mu - ig_L \tfrac{\vec{\sigma}}{2} \overrightarrow{W}_{L\mu}\right) \psi_L \ , \\ D_\mu \psi_R &= \left(\partial_\mu - ig' \tfrac{Y}{2} B_\mu - ig_R \tfrac{\vec{\sigma}}{2} \overrightarrow{W}_{R\mu}\right) \psi_R \ . \end{aligned} \tag{3.29}$$

So the model has seven gauge fields that will create seven gauge particles after the spontaneous symmetry breaking. Those known from the SM (γ, $Z_1 = Z$, $W_1^\pm = W^\pm$), and three additional: Z_2, $W_2^\pm$

$$\overrightarrow{W}_{L\mu},\ \overrightarrow{W}_{R\mu},\ B_\mu \xrightarrow[[\boldsymbol{SSB}]]{} W_1^\pm,\ W_2^\pm,\ Z_1,\ Z_2,\ \gamma.$$

But to break that $SU(3)_C \times SU(2)_L \times SU(2)_R \times U(1)_{B-L}$ symmetry, also the scalar sector needs to be extended. Historically, two scalar doublets and one bidoublet were used. Later two triplets instead of doublets were introduced since that model connects the small neutrino masses with a large scale of the right-handed symmetry breaking. In this thesis, I am also using this version of MLRSM

$$\phi = \begin{pmatrix} \phi_1^0 & \phi_1^+ \\ \phi_2^- & \phi_2^0 \end{pmatrix}, \quad \Delta_{L,R} = \begin{pmatrix} \delta_{L,R}^+/\sqrt{2} & \delta_{L,R}^{++} \\ \delta_{L,R}^0 & -\delta_{L,R}^+/\sqrt{2} \end{pmatrix}. \tag{3.30}$$

As in the previous case, the scalar potential, kinetic term, and Yukawa part of the Lagrangian are needed. The most general scalar part is, of course, more complicated. Here it is

$$
\begin{aligned}
V=&-\mu_1^2\left(Tr[\phi^\dagger\phi]\right)-\mu_2^2\left(Tr[\tilde{\phi}\phi^\dagger]+Tr[\tilde{\phi}^\dagger\phi]\right)-\mu_3^2\left(Tr[\Delta_L\Delta_L^\dagger]+Tr[\Delta_R\Delta_R^\dagger]\right)\\
&+\lambda_1\left(\left(Tr[\phi\phi^\dagger]\right)^2\right)+\lambda_2\left(\left(Tr[\tilde{\phi}\phi^\dagger]\right)^2+\left(Tr[\tilde{\phi}^\dagger\phi]\right)^2\right)+\lambda_3\left(Tr[\tilde{\phi}\phi^\dagger]Tr[\tilde{\phi}^\dagger\phi]\right)\\
&+\lambda_4\left(Tr[\phi\phi^\dagger]\left(Tr[\tilde{\phi}\phi^\dagger]+Tr[\tilde{\phi}^\dagger\phi]\right)\right)+\rho_1\left(\left(Tr[\Delta_L\Delta_L^\dagger]\right)^2+\left(Tr[\Delta_R\Delta_R^\dagger]\right)^2\right)\\
&+\rho_2\left(Tr[\Delta_L\Delta_L]Tr[\Delta_L^\dagger\Delta_L^\dagger]+Tr[\Delta_R\Delta_R]Tr[\Delta_R^\dagger\Delta_R^\dagger]\right)+\rho_3Tr[\Delta_L\Delta_L^\dagger]Tr[\Delta_R\Delta_R^\dagger]\\
&+\rho_4\left(Tr[\Delta_L\Delta_L]Tr[\Delta_R^\dagger\Delta_R^\dagger]+Tr[\Delta_L^\dagger\Delta_L^\dagger]Tr[\Delta_R\Delta_R]\right)\\
&+\alpha_1\left(Tr[\phi\phi^\dagger]\left(Tr[\Delta_L\Delta_L^\dagger]+Tr[\Delta_R\Delta_R^\dagger]\right)\right)\\
&+\alpha_2\left(Tr[\phi\tilde{\phi}^\dagger]Tr[\Delta_R\Delta_R^\dagger]+Tr[\phi^\dagger\tilde{\phi}]Tr[\Delta_L\Delta_L^\dagger]\right)\\
&+\alpha_2^*\left(Tr[\phi^\dagger\tilde{\phi}]Tr[\Delta_R\Delta_R^\dagger]+Tr[\tilde{\phi}^\dagger\phi]Tr[\Delta_L\Delta_L^\dagger]\right)\\
&+\alpha_3\left(Tr[\phi\phi^\dagger\Delta_L\Delta_L^\dagger]+Tr[\phi^\dagger\phi\Delta_R\Delta_R^\dagger]\right)\\
&+\beta_1\left(Tr[\phi\Delta_R\phi^\dagger\Delta_L^\dagger]+Tr[\phi^\dagger\Delta_L\phi\Delta_R^\dagger]\right)+\beta_2\left(Tr[\tilde{\phi}\Delta_R\phi^\dagger\Delta_L^\dagger]+Tr[\tilde{\phi}^\dagger\Delta_L\phi\Delta_R^\dagger]\right)\\
&+\beta_3\left(Tr[\phi\Delta_R\tilde{\phi}^\dagger\Delta_L^\dagger]+Tr[\phi^\dagger\Delta_L\tilde{\phi}\Delta_R^\dagger]\right).
\end{aligned}
\tag{3.31}
$$

The potential parameters μ_i, λ_i, ρ_1, and α_i will be used to express the scalars' masses. To avoid the fine-tuning problem, parameters β_i will be set to zero [157]. For one bidoublet and two triplets the scalar sector has four VEVs.

$$
<\phi>=\begin{pmatrix}\kappa_1/\sqrt{2} & 0\\ 0 & \kappa_2/\sqrt{2}\end{pmatrix},\quad <\Delta_{L,R}>=\begin{pmatrix}0 & 0\\ v_{L,R}/\sqrt{2} & 0\end{pmatrix}. \tag{3.32}
$$

To avoid the fine-tuning in the light neutrino mass spectrum [158] and to keep the ρ parameter (see section 3.2) close to one at the three level, the left-handed triplet VEV v_L has to be small, in particular I consider a model with $v_L = 0$. For convenience, I introduce the notation

$$
\kappa_+ = \sqrt{\kappa_1^2+\kappa_2^2}\quad ,\qquad \kappa_- = \sqrt{\kappa_1^2-\kappa_2^2}. \tag{3.33}
$$

The bidoublet VEVs $\kappa_{1,2}$ are in the range of the electroweak symmetry scale. I follow the convention where $\kappa_1 \gg \kappa_2$, $\kappa_1 \simeq 246$ GeV and $\kappa_2 \to 0$, which makes $W_L - W_R$ mixing between light and heavy charged gauge bosons very small. The triplet VEV v_R

has to reach at least a few TeV range to meet the experimental criteria for non-standard neutrinos, scalar, and gauge bosons masses. I will discuss those limits in section 4.2
As the potential should be invariant under the parity transformation, the potential parameters are real, except α_2, but this parameter should not be complex to avoid the explicit CP symmetry breaking [156]. From the scalar sector, ten physical fields are obtained, two doubly charged scalars, two singly charged scalars, four neutral (the SM-like Higgs particle will be denoted as H_0^0), and two pseudoscalars

$$H_1^{\pm\pm}\ ,\ H_2^{\pm\pm}\ ,\ H_1^{\pm}\ ,\ H_2^{\pm}\ ,\ H_0^0\ ,\ H_1^0\ ,\ H_2^0\ ,\ H_3^0\ ,\ A_1^0\ ,\ A_2^0.$$

The physical fields are connected with the doublet and triplet fields. The more detailed discussion is presented in [156], but for $\kappa_+ \ll v_R$ the following approximations are valid:

$$\begin{aligned}
H_1^{\pm\pm} &= \delta_L^{\pm\pm},\\
H_2^{\pm\pm} &= \delta_R^{\pm\pm},\\
H_1^{\pm} &= \delta_L^{\pm},\\
H_2^{\pm} &= \frac{\kappa_-^2}{\kappa_+^2\sqrt{1+\left(\frac{\kappa_-^2}{\sqrt{2}\kappa_+ v_R}\right)^2}}\left(\frac{\kappa_1}{\kappa_+}\phi_1^+ - \frac{\kappa_2}{\kappa_+}\phi_2^+\right),\\
H_0^0 &= \sqrt{2}/\kappa_+ \mathrm{Re}\left(\kappa_1\phi_1^0 - \kappa_2(\phi_2^0)^*\right),\\
H_1^0 &= \sqrt{2}/\kappa_+ \mathrm{Re}\left(\kappa_1(\phi_2^0)^* - \kappa_2\phi_1^0\right),\\
H_2^0 &= \sqrt{2}\ \delta_R^0,\\
H_3^0 &= \sqrt{2}\ \mathrm{Re}(\delta_L^0),\\
A_1^0 &= \sqrt{2}/\kappa_+ \mathrm{Im}\left(\kappa_1(\phi_2^0)^* - \kappa_2\phi_1^0\right),\\
A_2^0 &= \sqrt{2}\ \mathrm{Im}(\delta_L^0).
\end{aligned} \tag{3.34}$$

The formulas for scalar boson masses will be presented in section 4.2, where I discuss the experimental bounds on those masses.

As in the case of `HTM`, the Yukawa part of the Lagrangian creates the masses of neutrinos. However, within `MLRSM` the right-handed neutrino fields are introduced, so as distinct from `SM` and `HTM`, right-handed leptonic fields do not form singlets but

become a part of doublets under the $SU(2)_R$ group. The same is true for the right-handed quark fields (Eqs. (3.26) and (3.27)) thus

$$\mathcal{L}_Y = -\left\{\bar{L}_L\left[h_l\phi + \tilde{h}_l\tilde{\phi}\right]L_R + h.c.\right\} - \bar{L}_R^c i\sigma_2\Delta_L h_M L_L - \bar{L}_R^c i\sigma_2\Delta_R h_M L_L + h.c. \quad (3.35)$$

where $\tilde{\phi} = \sigma_2\ \phi^*\sigma_2$, $\tilde{h}_l = \sigma_2\ h_l^*\sigma_2$. $L_{R,L}^c$ denotes $C\bar{L}_{R,L}^T$, where C is the same charge conjugate operator as in Eq. (3.22). h_M is a complex symmetric matrix ($h_M = h_M^T$). The above Lagrangian contains the mass term for charged leptons, as well as the neutrino mass term, which can be written in the following form

$$\mathcal{L}_{\text{mass}}^{\nu} = -\frac{1}{2}\left(\bar{n}_L'^{\,c} M_\nu n_R' + \bar{n}_R'^{\,c} M_\nu n_L'\right) \quad (3.36)$$

where for convenience left- and right-handed neutrino fields are combined

$$n_R' = \begin{pmatrix} \nu_R'^{\,c} \\ \nu_R' \end{pmatrix}, \quad n_L' = \begin{pmatrix} \nu_L'^{c} \\ \nu_L'^{\,c} \end{pmatrix}. \quad (3.37)$$

M_ν denotes the famous seesaw neutrino matrix presented below. The element M_D is proportional to the electroweak symmetry breaking scale whereas M_R depends on the right-handed triplet VEV v_R

$$M_\nu = \begin{pmatrix} 0 & M_D \\ M_D^T & M_R \end{pmatrix}\ ,\ M_D = \frac{1}{\sqrt{2}}\left(h_l\kappa_1 + \tilde{h}_l\kappa_2\right)\ ,\ M_R = \sqrt{2}h_M v_R. \quad (3.38)$$

To calculate masses of physical states, the M_ν matrix needs to be diagonalized

$$(M_\nu)_{\text{diag}} = U^T M_\nu\, U \quad (3.39)$$

where U is a unitary 6×6 matrix [159]. The common solution is to choose the seesaw mixing matrix: $|U_{\nu_i j}| \simeq \frac{|<M_D>|}{M_R}\delta_{i,j-3}$. Masses of non-standard heavy neutrinos are proportional to M_R when masses of SM neutrinos are proportional to $\frac{M_D^2}{M_R}$. For the GUT symmetry breaking scale much higher than the electroweak one ($v_R \gg \kappa_+$), those relations explain the smallness of neutrino masses. I will denote the light SM-like neutrinos by ν_i, the heavy neutrinos by N_j, and their masses by M_{ν_i} and M_{Nj} respectively, where

$i = e, \mu, \tau,\ j = 1, 2, 3.$

As in the case of HTM, the Yukawa Lagrangian in Eq. (3.35) characterizes particles interactions including the lepton number violating vertices $H^{\pm\pm}_{1,2} - l^{\mp}_i - l^{\mp}_j$. The couplings depend on the general shape of the unitary matrix U. The matrix can be written in the form: $U = \begin{pmatrix} K^*_L \\ K_R \end{pmatrix}$. I am choosing the case when the off-diagonal elements of the K_L and K_R vanished: $H^{\pm\pm}_{1,2} - l^{\mp}_i - l^{\mp}_j \sim \delta_{ij}$. More about that choice and the detailed discussion of why it is justified can be found in [135]. I will shortly sum up that the off-diagonal elements are of the range of inverted triplet VEV, where the vertices can be expressed in the following way

$$H^{\pm\pm} - l_i - l_i = \frac{\sqrt{2}}{v_R} M_{N_i}. \tag{3.40}$$

The structure of the couplings within HTM in Eq. (3.24) and MLRSM in Eq. (3.40) will be crucial for the studies presented in the thesis. $H^{\pm\pm} - l_i - l_i$ vertex is vital for calculating scalar decay branching ratios and possible detection signals. It will bring essential bounds on models' parameters since it contributes to lepton flavor and number-violating processes.

4 Phenomenology of particle physics with doubly charged Higgs bosons

The doubly charged scalar particles have been in the physicists' circle of interest for years. Direct searches of those particles were performed, among others, at LEP, Tevatron, and LHC. For recent LHC searches for these particles, see [160]. More references will follow in the next sections. The doubly charged scalars' decay modes can be different depending on the model, which, in the case of an observation of this kind of particle, can enable us to distinguish between extensions of the Standard Model and, potentially, reject a part of theoretical solutions. The distinction between the models is one of the main threads of this thesis.

Starting with a model-independent analysis, the doubly charged scalar particles' decay channels can be split into three categories. In the first category, I put decays to other non-standard particles like, in the case of `HTM` and `MLRSM`, a pair of singly charged scalars ($H^{\pm}_{(1,2)}H^{\pm}_{(1,2)}$) or charged scalar and charged gauge bosons (`SM`-like or beyond the `SM`: $H^{\pm}_{(1,2)}W^{\pm}_{1}$, $H^{\pm}_{1,2}W^{\pm}_{2}$), or a pair of same-sign charged gauge bosons $W^{\pm}_{i}W^{\pm}_{j}$, $i,j = 1,2$. Two other cases are decays into Standard Model particles: pair of gauge bosons ($W^{\pm}W^{\pm}$) or leptons ($l^{\pm}_{i}l^{\pm}_{j}$). Those last two decay channels were mainly studied, and there is no evidence of doubly charged scalars. However, experimental limits and bounds on the non-standard scalar masses and couplings are set. The decay into a pair of same-sign leptons is often considered the most promising channel to discover the doubly charged scalar since the same-sign dilepton signal can be directly seen in the detector. The kinematics of such a decay differs from the SM background as dileptons originate from the same particle. This channel is also interesting since, depending on the model, analysis of that decay potentially brings information about the neutrino mixing matrix, see Eq. (3.24) and [161]. Searches for doubly charged scalars through decay to a pair of same-sign leptons have been performed, among others, at LEP [162, 163], Tevatron [164–167] and LHC. In section 4.4, I will shortly sum up the bounds from high energy experiments.

In this thesis, I am concentrating on leptonic final state signals. Phenomenological analysis of diboson signals at high-energy colliders can be found in [168–170]. See also my collaborative work [171].

4.1 Doubly charged scalar mass spectrum within HTM

The range of charged scalar masses is crucial to study their production at colliders. Theoretical and experimental constraints on their masses are discussed in sections 3.2, 4.3 and 4.4. Masses of scalar particles in HTM depend on the scalar potential parameters and the triplet VEVs in Eq. (3.17) (assuming that the ratio $2\frac{v_\Delta}{v_\Phi} \to 0$ [144])

$$M_A^2 = \frac{\mu}{\sqrt{2}v_\Delta}(v_\Phi^2 + 4v_\Delta^2), \tag{4.1}$$

$$\begin{aligned} M_h^2 &= \lambda v_\Phi^2 \cos^2\alpha + \left(\frac{\mu v_\Phi^2}{\sqrt{2}v_\Delta} + 2v_\Delta^2(\lambda_2+\lambda_3)\right)\sin^2\alpha \\ &\quad + 2\left(v_\Phi v_\Delta(\lambda_1+\lambda_4) - \sqrt{2}\mu v_\Phi\right)\cos\alpha\sin\alpha, \end{aligned} \tag{4.2}$$

$$\begin{aligned} M_{H^0}^2 &= \lambda v_\Phi^2 \sin^2\alpha + \left(\frac{\mu v_\Phi^2}{\sqrt{2}v_\Delta} + 2v_\Delta^2(\lambda_2+\lambda_3)\right)\cos^2\alpha \\ &\quad - 2\left(v_\Phi v_\Delta(\lambda_1+\lambda_4) - \sqrt{2}\mu v_\Phi\right)\cos\alpha\sin\alpha, \end{aligned} \tag{4.3}$$

$$M_{H^\pm}^2 = \frac{(2\sqrt{2}\mu - \lambda_4 v_\Delta)}{4v_\Delta}(v_\Phi^2 + 2v_\Delta^2), \tag{4.4}$$

$$M_{H^{\pm\pm}}^2 = \frac{\mu v_\Phi^2}{\sqrt{2}v_\Delta} - \frac{\lambda_4}{2}v_\Phi^2 - \lambda_3 v_\Delta^2\,. \tag{4.5}$$

First, I discuss the potential stability and unitarity, as well as the ρ and T parameters within HTM. This subject was covered, for example, in [172], [173] and [174], here I will present the most important conclusions.

As discussed already in section 3.2 the S, T and U (Peskin–Takeuchi) parameters can be used to parameterize the new physics contributions to electroweak radiative corrections [129, 175], so-called oblique corrections. Among them, the T-parameter is considered the most significant in comparison to the other oblique parameters (although

for the models with the custodial symmetry it might not be true [176]), because of its quadratic, instead of logarithmic, dependence on the masses of new particles. The T-parameter is connected with the ρ-parameter by the relation $\Delta\rho = \alpha T$ [129], where α is the fine-structure constant. The ρ-parameter is also bounded directly by the triplet VEV, see Eq. (3.13) and [177].

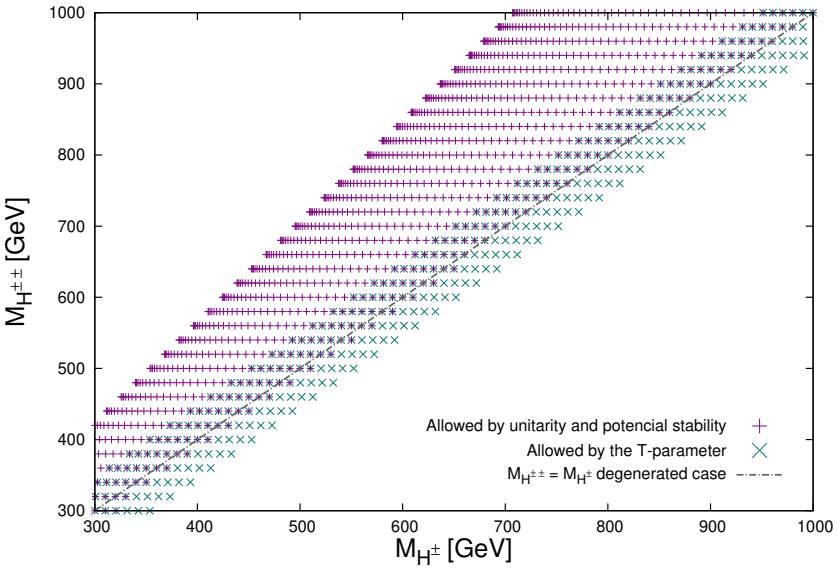

Figure 13: Parameter space for singly and doubly charged scalars, allowed by the `HTM` scalar potential's unitarity, stability, and T-parameter. Triplet VEV is small, $v_\Delta \simeq 10$ eV, see next sections and [174].

The accurate formulas for potential stability, unitarity, and the T-parameter within the `HTM` are presented in Appendix A.5. In Fig. 13 I am presenting the allowed mass region for $M_{H^{\pm\pm}}$ and $M_{H^\pm}$. From that plot, it is justified to choose degenerate masses $M_{H^{\pm\pm}}$=$M_{H^\pm}$. Another important conclusion from the plot is that the mass gap between the doubly and singly charged scalars is less than the mass of the boson W. This will suppress decay channel $H^{\pm\pm} \to H^\pm W^\pm$. It is also consistent with the electroweak precision data from the $H^0 \to \gamma\gamma$ decay, which gives the mass gap between the singly and charged scalar masses $|M_{H^{\pm\pm}} - M_{H^\pm}|$ less than 40 GeV [172, 178, 179]. A similar analysis for the possible difference between the charged and heavy neutral scalar par-

ticles is presented in [144], with the conclusion that within the mass range below 1000 GeV, the mass gap $|M_{H^\pm} - M_H|$ equal to zero fulfil the potential stability, unitarity and T-parameter bounds. So finally, it is natural to assume that the scalar sector is degenerated (excluding the SM-like scalar): $M_{H^{\pm\pm}} = M_{H^\pm} = M_H = M_A$.

I am interested in the scalar particle masses around a few hundred GeV, but to discuss the possible mass range, it is necessary to analyze the decay channels. Those studies are presented in section 4.5.

4.2 Doubly charged mass spectrum within `MLRSM`

tThe subject of the `MLRSM` mass spectrum was covered in [180]. Comparing to `HTM` the situation is different. Here the most relevant scale is connected with the $SU(2)_R$ triplet vacuum expectation value which necessarily needs to be high, at the range of at least several TeV, to explain the fact, that heavy gauge bosons and heavy neutrinos are not visible in the experiments. The leading terms of the ρ-parameter in Eq. (3.3) connected with the scale v_R of the heavy sector of the theory can be found in [132,133]. Below I am presenting the formulas for the scalar sector particles' masses as functions of the scalar potential parameters in Eq. (3.31), and v_R

$$M^2_{H^0_1} = \frac{1}{2}\alpha_3 v_R^2 \qquad > (10\text{ TeV})^2, \tag{4.6}$$

$$M^2_{H^0_2} = 2\rho_1 v_R^2, \tag{4.7}$$

$$M^2_{H^0_3} = \frac{1}{2}(\rho_3 - 2\rho_1)v_R^2 \qquad > (55.4\text{ GeV})^2, \tag{4.8}$$

$$M^2_{A^0_1} = \frac{1}{2}\alpha_3 v_R^2 - 2(\kappa_1^2+\kappa_2^2)(2\lambda_2-\lambda_3) \qquad > (10\text{ TeV})^2, \tag{4.9}$$

$$M^2_{A^0_2} = \frac{1}{2}(\rho_3 - 2\rho_1)v_R^2 \qquad > (55.4\text{ GeV})^2, \tag{4.10}$$

$$M^2_{H^\pm_1} = \frac{1}{2}(\rho_3 - 2\rho_1)v_R^2 + \frac{1}{4}\alpha_3(\kappa_1^2+\kappa_2^2), \tag{4.11}$$

$$M^2_{H^\pm_2} = \frac{1}{2}\alpha_3 v_R^2 + \frac{1}{4}\alpha_3(\kappa_1^2+\kappa_2^2) \qquad > (10\text{ TeV})^2, \tag{4.12}$$

$$M^2_{H^{\pm\pm}_1} = \frac{1}{2}(\rho_3 - 2\rho_1)v_R^2 + \frac{1}{2}\alpha_3(\kappa_1^2+\kappa_2^2), \tag{4.13}$$

$$M^2_{H^{\pm\pm}_2} = 2\rho_2 v_R^2 + \frac{1}{2}\alpha_3(\kappa_1^2+\kappa_2^2), \tag{4.14}$$

and, for SM-like Higgs I am applying the following conditions

$$M^2_{H^0_0} \simeq 2\kappa_+^2\lambda_1, \tag{4.15}$$

$$124.7\text{ GeV} < M_{H^0_0} < 126.2\text{ GeV}. \tag{4.16}$$

I have already added some experimental limits to the above equations. Limits on $M^2_{H^0_3}$ (4.8) and $M^2_{A^0_2}$ (4.10) come from LEP studies on the $e^+e^- \to \gamma + \not{E}_T$ [181]. But more severe limits are introduced to suppress Flavour Changing Neutral Currents (FCNC). The Yukawa Lagrangian, apart from the lepton part of Eq. (3.35), contains the term responsible for quarks' masses $\mathcal{L}_Y = Y_u\bar{Q}_{iL}\phi Q_{iR} + Y_d\bar{Q}_{iRL}\tilde{\phi}Q_{iR} + h.c.$ This term brings interactions between the neutral scalar fields and quarks, including changing quarks' flavour. However, only H^0_1 and A^0_1 particles can contribute to this process, bringing the lowest limit on their masses at the range of 10-15 TeV [182]. The Feynman diagram of an exemplary process is presented in Fig. 14.

Even though this limit is applied only to neutral particles, it will influence the mass bound on the singly charged scalar $H^\pm_2$ since the mass of this particle is expressed as

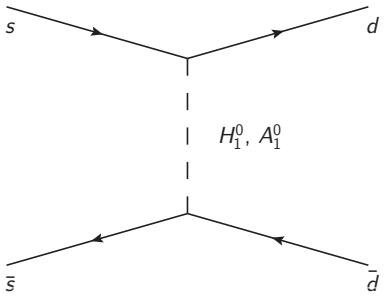

Figure 14: An exemplary diagram for the FCNC process.

a function of the same parameters as for $M_{H_1^0}$ (compare (4.6) and (4.12), keeping in mind that α_3 and both κ_1 and κ_2 are not negative parameters). But it is still possible to choose the parameter space, where the doubly charged scalar particles' masses are relatively low, in the range of a few hundreds GeV. The detailed discussion with an exemplary parameter set can be found in [180].

In the case of the `MLRSM` I will consider a non-degenerated case with low masses of doubly charged scalars and possible very high masses of neutral and singly charged scalars. That will suppress some decay channels too. I will discuss this subject in the next section. The potential unitarity and stability conditions are presented in Appendix A.5. The `MLRSM` potential has a lot of free parameters, so it is possible to provide potential stability and unitarity for a wide range of scalar particles' masses, including non-degenerated cases.

An example set of generated mass spectra of Higgs bosons for $v_R = 8$ TeV is presented in Fig. 15 (left figure). Mass spectra have been obtained by varying uniformly the Higgs potential parameters in the range (-10,10). We have also taken into account the bounds on neutral Higgs bosons obtained from FCNC constraints assuming $m_{A_1^0}, m_{H_1^0} > 15$ TeV by fixing $\alpha_3 = 7.1$. The spectra which did not fulfill relation (4.6)

were rejected. Altogether we have 6 neutral, 2 singly charged and 2 doubly charged Higgs boson particles in the MLRSM. The figure includes possible spectra of singly and doubly charged as well as neutral Higgs bosons. Some of them can be degenerated or nearly degenerated.

Although the Higgs particles naturally tend to have masses of the order of the v_R scale, it is still possible to choose the potential parameters such that some of the scalar particles can have masses much below 1 TeV. We aim at such spectrum which can be tested at LHC and future colliders. The cumulative distribution function P of the lowest masses of singly and doubly charged and next to lightest neutral scalar particles are plotted on right of Fig. 15. These results show that for $v_R = 8$ TeV a fraction of the parameter space that gives lightest scalar masses below 1 TeV is at the level of several percent. It means that it is possible to generate the low mass spectra of Higgs boson masses in MLRSM keeping large v_R scale.

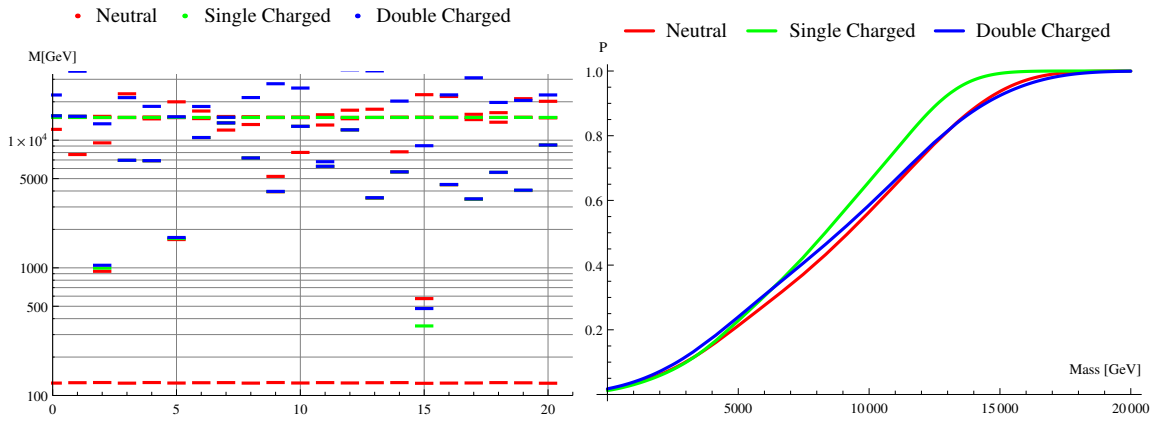

Figure 15: On left an example of 20 Higgs mass spectra obtained by randomly chosen Higgs potential parameters in Eq. (3.31). The constrain on the lowest SM-like neutral Higgs mass Eq. (4.16) was imposed and the bounds coming from FCNC were taken into account. On right cumulative distribution function P of the lowest mass of singly and doubly charged and next to lightest neutral scalars. For both figures, $v_R = 8$ TeV. Figures taken from [180].

In [180] we have analyzed what can be the lowest masses of $H^{\pm\pm}$ scalars based on the potential analysis and experimental data. Due to the freedom in the parameter space of the full scalar potential, there is no lowest limit on the mass of $H_2^{\pm\pm}$. On the other hand, taking into account experimental limits one can obtain the following bound on $M_{H_1^{\pm\pm}}$

$$\sqrt{\min(M_{H_3^0}^2) + M_{H_1^0}^2 \kappa_1^2 / v_R^2} \approx \frac{2.41 \text{ TeV}^2}{v_R}. \tag{4.17}$$

In the above relation neutral scalars are related to $H^{\pm\pm}$ as the same coefficients in mass relations (4.6)-(4.14) are involved. The lowest limit depends of course on v_R, e.g. for $v_R = 8$ TeV, the lowest mass of $H_1^{\pm\pm}$ is 465 GeV.

HTM	$\mu = 1.7 \times 10^{-7}, \quad \lambda = 0.519, \quad \lambda_1 = 0.519, \quad \lambda_2 = 0, \quad \lambda_3 = -1, \quad \lambda_4 = 0.$ $M_h = 125.3 \text{ GeV}, \quad M_H = 700 \text{ GeV}, \quad M_{H^\pm} = 700 \text{ GeV}, \quad M_{H^{\pm\pm}} = 700 \text{ GeV}.$
MLRSM	$\lambda_1 = 0.129, \ \rho_1 = 0.0037, \ \rho_2 = 0.0037, \ \rho_3 - 2\rho_1 = 0.015, \ \alpha_3 = 4.0816, \ 2\lambda_2 - \lambda_3 = 0.$ $M_{H_0^0} = 125.3 \text{ GeV}, \quad M_{H_1^0} = 10 \text{ TeV}, \quad M_{H_2^0} = 600 \text{ GeV}, \quad M_{H_3^0} = 605.4 \text{ GeV},$ $M_{H_1^{\pm\pm}} = 700 \text{ GeV}, \quad M_{H_2^{\pm\pm}} = 700 \text{ GeV}, \quad M_{H_1^\pm} = 654.4 \text{ GeV}, \quad M_{H_2^\pm} = 10\,003.1 \text{ GeV}.$

Table 5: Benchmark points and corresponding potential parameters for HTM and LRSM with $M_{H^{\pm\pm}} = M_{H_{1,2}^{\pm\pm}} = 700$ GeV. The scalar potential parameters, fields and relations for masses are defined in Eqs. (3.17), (3.19a) - (3.19d) and (4.1) - (4.5) for HTM and Eqs. (3.31), (3.34) and (4.6) - (4.14) for MLRSM. I identify h and H_0^0 as the SM Higgs boson (H^0).

The mass benchmark points are constructed in order to satisfy several theoretical conditions like potential stability, unitarity and the T-parameter restriction and

bounds from $H^0 \to \gamma\gamma$ [144, 149, 172, 174, 178, 179], see also section 4.1.

Finally, in Tab. 5 possible benchmarks for two considered models are given. Obviously, there are more scalar fields in `MLRSM` than in `HTM`. Then any detectable signal connected with a neutral, singly or doubly charged Higgs bosons which are present in `MLRSM` but are not present in `HTM` would be in favour of `MLRSM`. However, none of these extra particles has been identified/discovered so far and what we get so far are exclusion limits on the parameters of this model. There is no indication for neutral, singly or doubly charged scalars, extra neutral heavy leptons, extra gauge bosons. So we do not know if and which BSM model is realized in nature and we are still looking for a first experimental indication towards any non-standard signals in one or another model. As the models' parameters are already severely constrained, we have to consider very rare processes and hence faint signals.

We will compare $H^{\pm\pm}$ signals from two models in the next sections as the doubly charged Higgs bosons $H^{\pm\pm}_{1,2}$ would undoubtedly be clear messengers of the new physics.

4.3 Low energy $H^{\pm\pm}$ physics with lepton number and lepton flavour violation

Low energy physics makes it possible to study the charged Higgs bosons and their parameters as charged scalars can intermediate in low energy processes, breaking lepton flavour numbers. Those processes will be particularly interesting in the case of `HTM`, as within `MLRSM`, I assume that the off-diagonal vertex between the doubly charged scalars and different flavour leptons are negligible, see Eq. (3.40). In the context of `HTM`, those processes have been discussed, for example, in [151, 161, 183–188].

Examples of the LFV processes and corresponding diagrams are presented in Fig. 16. Among them I mention: radiative decay $l_i \to l_j\gamma$ — diagrams (a) and (b), μ to e conversion in the presence of atomic nuclei — diagrams (c) and (d), three body decay $l_i \to l_j l_k l_m$ — diagram (e), and muonium-antimuonium conversion — diagram (f). The

singly and doubly charged scalars can contribute to the muon $(g-2)_\mu$ parameter, too (see, for example, [189]). Feynman diagrams for this process are presented in Fig. 17. In Tables 6 and 8 the present and predicted future limits on LFV processes are presented. Amplitudes for those processes are discussed in [135].

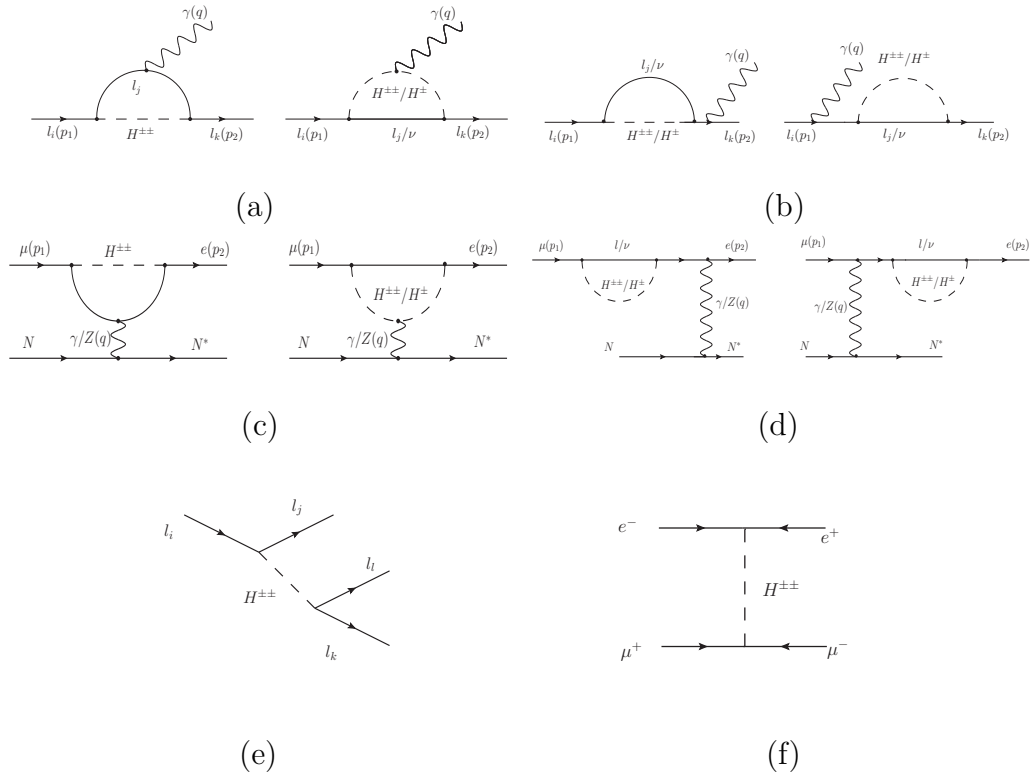

Figure 16: Feynman diagrams representing the contributions to various lepton flavour violating processes mediated by charged scalars in `HTM`. (a) and (b) are representing the radiative decay $l_i \to l_j\gamma$, (c) and (d) corresponds to the μ to e conversion. Three body lepton decay of a lepton is represented by diagram (e), finally diagram (f) represents the muonium-antimuonium conversion.

Another specific case of LFV processes which appears especially important for testing the HTM model are neutrino oscillations data. The $H^{\pm\pm}$ decay within `MLRSM` is not sensitive to the neutrino oscillation parameters. There is a strict relation between

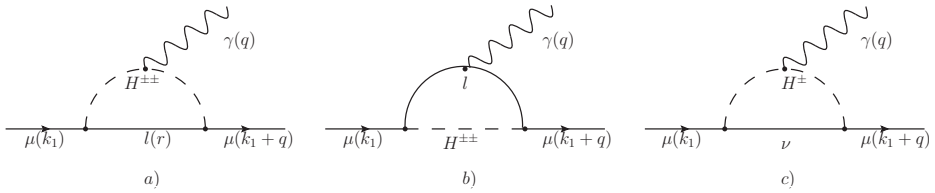

Figure 17: Feynman vertex diagrams representing $(g-2)_\mu$ within HTM.

	Process	Present limits	
LFV processes	BR($\mu \to e\gamma$)	4.2×10^{-13}	[190]
	BR($\tau \to e\gamma$)	3.3×10^{-8}	[191]
	BR($\tau \to \mu\gamma$)	4.4×10^{-8}	[191]
	BR($\mu \to eee$)	1.0×10^{-12}	[192]
	BR($\tau \to eee$)	2.7×10^{-8}	[193]
	BR($\tau \to \mu\mu\mu$)	2.1×10^{-8}	[193]
	BR($\tau^- \to \mu^+e^-\mu^-$)	2.7×10^{-8}	[193]
	BR($\tau^- \to \mu^+e^-e^-$)	1.5×10^{-8}	[193]
	BR($\tau^- \to e^+\mu^-\mu^-$)	1.7×10^{-8}	[193]
	BR($\tau^- \to e^+e^-\mu^-$)	1.8×10^{-8}	[193]
	R($\mu N \to eN^*$)	7.0×10^{-13} (for Au)	[194]
	$\mu^+e^- \to \mu^-e^+$	$\sqrt{\mathcal{Y}_{ee}\cdot\mathcal{Y}_{\mu\mu}} < \frac{0.44}{10^3\,\mathrm{GeV}}\cdot M_{H^{\pm\pm}}$	[195]

Table 6: Limits on the processes with doubly charged scalar contributions, LFV processes (90% CL).

neutrino parameters and the Yukawa coupling $\mathcal{Y}_{\ell\ell'}$ which enters discussed in the thesis collider processes, see Eq. (3.24).

The HTM model is thus sensitive to the neutrino oscillation data, as discussed already in [161] and [144, 196, 197]. It means that also such details as neutrinos hierarchy and the lightest neutrino mass play a role in studies of $H^{\pm\pm}$ signals at lepton colliders. In analysis I use the following standard parametrization of the $V_{\texttt{PMNS}}$ matrix

$$V_{\texttt{PMNS}} = \begin{bmatrix} c_{12}c_{13}e^{i\alpha_1} & s_{12}c_{13}e^{i\alpha_2} & s_{13}e^{-i\delta_{CP}} \\ (-s_{12}c_{23} - c_{12}s_{23}s_{13}e^{i\delta_{CP}})e^{i\alpha_1} & (c_{12}c_{23} - s_{12}s_{23}s_{13}e^{i\delta_{CP}})e^{i\alpha_2} & s_{23}c_{13} \\ (s_{12}s_{23} - c_{12}c_{23}s_{13}e^{i\delta_{CP}})e^{i\alpha_1} & (-c_{12}s_{23} - s_{12}c_{23}s_{13}e^{i\delta_{CP}})e^{i\alpha_2} & c_{23}c_{13} \end{bmatrix}. \tag{4.18}$$

By s_{ij} and c_{ij} I understand $\sin(\theta_{ij})$ and $\cos(\theta_{ij})$. The values of those angles are presented in Table 7. Depending on the hierarchy scenarios defined in (4.19), for atmospheric neutrino oscillations either $\Delta m^2_{3l} = \Delta m^2_{31} > 0$ (NH) or $\Delta m^2_{3l} = \Delta m^2_{32} < 0$ (IH).

Normal mass hierarchy:	Inverted mass hierarchy:	
$m_{\nu_1} = m_{\nu_0}$,	$m_{\nu_1} = \sqrt{m^2_{\nu_0} - \Delta m^2_{21} - \Delta m^2_{32}}$,	(4.19)
$m_{\nu_2} = \sqrt{m^2_{\nu_0} + \Delta m^2_{21}}$,	$m_{\nu_2} = \sqrt{m^2_{\nu_0} - \Delta m^2_{32}}$,	
$m_{\nu_3} = \sqrt{m^2_{\nu_0} + \Delta m^2_{31}}$,	$m_{\nu_3} = m_{\nu_0}$,	

	Normal hierarchy (NH)				Inverted hierarchy (IH)			
	Best fit (bf):	σ	bf$\pm 1\sigma$	bf$\pm 2\sigma$	Best fit (bf):	σ	bf$\pm 1\sigma$	bf$\pm 2\sigma$
$\sin^2\theta_{12}$	0.310	$^{+0.013}_{-0.012}$	0.298 $\div$ 0.323	0.286 $\div$ 0.336	0.310	$^{+0.013}_{-0.012}$	0.298 $\div$ 0.323	0.286 $\div$ 0.336
$\sin^2\theta_{23}$	0.558	$^{+0.020}_{-0.033}$	0.525 $\div$ 0.578	0.492 $\div$ 0.598	0.563	$^{+0.019}_{-0.026}$	0.537 $\div$ 0.582	0.511 $\div$ 0.601
$\sin^2\theta_{13}$	0.02241	$^{+0.00066}_{-0.00065}$	0.02176 $\div$ 0.02307	0.02111 $\div$ 0.02373	0.02261	$^{+0.00067}_{-0.00064}$	0.02197 $\div$ 0.02328	0.02133 $\div$ 0.02395
$\delta_{CP}[^o]$	222	$^{+38}_{-28}$	194 $\div$ 260	166 $\div$ 298	285	$^{+24}_{-26}$	259 $\div$ 309	233 $\div$ 333
$\frac{\Delta m^2_{21}}{10^{-5}\ \mathrm{eV}^2}$	7.39	$^{+0.21}_{-0.20}$	7.19 $\div$ 7.60	6.99 $\div$ 7.81	7.39	$^{+0.21}_{-0.20}$	7.19 $\div$ 7.60	6.99 $\div$ 7.81
$\frac{\Delta m^2_{3l}}{10^{-3}\ \mathrm{eV}^2}$	+2.523	$^{+0.032}_{-0.030}$	2.463 $\div$ 2.527	2.463 $\div$ 2.587	-2.509	$^{+0.032}_{-0.030}$	-2.539 $\div$ -2.477	-2.569 $\div$ -2.445

Table 7: Neutrino oscillation data [198], best fit (bf) and parameter ranges for $bf \pm 1\sigma$ and $bf \pm 2\sigma$. $\Delta m^2_{ij} = m^2_i - m^2_j$, see Eq. (4.19).

4.4 Collider physics limits on $H^{\pm\pm}$

Collider experiments bring bounds on the charged scalars too. The most strict limits come from LHC. The direct mass limits on doubly charged Higgs mass depend on the analyzed decay channel. The ATLAS experiment sets the minimum on the $H^{\pm\pm}$ mass at 870 GeV for the 100 % leptonic decay in the case of a pair of left-handed leptons and 760 GeV for decays into right-handed leptons. By the 'leptonic decay', I

mean here a decay into a pair of muons, electrons, or their combination. Some results regarding the decay into the tau lepton are already published [160], but in this work I am exploring the electron and muon signals. However, the above ATLAS limits can be circumvented by assuming that the doubly charged scalar particles do not decay purely into electrons or muons. For example, if that decay channel drops to 10% branching ratio (BR) those limits decline to around 450 GeV. To reduce that BR, other decay channels have to be enhanced, for example, $H^{\pm\pm}_{(1,2)} \to W^{\pm}W^{\pm}$, or $H^{\pm\pm}_{(1,2)} \to \tau^{\pm}\tau^{\pm}$ or decay into the tau and another charged lepton. Regarding the diboson channel, for 100% BR, the mass bounds are set around 200-220 GeV [199], so considering this decay channel, it is possible to reduce the experimental limits on the doubly charged scalar mass. In this thesis I will follow this direction and, thanks to studying different decay channels, lower mass bounds will be obtained. The detailed discussion can be found in section 4.5. Other scenarios with possible low $H^{\pm\pm}$ mass limits have been considered recently in [76], see also [77].

The high-energy lepton collider physics also brings some limits on the doubly charged scalar particle couplings. Those particles can intermediate in well-known processes like the Bhabha or Møller scattering or the $e^+e^- \to l^+l^-$ process. The doubly charged scalars contribute to the $t-$channel (Feynman diagram is similar to the diagram (f) in Fig. 16). In Tab. 8, some important (lepton conserving) SM processes with the corresponding bounds on the doubly charged scalars' couplings are gathered, which will also be used in sections on the high-energy colliders $H^{\pm\pm}$ analysis.

	Process	Present limits	Refs.
SM processes		$\lvert\mathcal{Y}_{ee}\rvert \leq \frac{\sqrt{4\pi}\, M_{H^{\pm\pm}}}{8.7\times10^3\ \text{GeV}}$	[200]
	$e^+e^- \to l^+l^-$ (LEP)	$\lvert\mathcal{Y}_{e\mu}\rvert \leq \frac{1}{\sqrt{2}} \frac{\sqrt{4\pi}\, M_{H^{\pm\pm}}}{12.2\times10^3\ \text{GeV}}$	[200]
		$\lvert\mathcal{Y}_{e\tau}\rvert \leq \frac{1}{\sqrt{2}} \frac{\sqrt{4\pi}\, M_{H^{\pm\pm}}}{9.1\times10^3\ \text{GeV}}$	[200]
	$e^-e^- \to e^-e^-$ (MØLLER)	$\lvert\mathcal{Y}_{ee}\rvert \leq \frac{M_{H^{\pm\pm}}}{3.7\times10^3\ \text{GeV}}$	[201]

Table 8: Important other than LHC limits on the Standard Model processes with doubly charged scalar contributions (95% CL).

4.5 $H^{\pm\pm}$ decay channels and widths

Let us first study $H^{\pm\pm}$ decays, which depend on particles' mass spectrum. The situation is quite simple in the case of `HTM`. In Table 9, I have collected all possible vertices. The situation is more complicated in the case of `MLRSM`. Theoretically, there are twenty bosonic decay channels, apart from the three leptonic decays. I have presented them in Table 9. Still, most of them can vanish by choosing the parameter space, for example, due to $SU(2)_L$ triple VEV, v_L set to zero (to avoid problems with the ρ and T-parameter constraints) or the experimental limits on the $W_1 - W_2$ mixing angle $\xi < 10^{-2}$ [202,203]. The non-vanishing decay channels are also presented in Table 9.

HTM		MLRSM			
(i)	$H^{\pm\pm} \to l_i\, l_j,$	(v)	$H_1^{\pm} \to l_i\, l_i$	(vii)	$H_2^{\pm\pm} \to l_i\, l_i$
(ii)	$H^{\pm\pm} \to W^{\pm}\, W^{\pm}$	(vi)	$H_1^{\pm\pm} \to H_1^{\pm}\, W_1^{\pm}$	(viii)	$H_2^{\pm\pm} \to W_2^{\pm}\, W_2^{\pm}$
(iii)	$H^{\pm\pm} \to H^{\pm}\, W^{\pm}$			(ix)	$H_2^{\pm\pm} \to H_2^{\pm}\, W_2^{\pm}$
(iv)	$H^{\pm\pm} \to H^{\pm}\, H^{\pm}$			(x)	$H_2^{\pm\pm} \to H_2^{\pm}\, W_2^{\pm}$

Table 9: Non-vanishing vertices for doubly charged scalar particle decays within the `HTM` and `MLRSM` models, $i, j = e, \mu, \tau$.

Some of the decays in Table 9 will be suppressed, too, due to the mass spectrum discussed in sections 4.1 and 4.2. In case of mass degeneration in `HTM` ($H^{\pm\pm} = H^{\pm}$), and due to the large mass of the $H_2^{\pm}$ scalar ($M_{H_2^{\pm}} > 10$ TeV) within `MLRSM`, I will skip the channels (iii), (iv), (ix) and (x). The channel (viii) depends on the heavy gauge boson masses. From [202] and [203], the mass of the non-standard charged gauge boson $M_{W_2} > 700$ GeV, so the channel (viii) will also be kinematically suppressed for low $M_{H_2^{\pm\pm}}$. Choosing the benchmark masses by choosing the particular potential parameters (Tab. 5), the process (vi) is also suppressed. In Table 10, I am presenting the left processes with the vertex dependence.

Within `HTM`, the leptonic vertex is inversely proportional to the triplet VEV v_Δ while the $H^{\pm\pm} \to W^{\pm}W^{\pm}$ vertex is proportional to v_Δ. That dependence is presented in Fig. 18. So to find the dominating decay channel, I first study the appropriate range of v_Δ.

HTM		MLRSM			
(i)	$H^{\pm\pm} \to l_i\, l_j$, $f(\frac{1}{v_\Delta}, V_{\rm PMNS})$	(v)	$H_1^{\pm} \to l_i\, l_i$ $f(\frac{1}{v_R}, M_{N_i})$	(vii)	$H_2^{\pm\pm} \to l_i\, l_i$ $f(\frac{1}{v_R}, M_{N_i})$
(ii)	$H^{\pm\pm} \to W^{\pm}\, W^{\pm}$ $f(v_\Delta)$				

Table 10: Decay modes with the greatest impact for low $H^{\pm\pm}$ mass, $M_{H^{\pm\pm}_{(1,2)}} = 700$ GeV. The f function shows dependence of corresponding vertices on key parameters $v_\Delta, v_R, M_{N_i}, V_{\rm PMNS}$. Indices i, j denote lepton flavours e, μ, τ. The numbering of the processes stays the same as in Table 9.

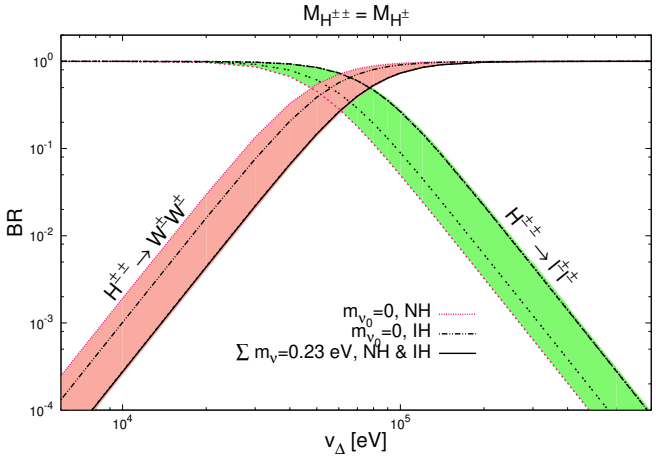

Figure 18: Branching ratios for `HTM` scalar particle $H^{\pm\pm}$ decays, the degenerate case $m_{H^{\pm\pm}} = m_{H^{\pm}} = 700$ GeV. The plot has a band because the neutrino parameters are taken within the $\pm 2\sigma$ range, and neutrino masses are taken from 0 to the maximum value that meets the conservative astrophysics limit $\sum_i m_{\nu_i} < 0.23$ eV [204].

The first limit on the $SU(2)_L$ triplet came from the ρ-parameter and was presented in section 3.2, Eq. (3.13). From that condition, the triplet VEV v_Δ can reach the level of $\mathcal{O}(1)$ GeV. But v_Δ is bounded from below, too, by the LFV processes, as well as the $(g-2)_\mu$ and high energy data (see Tables 6 and 8). All those constraints provide

bounds on the $H^{\pm\pm} - l_i - l_j$ and $H^{\pm} - l_i - \nu_j$ vertices, so on the coupling $\mathcal{Y}_{ij}$, Eq. (3.24). Fig. 19 presents the most severe limits. Since the $H^{\pm\pm} - l_i^{\pm} - l_j^{\pm}$ vertex depends not only on the triplet VEV but also on the neutrino parameters, the plot presents the limits in the case of normal and inverted neutrino mass hierarchies, with the neutrino parameters in the range of $\pm 2\sigma$. The exact parametrization of the V_{PMNS} matrix and used neutrino parameters were presented in section 4.3.

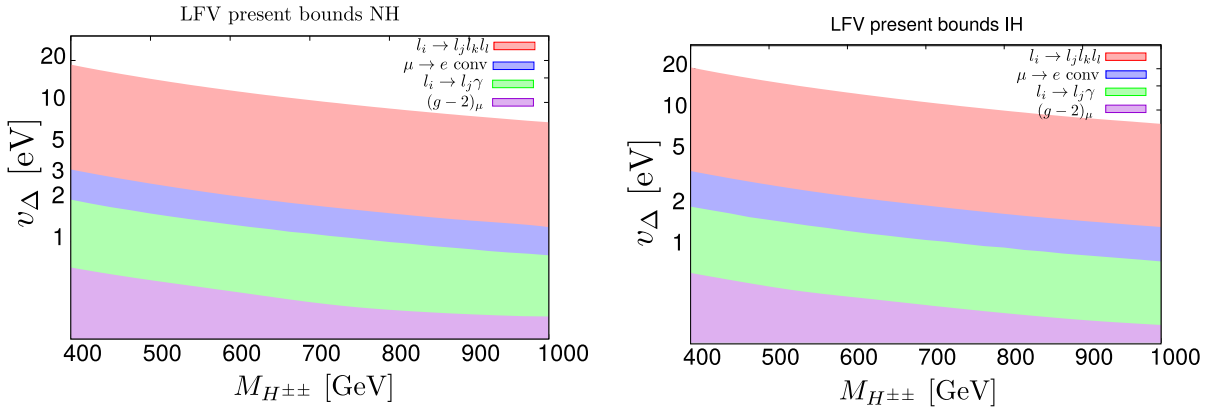

(a) (b)

Figure 19: Limits on the triplet VEV v_Δ as a function of the doubly charged scalar particle's mass within HTM. The LFV processes and muon $(g-2)_\mu$ exclude the shaded region. Normal and inverted neutrino mass hierarchies are tested. The neutrino oscillation data are taken in the 2σ range (see section 4.3).

From Fig. 19 we can see that the triplet VEV for $M_{H^{\pm\pm}} = 700$ GeV is bound till 10 eV. To satisfy that limit, I take $v_\Delta = 15$ eV for further calculations.

For `MLRSM` scenario, in section 3.3.2, I explained that I am taking into account only the diagonal couplings $H^{\pm\pm}_{1,2} - l_i - l_i$, Eq. (3.40). That means that the limits from the LFV processes are not applied here. Also, the constraints from the ρ-parameter are suppressed by large values of v_R [132, 133]. The most important experimental limits come from the bounds on the non-standard particles' masses, like M_{W_2} and heavy neu-

trino masses M_{N_i}. Those bounds are often connected since one of the most crucial processes used to calculate those bounds is a high-energy analogue of the neutrinoless double beta decay process: $pp \to Nl \to W_R ll \to jjll$. In [135], I discussed two cases of the triplet VEV value, $v_R = 6000$ GeV and $v_R = 15\,000$ GeV. That corresponds to the heavy charged gauge boson mass around 3500 GeV and 7500 GeV, since $M_{W_2} \simeq \frac{g v_R}{\sqrt{2}} = 0.47 v_R$. Here I will present the most interesting results for $v_R = 15\,000$ GeV. That value lies beyond the parameter space examined by the LHC, and there are no limits on the heavy neutrino masses.

To calculate the triplet VEV's bounds, it was essential to determine whether the dominating decay channels in both models could be the leptonic ones. I will study this case since the leptonic decay is the most promising for identification beyond the SM signals [135]. For this purpose, I will present the experimental data combining the leptonic branching ratios with bounds on the doubly charged scalars.

Table 11 shows that even though the most severe bound on the doubly charged scalar particle's masses is around 875 GeV (for 100% $e\mu$), it is possible to find lower limits, assuming that BR is also respectively lower.

Within HTM it is not possible to obtain the pure 100% decay into electrons and muons anyway, see Fig. 20.

Within `MLRSM` for $v_R > 12\,000$ GeV, there are no experimental data about heavy neutrino masses and mixing, except for some rough lower mass limits mentioned earlier. So it is not an issue to find the allowed parameter space for desired doubly charged particle masses. The chosen parameters' set for $M_{H^{\pm\pm}_{1,2}} = 700$ GeV and $M_{H^{\pm\pm}_{1,2}} = 1000$ GeV will be presented in section 4.6 and Tab. 16.

While considering the doubly charged scalar's decays and limits on its couplings, calculating the total decay width is also important. The particle covered distance after production depends on the total decay width. Many extensions of the SM introduce new particles with macroscopic decay lengths ($c\tau > 1$ cm) [206]. Such particles are often called long-lived particles (LLPs). Since the doubly charged scalar particle was not been directly observed so far, it is important to ensure that the particle decays

BR	ll	ee	$e\mu$	$\mu\mu$
0.01	216.3	**249.2**	**216.3**	**309.7**
0.02	279.4	**310.9**	**300.0**	**335.7**
0.03	308.5	**323.7**	**316.6**	**367.5**
0.04	316.8	**333.9**	**329.5**	**418.2**
0.05	324.3	**342.5**	**339.5**	**434.1**
0.1	**473.7**	**478.5**	**473.7**	**480.7**
0.2	**493.5**	**613.7**	**573.1**	**557.9**
0.3	**518.1**	**638.9**	**648.0**	**683.4**
0.4	**645.4**	**658.4**	**671.78**	**714.6**
0.5	**662.7**	**691.5**	**690.08**	**734.0**
0.6	**679.6**	752.6	754.4	749.3
0.7	**695.6**	755.8	808.3	776.5
0.8	753.3	758.3	839.4	805.8
0.9	756.8	761.9	857.8	829.4
1.0	763.8	768.3	874.7	846.2

Table 11: Lowest limits on a mass of the doubly charged scalar boson for the $SU(2)_L$ triplet as a function of different leptonic branching ratios. Based on the data from [205]. I bolded the BR range allowed within HTM (see Fig. 20). I separated the BR range with a horizontal line that allows doubly charged scalars' masses lower than 700 GeV.

before entering the detector. In Figs. 21 and 22 I present the total decay widths for $H^{\pm\pm}$ within `HTM` (`MLRSM`). In both cases I assume $M_{H^{\pm\pm}} = M_{H^{\pm}}$, so dominating are dilepton and diboson decay channels. As $H^{++} - l^+ - l^+$ vertex is proportional to $1/v_\Delta$ and $H^{++} - W^+ - W^+$ vertex is proportional to v_Δ (see Tab. 9), their cotributions cross around 10^5 eV in Fig. 21 (minimum). For the left part (below $v_\Delta \sim 10^5$ eV) the lines are sensitive to neutrino parameters. In `MLRSM`, Fig. 22, characteristic line kinks for the region $v_R \lesssim 10\ 000$ GeV are due to the LHC exclusion analysis. For reader convenience, I added here the corresponding figure from [207], Fig. 23, from which I extracted the CMS exclusion limits, $M_{W_2} \simeq 0.48\ v_R$.

As we can see, in both models $H^{\pm\pm}$ are not LLPs.

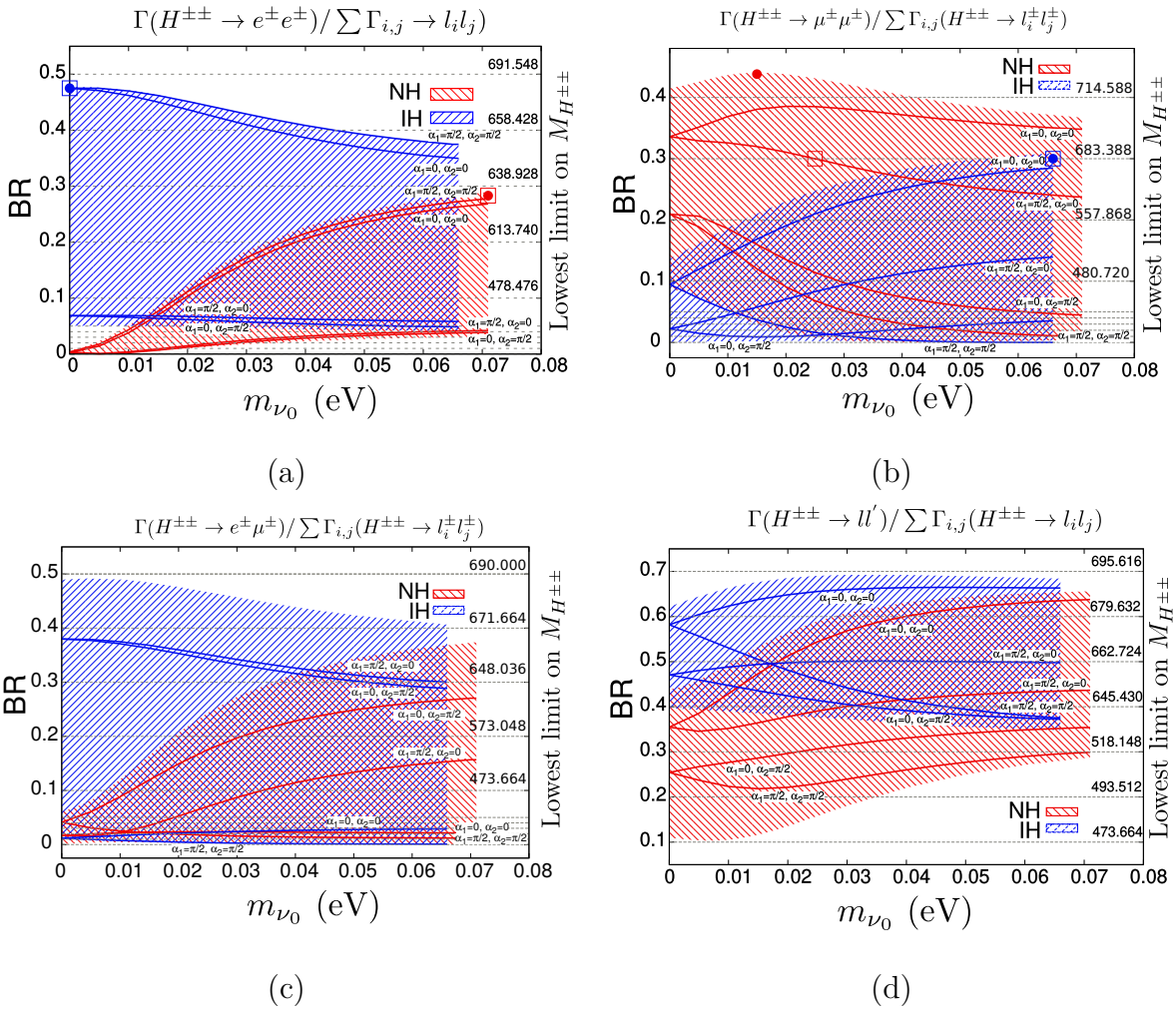

Figure 20: $H^{\pm\pm}$ decay branching ratios into ee — fig. (a), $\mu\mu$ — fig. (b), $e\mu$ — fig. (c) and $ee + e\mu + \mu\mu$ — fig. (d) within HTM as a function of the lowest neutrino mass m_{ν_0}. Corresponding lower limits on the doubly charged scalar particle's masses are marked (see Tab. 11). Neutrino parameters are taken within the $\pm 2\sigma$ range (see Tab. 7). Solid lines present the result for different Majorana phases and the best fit of neutrino parameters. Points marked with □ and • are used for further calculation for $M_{H^{\pm\pm}}$=700 GeV (□) and $M_{H^{\pm\pm}}$=1000 GeV (•).

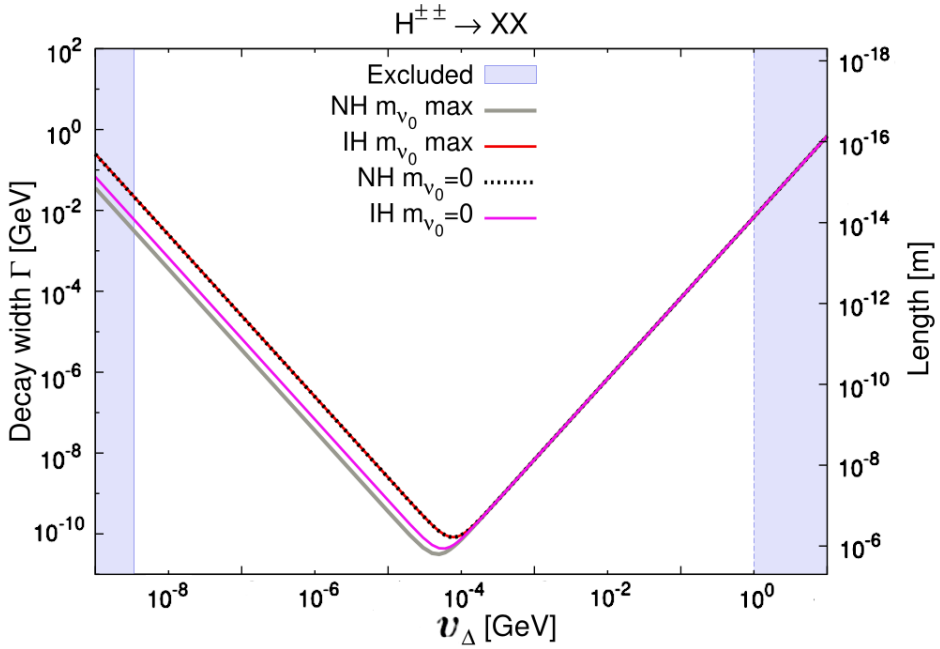

Figure 21: The total decay with for $H^{\pm\pm}$ in HTM. The excluded region for small values of v_Δ is due to Fig. 19 while for large values of v_Δ is due to the constraints on the ρ-parameter, Eq. (3.13).

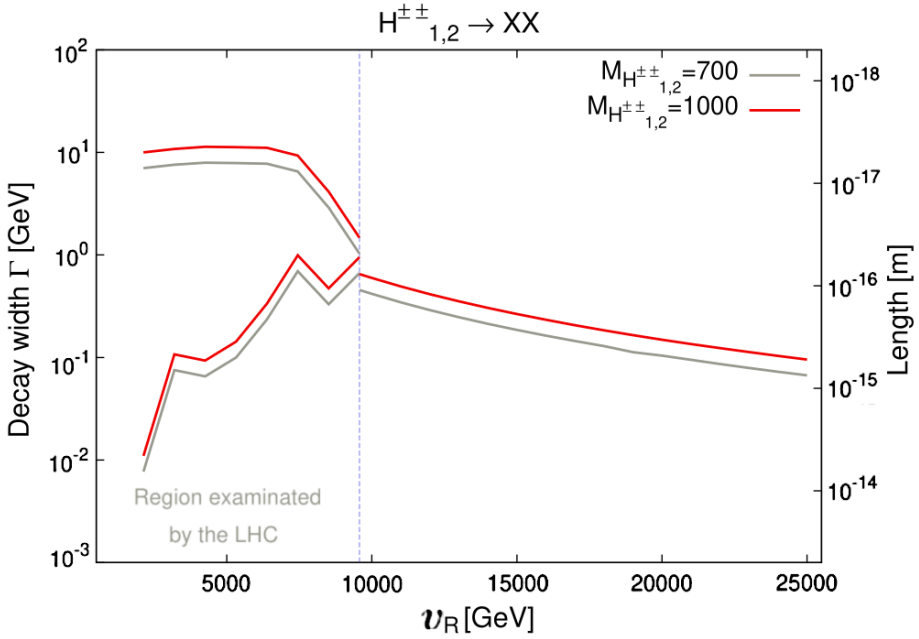

Figure 22: The total decay width for $H^{\pm\pm}_{1,2}$ in MLRSM. In the legend, $H^{\pm\pm}_{1,2}$ masses are given in GeV.

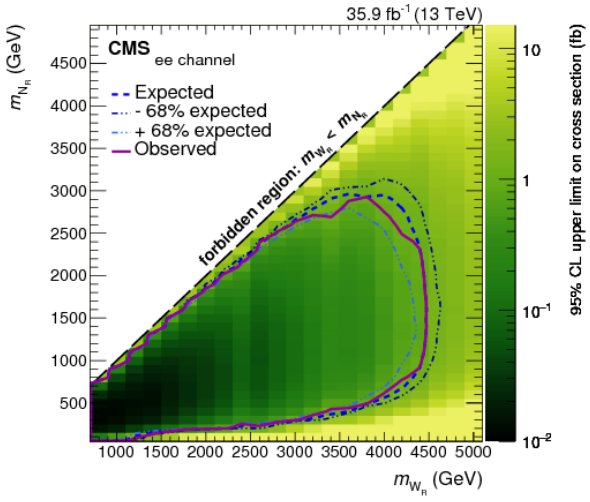

Figure 23: Upper limit on the $pp \to eejj$ cross section for different $M_{W_R} \equiv M_{W_2}$ and $M_{N_R} \equiv M_N$ mass hypotheses. The thin-dotted (blue) curves indicate the region in (M_{W_2}, M_{N_i}) parameter space that is expected to be excluded at 68% CL. Figure taken from [208].

4.6 $H^{\pm\pm}$ production and decays in lepton and hadron colliders

There are two attractive options with singly and doubly charged $H^{\pm\pm}$ production which after decays may lead to tri- and four-leptons in the final state. As already discussed, we have chosen the parameter space in such a way that the doubly charged scalars decay to charged leptons with almost 100% branching ratio. Thus, the four lepton final state contains two pairs of same sign and same flavoured charged leptons where each pair has opposite charges to each other. As there is no neutrino (missing energy) or jet involved it is easy to reconstruct the momentum of the final state particles. We have reconstructed invariant masses for a lepton pair defined as $m_{\ell_1\ell_2} = \sqrt{(E_1+E_2)^2 - (\vec{P_1}+\vec{P_2})^2}$, where E_i and $\vec{P_i}$ are the energy and three momentum of ℓ_i, respectively, for the same sign dileptons (SSDL) and the opposite sign dileptons (OSDL). As the doubly charged scalars are the 'parents' of the dilepton pairs, invariant mass of the SSDL should lead to a clean peak around the mass of the doubly charged scalar, which is not necessarily a case for OSDL.

There is another interesting variable which can be used for determination of signals

$$\Delta R_{\ell_1\ell_2} = \sqrt{(\eta_1-\eta_2)^2 + (\phi_1-\phi_2)^2}, \tag{4.20}$$

where η_i and ϕ_i denote pseudorapidity and azimuth of ℓ_i, respectively. $\Delta R_{\ell\ell}$ amounts the separation between two light charged leptons (ℓ) in azimuth-pseudorapidity plane. Its physical importance is that in the detector if $\Delta R_{\ell\ell}$ is smaller than the specified value then one can not distinguish whether the deposited energy is really by one or two leptons. So, one chooses only events for which leptons are well separated. *We expect that the leptons originated from a single doubly charged scalar will be less separated than the leptons coming from different charged scalars.* This statement is very distinctively clear from the invariant mass distributions of the same sign dileptons, as shown in Fig. 24. Maximum number of same dilepton events are with an invariant mass peak around $M_{H_1^{\pm\pm}} = 400$ GeV and that around $M_{H_2^{\pm\pm}} = 500$ GeV is much smaller, as expected. *For the opposite sign lepton pairs, the two leptons have different origin, thus their invariant mass distribution is continuous while the same sign dilepton invariant*

mass distributions always peak around the mass of the doubly charged scalars. This is the first analysis in which I was involved [209] where we have undertaken the study of production and decay processes with $H^{\pm\pm}$. We also performed the $\Delta R_{\ell\ell}$ distribution

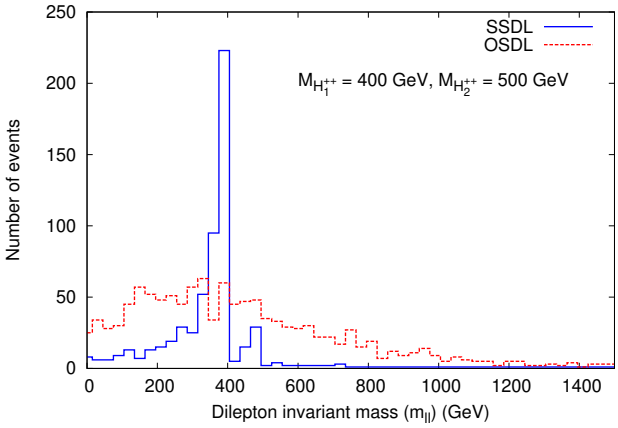

Figure 24: Invariant mass for SSDL and OSDL signals in the $pp \to H_{1,2}^{++} H_{1,2}^{--} \to 4l$ process in the non-degenerate mass scenario with $M_{H_1^{\pm\pm}} = 400$ GeV and $M_{H_2^{\pm\pm}} = 500$ GeV for $\sqrt{s} = 14$ TeV and $L = 300\ fb^{-1}$.

for the same benchmark point. For the same reason as explained before our expectation is reflected in Fig. 25 where the distribution for SSDL is narrower than for OSDL.

In [209] we have also considered the trilepton signals with missing p_T by analyzing processes $pp \to H_1^{\pm\pm} H_1^{\mp}$ and $pp \to H_2^{\pm\pm} H_2^{\mp}$. We can have $\ell^+\ell^+\ell^-$ or $\ell^-\ell^-\ell^+$ signals in this case. We can estimate the ratio R_-^+ defined as

$$R_-^+ = \frac{\#\text{ of events for } \ell^+\ell^+\ell^-}{\#\text{ of events for } \ell^-\ell^-\ell^+}. \tag{4.21}$$

For $\sqrt{s} = 14$ TeV and integrated luminosity 300 fb^{-1}, $v_R = 8$ TeV, $M_{H_1^{\pm\pm}} = 483$ GeV, $M_{H_2^{\pm\pm}} = 527$ GeV, $M_{H_1^{\pm}} = 355$ GeV, $M_{H_2^{\pm}} = 15066$ GeV, the estimate is $R_-^+ = \frac{396}{158} \simeq 2.51$. In SM we got $R_{-SM}^+ \simeq \frac{17.8}{15.0} = 1.19$ which differs substantially from the MLRSM prediction for the above choices of charged scalar masses. We find 554 trilepton signal events after all the cuts as given in Appendix A.1.

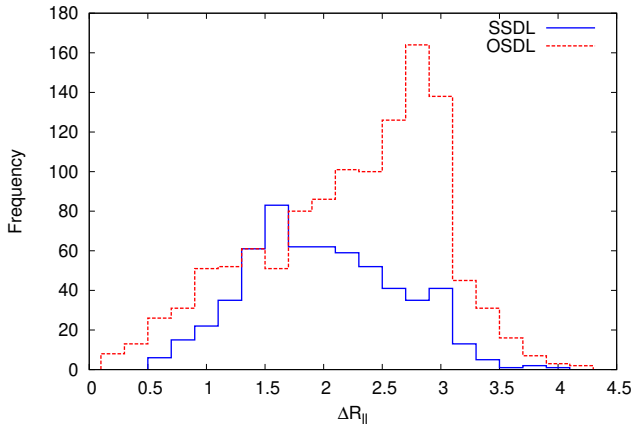

Figure 25: Lepton - lepton separations for the same sign lepton pairs ($\Delta R_{\ell^\pm\ell^\pm}$) and opposite sign lepton pairs ($\Delta R_{\ell^\pm\ell^\mp}$) in $pp \to H_{1,2}^{++} H_{1,2}^{--} \to 4l$. Benchmark parameters as in Fig. 24.

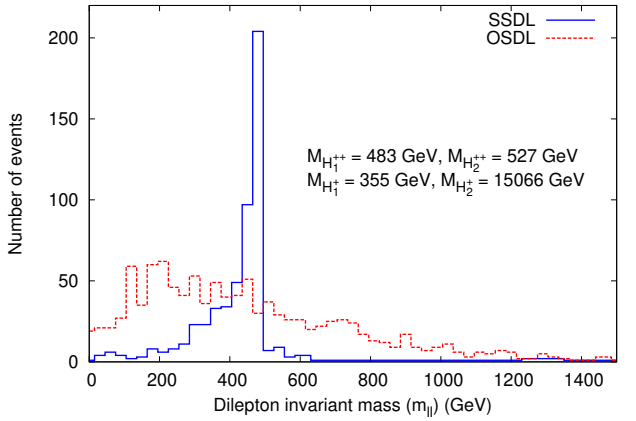

Figure 26: Invariant mass plots for SSDL and OSDL for the signals $\ell^\pm\ \ell^\pm\ \ell^\mp$ + missing p_T ($l = e, \mu$), at the LHC with $\sqrt{s} = 14$ TeV and integrated luminosity 300 fb^{-1}.

From Fig. 26 it is distinctly seen that the significant amount of same sign dilepton pair peaks again at smaller $H_1^{\pm\pm}$ than $H_2^{\pm\pm}$ mass (here specific benchmark points defined in [209] are chosen for higher $M_{H_1^{\pm\pm}}$ than in Fig. 24). This implies that the dominant contribution to this trilepton events are generated through $pp \to H_1^{\pm\pm} H_1^{\mp}$ process and the further leptonic decays of the charged scalars.

In [171] we analysed all the associated processes of $H^{\pm\pm}$ with gauge and scalar bosons in `HTM` and found that five of them are worth further studies. In Tab. 12 we gathered the results, for basic Feynman diagrams see Appendix A.4.

Process		Cross section [pb]	Process		Cross section [pb]
a)	$pp \to H^{\pm\pm} W^{\mp}$	$\sim 10^{-22}$ ($\sim 10^{-20}$)	*b)*	$pp \to H^{\pm\pm} H^{\mp}$	8.13×10^{-5} (8.78×10^{-3})
c)	$pp \to H^{\pm\pm} Z W^{\mp}$	$\sim 10^{-12}$ (2.7×10^{-9})	*d)*	$pp \to H^{\pm\pm} Z H^{\mp}$	6.29×10^{-7} (1.56×10^{-4})
e)	$pp \to H^{\pm\pm} W^{\mp} W^{\mp}$	$\sim 10^{-10}$ (1.87×10^{-9})	*f)*	$pp \to H^{\pm\pm} W^{\mp} h$	$\sim 10^{-12}$ (3.47×10^{-8})
g)	$pp \to H^{\pm\pm} W^{\mp} H$	1.35×10^{-6} (2.44×10^{-4})	*h)*	$pp \to H^{\pm\pm} W^{\mp} H^{\mp}$	2.88×10^{-6} (6.81×10^{-4})
i)	$pp \to H^{\pm\pm} h H^{\mp}$	1.07×10^{-7}) (1.63×10^{-6}	*j)*	$pp \to H^{\pm\pm} H H^{\mp}$	$\sim 10^{-29}$ ($\sim 10^{-26}$)
k)	$pp \to H^{\pm\pm} H^{\mp} H^{\mp}$	$\sim 10^{-31}$ ($\sim 10^{-28}$)			

Table 12: Cross sections for a production of a single $H^{\pm\pm}$ boson with associated SM gauge bosons and other `HTM` scalars at the pp colliders in $2 \to 2$ and $2 \to 3$ processes, calculated for $\sqrt{s} = 14$ TeV (100 TeV), in pb. Charged scalar masses are degenerated, $M_{H^{\pm\pm}} = M_{H^{\pm}} = 1$ TeV. Basic Feynman diagrams can be found in Appendix A.4.

In Tables 13 and 14 we gathered results for $pp \to H^{\pm\pm} H^{\pm}$ after decays as we found that the largest cross section, similarly to `MLRSM` is for the $pp \to H^{\pm\pm} H^{\pm}$ process. However, as we can see from our preliminary studies, the background signals for considered processes are substantial, and more detailed analysis of kinematic conditions

and appropriate distributions or choice of final states which can enhance new physics signals over the SM background are needed.

v_Δ	Process:		Signal [pb]:	Background [pb]:
50 eV	$pp \to H^{\pm\pm}H^{\mp} \to$	$e^{\pm}\, e^{\pm}\, e^{\mp}\, \not{E}_T$	1.79×10^{-5}	5.05×10^{-2}
			(2.00×10^{-3})	(3.15×10^{-1})
		$\mu^{\pm}\mu^{\pm}\mu^{\mp}\, \not{E}_T$	1.43×10^{-5}	5.05×10^{-2}
			(1.55×10^{-3})	(3.15×10^{-1})
0.5 GeV	$pp \to H^{\pm\pm}H^{\mp} \to$	$W^{\pm}W^{\pm}W^{\mp}\, Z$	3.62×10^{-5}	7.00×10^{-4}
			(3.93×10^{-3})	(1.60×10^{-2})
		$W^{\pm}W^{\pm}W^{\mp}h$	3.53×10^{-5}	6.19×10^{-5}
			(3.84×10^{-3})	(1.12×10^{-3})
		$W^{\pm}W^{\pm}jj$	3.68×10^{-10}	3.09×10^{-1}
			(4.01×10^{-8})	(5.65)

Table 13: Singly and doubly charged scalar production $pp \to H^{\pm\pm}H^{\mp}$ with primary decays to the SM particles for CM energy 14 TeV (100 TeV).

Process:	Signal:		Background:	
	Before cuts [pb]:	After cuts [fb]:	Before cuts [pb]:	After cuts [fb]:
$e^{\pm}\, e^{\pm}\, e^{\mp}\, \not{E}_T$	1.79×10^{-5}	5.46×10^{-3}	5.05×10^{-2}	0.94
$\mu^{\pm}\, \mu^{\pm}\, \mu^{\mp}\, \not{E}_T$	1.43×10^{-5}	9.68×10^{-3}	5.05×10^{-2}	1.77

Table 14: Results from the Table 13 for $v_\Delta = 50$ eV, after cuts. Centre mass energy: $\sqrt{s} = 14$ TeV.

To the end of this section I will present the final results for doubly charged scalar particles' pair production in pp and e^+e^- colliders, aiming to compare signals in the case of the same $H^{\pm\pm}$ masses in two considered models. The decays of those particles, disscussed in section 4.5 will be used to calculate the possible detector signals.

First I will present the results for lepton colliders. In section 1.3 I have shortly summarized main plans regarding future lepton and hadron colliders. Among lepton

colliders, the higher centre-mass energy is planned in the CLIC, which can reach energy of 3 TeV. However, that will be possible not until the last stage of this experiment. Till that, the accelerator will operate with the energy of 1.5 TeV, maximally. That is the reason that I study relatively low doubly charged scalars's masses, for $M_{H^{\pm\pm}_{(1,2)}} = 700$ GeV it is possible to consider the direct pair production in lepton collider at the energy of 1.5 TeV. In Tables 15 and 16 I am presenting the models parameters for benchmark points $M_{(1,2)^{\pm\pm}} = 700$ GeV and $M_{(1,2)^{\pm\pm}} = 1000$ GeV, for `HTM` and `MLRSM`.

$M_{H^{\pm\pm}}$	$H^{\pm\pm} \to XX$	HTM			
		NH		IH	
700 GeV (□)	eemax $BR < 0.5$	BR=0.283	$\alpha_1 = \frac{\pi}{2}$ $\alpha_2 = \frac{\pi}{2}$ $m_{\nu_0} = 0.071$	BR=0.475	$\alpha_1 = \frac{\pi}{2}$ $\alpha_2 = \frac{\pi}{2}$ $m_{\nu_0} = 0$
	$\mu\mu$max $BR < 0.3$	BR=0.3	$\alpha_1 = \frac{\pi}{2}$ $\alpha_2 = 0$ $m_{\nu_0} = 0.025$	BR=0.3	$\alpha_1 = 0$ $\alpha_2 = 0$ $m_{\nu_0} = 0.066$
1000 GeV (•)	eemax	BR=0.283	$\alpha_1 = \frac{\pi}{2}$ $\alpha_2 = \frac{\pi}{2}$ $m_{\nu_0} = 0.071$	BR=0.475	$\alpha_1 = \frac{\pi}{2}$ $\alpha_2 = \frac{\pi}{2}$ $m_{\nu_0} = 0$
	$\mu\mu$max	BR=0.438	$\alpha_1 = 0$ $\alpha_2 = 0$ $m_{\nu_0} = 0.015$	BR=0.3	$\alpha_1 = 0$ $\alpha_2 = 0$ $m_{\nu_0} = 0.066$

Table 15: Parameters for the benchmark points $M_{H^{\pm\pm}} = 700$ GeV and $M_{H^{\pm\pm}} = 1000$ GeV. The neutrino masses and Majorana phases are fitted to obtain the maximal possible signal for ee and $\mu\mu$ decays (maximal branching ratios), as well as to meet the experimental limits on the neutrino parameters. The other parameters are set to the best fit from Table 7. The benchmark points are also marked in Fig. 20 by □ ($M_{H^{\pm\pm}} = 700$ GeV) and • ($M_{H^{\pm\pm}} = 1000$ GeV). Neutrino masses given in electronvolts.

$M_{H^{\pm\pm}_{1,2}}$	$H^{\pm\pm}_{1,2} \to XX$	MLRSM	
700 GeV	eemax $BR < 0.5$	BR=0.5	$M_{N_1} = 1300$ $M_{N_{2,3}} = 918$
	$\mu\mu$max $BR < 0.3$	BR=0.3	$M_{N_2} = 1300$ $M_{N_{1,2}} = 1130$
1000 GeV	eemax	BR~ 1	$M_{N_1} = 5733$ $M_{N_{2,3}} = 300$
	$\mu\mu$max	BR~ 1	$M_{N_2} = 5000$ $M_{N_{1,2}} = 300$

Table 16: Parameters for the benchmark points $M_{H^{\pm\pm}_{1,2}} = 700$ GeV and $M_{H^{\pm\pm}_{1,2}} = 1000$ GeV within the MLRSM for $v_R = 15\,000$ GeV. The heavy neutrino masses are fitted to obtain the maximal possible signal for ee and $\mu\mu$ decays (maximal branching ratios). Neutrino masses are given in GeV.

Compared to the hadron colliders, lepton colliders offer significantly lower energies, but the signal can potentially be evident over the SM background. In Figs. 27 and 29, the results are given for HTM and MLRSM, respectively. In Fig. 28, I present the Feynman diagrams for doubly charged scalars' pair production in e^+e^- collisions. Even though the MLRSM has rich phenomenology, the main contribution to the s-channel within both models will be at the same range since the non-standard scalars are very heavy. Regarding the t-channel, it is suppressed within HTM by the LFV processes (see Fig. 27). Within MLRSM, the t-channel is bounded mainly by the Bhabha scattering data (see Tab. 6), and the impact of the t-channel might reach around 20% of the s-channel contribution. For the t-channel, the $M_{W_2} - M_N$ space is restricted by the LHC exclusion plots [208, 210]. To use this data, we take $M_{W_2} \geq M_N$ with the same CP-parities of heavy neutrinos and a correlation between heavy masses which are proportional to v_R [149, 159]. Let us note that most of the experimental LHC analyses are based on simplified scenarios where heavy neutrinos are mass degenerate with diagonal mixings and where CP-violating effects are not taken into account. However,

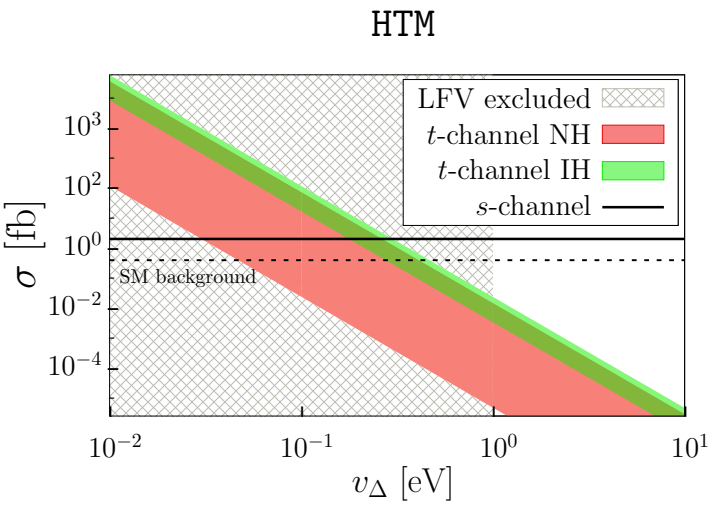

Figure 27: Doubly charged Higgs boson pair production in e^+e^- collision within the HTM. $M_{H^{\pm\pm}} = 700$ GeV and collider energy $E_{CM} = 1.5$. The low energy data excludes the shaded region (Tab. 6). Neutrino oscillation parameters are within the $\pm 2\sigma$ range (Tab. 7). A dashed line marked the SM background for four leptons production $\sigma = 0.415$ fb, with the cuts presented in the Appendix A.1. Basic diagrams are given in Fig. 28.

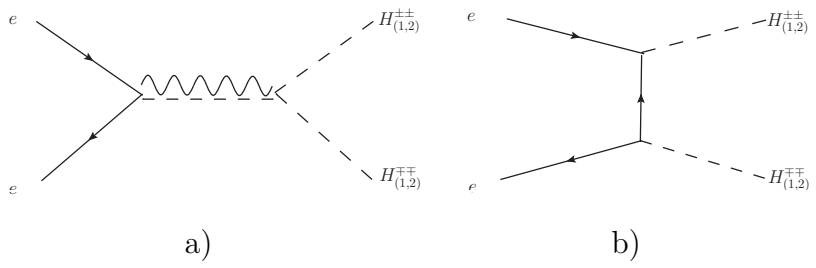

Figure 28: Pair production of doubly charged scalars in e^+e^- colliders.
The following particles contribute to the diagrams:
HTM: γ, Z, h and H (s-channel); e, μ, τ (t-channel),
MLRSM: γ, Z_1, Z_2, H_0^0, H_1^0, H_2^0 (s-channel).

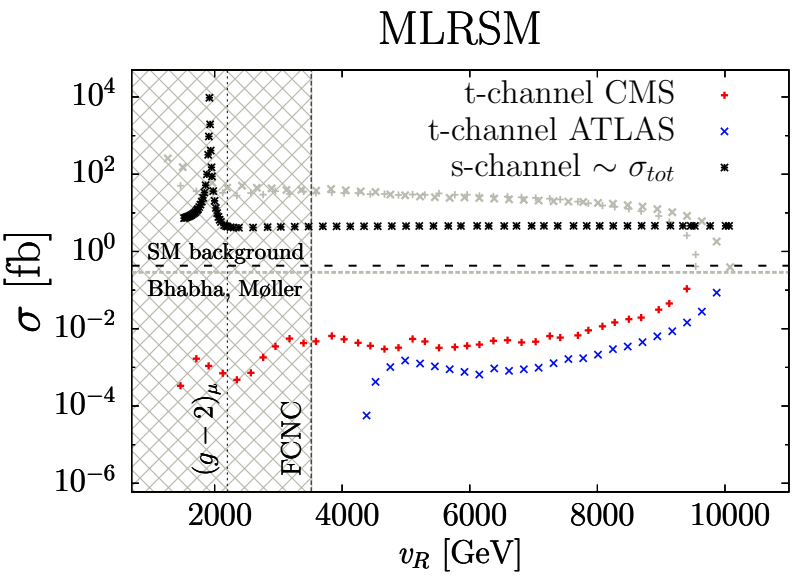

Figure 29: Doubly charged Higgs boson pair production $e^+e^- \to H_1^{++}H_1^{--} + H_2^{++}H_2^{--}$ for $M_{H^{\pm\pm}_{(1,2)}} = 700$ GeV and CM energy 1.5 TeV in `MLRSM`. The crossed area on the left is excluded by $(g-2)_\mu$ and FCNC. The maximum for $v_R = 1900$ GeV comes from the Z_2 resonance, $M_{Z_2} = 1.9$ TeV. The horizontal grey dashed line "Bhabha, Møller" separates the t-channel contribution to the cross-section, which is still allowed by the CMS and ATLAS exclusion analysis from constraints by the Bhabha and Møller processes (Tab. 8). The t-channel contribution above this line is forbidden. The SM background (black dashed horizontal line) after applying kinematic cuts is $\sigma = 0.415$ fb, see section A.1.

CP-parities of neutrinos can be different, leading to destructive interference effects, relaxing limits on the v_R scale, see [202, 211, 212]. We vary the M_{W_2} mass from 600 GeV to 5.5 TeV and the heavy neutrino mass up to 4.8 TeV and take the best fit expected values for the LHC exclusion data. As we can see, *in both e^+e^- and pp cases, the production processes can exceed the SM background.* We will quantify the results in the following tables after including $H^{\pm\pm}$ decays to four lepton final states.

Regarding the pair production in hadron colliders, only the s-channel will contribute

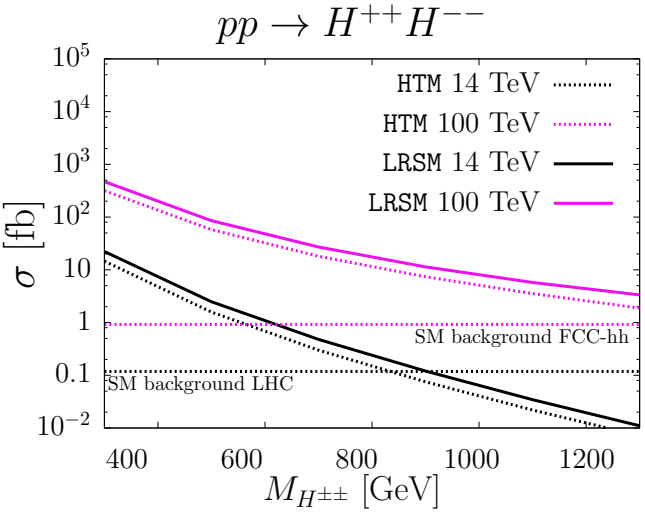

Figure 30: Doubly charged scalars' pair production at pp colliders for LHC and FCC-hh center-of-mass energies. Horizontal line marks the background for the process $pp \to 4l$, with kinematic cuts defined in the Appendix A.1. Basic diagrams are given in Fig. 31.

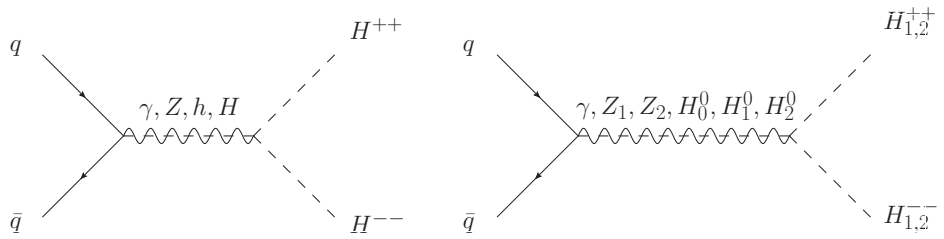

a) HTM b) MLRSM

Figure 31: Feynman diagrams for the doubly charged scalar particles' pair production in proton-proton colliders within (a) HTM and (b) MLRSM models.

to this process. The result for both HTM and MLRSM models are presented in Fig. 30 with basic Feynman diagrams shown in Fig. 31. In both Fig. 27 and Fig. 30 by a dashed line the SM background with four lepton in the final state is marked $4l$, $l = e, \mu$, with cuts presented in the Appendix A.1. The processes contributing to the background are gathered in Appendix A.2.

Finally, I will compare the four lepton signals within `HTM`, `MLRSM` and `SM` (background). I chose the $4e$ and 4μ final states and present the results in Table 17 for e^+e^- collider (CLIC: $E_{CM} = \sqrt{s} = 1500$ GeV, luminosity $L = 1500\ fb^{-1}$) and in Table 18 for pp colliders (HL-LHC: $E_{CM} = 14$ TeV, $L = 4000\ fb^{-1}$ and FCC-hh: $E_{CM} = 100$ TeV, $L = 25\,000\ fb^{-1}$). For the calculations, I used the cuts defined in Appendix A.1 to minimize the background contribution. The most promising result is obtained in the 4μ channel for e^+e^- colliders where both `HTM` and `MLRSM` signals are much higher than the background. I got 120 and 205 events for luminosity $L = 1500\ fb^{-1}$ within `HTM` and `MLRSM` respectively, versus 8 events of the SM background (Tab. 17). That gives a large significance $S = 14$ for `MLRSM` and $S = 11$ for `HTM`, where the significance if defined: $S \equiv S'/\sqrt{S' + B}$, S' and B are the total number of signal and background events, rspectively.

In the case of pp colliders, the significance for the 4μ signal can reach $S \sim 1$ for `HTM` (normal hierarchy case) and $S = 8$ for `MLRSM` for HL-LHC energies. For the signal and background numbers, see Tab. 18. That means that observing a 4μ signal with a significance $S > 1$ can discriminate the `HTM` model.

Apart from the significance, detailed analysis of the signal can bring some important information. For example, the invariant mass or the lepton-lepton separation can be studied. In Fig. 32 I am presenting this kind of distribution for $4e$ signal in e^+e^- colliders for benchmark points given in Tables 15 and 16. It is clear that good separation of final dilepton signals is possible. More distributions for $4e$ and 4μ signals are given in Appendix A.3.

Distributions presented in the thesis show that it is possible to extract clear signals for doubly charged scalars at the LHC and future colliders. For signal identification, crucial is how large are the SM background effects, and what are the significance values.

SM background: $e^+e^- \to 4l$				
$4e$	No cuts: $\sigma = 2.1$ fb After cuts: $\sigma = 0.13$ fb, N = **200**			
4μ	No cuts: $\sigma = 0.07$ fb After cuts: $\sigma = 0.005$ fb, N = **8**			
BSM signal: $e^+e^- \to H^{++}H^{--} \to 4l$		HTM		MLRSM
		NH	IH	
$4e$	No cuts:	0.19 fb	0.53 fb	0.924 fb
	After cuts:	0.02 fb N=**30**	0.06 fb N=**90**	0.113 fb N=**169**
4μ	No cuts:	0.22 fb	0.19 fb	0.33 fb
	After cuts:	0.08 fb N=**120**	0.08 fb N=**120**	0.137 fb N=**205**

Table 17: Doubly charged scalars' pair production with subsequent decays to four leptons at e^+e^- colliders, with $M_{H^{\pm\pm}} = 700$ GeV and centre-of-mass energy $\sqrt{s} = 1.5$ TeV. To study the $4e$ and 4μ signals, the paramaters set from Tables 15 and 16 were applied. "N" estimates a number of final events for luminosity $L = 1500\ fb^{-1}$.

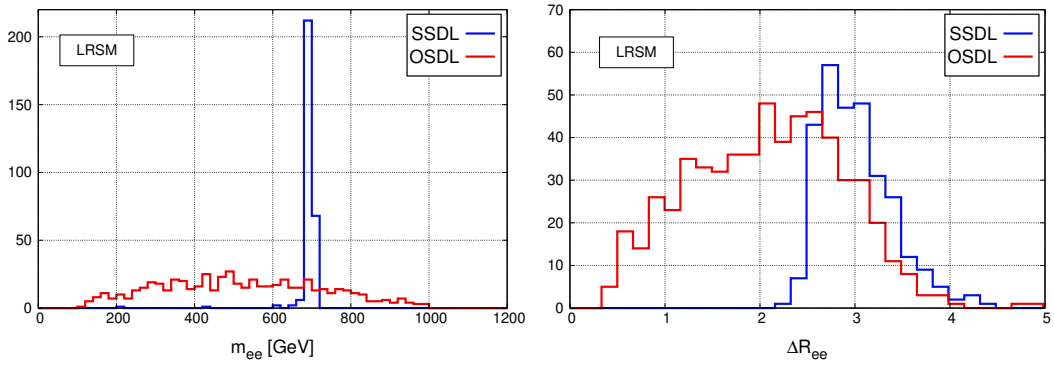

Figure 32: Dilepton distributions for $e^+e^- \to 4e$ in the LRSM. Benchmark parameters are given in Tab.16 (for $M_{H^{\pm\pm}_{1,2}} = 700$ GeV).

SM background: $pp \to 4l$	
$4e$	No cuts: $\sigma = 6.9$ [100.8] fb After cuts: $\sigma = 0.0061$ [0.192] fb, N = **24** [**4391**]
4μ	No cuts: $\sigma = 6.9$ [100.6] fb After cuts: $\sigma = 0.019$ [0.62] fb, N = **77** [**15 167**]

BSM signal: $pp \to H^{++}H^{--} \to 4l$		HTM		MLRSM
		NH	IH	
$4e$	No cuts:	0.0033 fb [0.39 fb]	0.0095 fb [1.11 fb]	0.085 fb [10.6 fb]
	After cuts:	0.00028 fb N=**1.1** [0.017 fb] [N=**421**]	0.0008 fb N=**3.2** [0.051 fb] [N=**1269**]	0.0072 fb N=**28** [0.53 fb] N=[**13 240**]
4μ	No cuts:	0.008 [0.944 fb]	0.0034 fb [0.41 fb]	0.085 fb [10.6 fb]
	After cuts:	0.0027 N=**10** [0.176 fb] [N=**4397**]	0.00115 fb N=**4.6** [0.078 fb] [N=**1967**]	0.028 fb N=**112** [2.1 fb] N=[**52 540**]

Table 18: Doubly charged scalars' pair production with subsequent decays to four leptons at hadron colliders, with $M_{H^{\pm\pm}} = 1000$ GeV and centre-of-mass energy $\sqrt{s} = 14$ [100] TeV. "N" estimates a number of final events with the assumed luminosity $L = 4000$ [25 000] fb^{-1}

5 Conclusions

The discovery of doubly charged Higgs bosons would signal the existence of a more complex potential for scalar fields. In the Thesis, I focused on a detailed study of theoretical constraints and possible phenomenological signals of the $H^{\pm\pm}$ pair production and decay to four leptons in future lepton and hadron colliders.

I considered the Higgs Triplet Model (`HTM`) not restricted by the custodial symmetry and the Minimal Left-Right Symmetric Model (`MLRSM`). The models include scalar triplets with different complexity of scalar potentials and, due to experimental restrictions, completely different scales of non-standard triplet vacuum expectation values. In both models, a doubly charged Higgs boson $H^{\pm\pm}$ can acquire a mass of hundreds of gigaelectronvolts, which can be probed at HL-LHC, future e^+e^-, and hadron colliders. I compared both models taking into account the consistent selection of all available experimental data.

I analyzed the possible decays of doubly charged scalar particles to estimate the lower bounds of their masses. It turned out that lepton decays dominate both models while other channels are suppressed. For example, doubly charged scalar particles can decay into singly charged particles, which are present in both models: $H^{\pm\pm} \to H^{\pm} + X$. However, these decays are limited in both models by mass differences between doubly and singly charged particles. Thus, in both cases, we expect lepton decays purely, although individual decay channels may differ in these models. In `HTM`, the decays of $H^{\pm\pm}$ depend on the parameters of neutrino oscillations, which strongly limit the possible phenomenology of the `HTM` model. The decays of this particle in the `MLRSM` model depend on the parameters of the heavy neutrino sector (see-saw type-I mechanism).

Using these calculations, I estimated the mass lower limits of the doubly charged scalar particles to assess whether they could be produced in e^+e^- accelerators with a maximum planned energy of 1.5 TeV (CLIC). In both models, we found parameters that allowed us to assume relatively low masses of these particles, and for e^+e^- collisions,

we assumed $M_{H^{\pm\pm}} = 700$ GeV. Next, we examined the production of doubly charged scalar particles in the e^+e^- and pp collisions. Our calculations showed that, despite the richer `MLRSM` phenomenology, also containing additional heavy gauge bosons and neutral scalar particles, their impact on the final result is negligible (due to the small couplings and large masses of these particles). The production of doubly charged particles scalars in the s channel is comparable in both models for e^+e^- (Figs. 27 and 29) pp collisions (Fig. 30). The situation is different in the t channel for e^+e^-. In this case, the cross-section may be drastically different for both models. Additionally, this channel is severely limited by the processes $\mu \to e\gamma$ and $\mu \to eee$ in the case of `HTM`, and the so-called Flavor Changing Neutral Currents (FCNC) and the Möller and Bhabha processes in the case of `MLRSM`. Interference between these channels had to be considered when calculating the total maximum output in the s and t channels.

I examined the decays of particles produced in this way up to four leptons, selecting the cuts and parameters of the model to obtain the maximum possible signal while minimizing the background.

The clean reconstruction of the invariant mass and SSDL, OSDL *separation signals are possible even in the hadronic environment. These measurements can be a smoking gun feature of BSM scenarios, indicating the presence of doubly charged scalars.* The most interesting results were obtained for decays up to 4 muons. The `MLRSM` model dominates over the HTM production and the background of the Standard Model. In Tab. 17 and Tab. 18 I present the results obtained for the e^+e^- and pp collisions.

The most interesting conclusions of my work:

1. The production probabilities of H^{++} particle pair in the e^+e^- and pp colliders are very similar. In both cases, the production is limited due to the correlation of parameters and the lack of signals of low-energy experiments breaking the lepton number, analysis of the Bhabha process and Möller with contributions from non-standard particles, and excluding analyzes for the $pp \to lljj$ process at the LHC.

2. There is a relatively small chance of discovering the production and decay signals of the H^{++} particle pair up to 4 electrons in the `HTM` and `MLRSM` models in the e^+e^- collisions. Analogous decays of up to 4 muons can be recorded and distinguished from the background.

3. The difference in prediction and the much larger possible muon detection signals within `MLRSM` allow distinguishing between the two models.

The most interesting part of the project is not so much looking at possible signals at future colliders under `HTM` and `MLRSM` but trying to compare these models. In other words, we were looking for an answer to whether, when a doubly charged scalar particle of a given mass is discovered, it is possible to determine which model it belongs to or exclude specific models. We managed to show that it is possible, thanks to appropriate kinematic cuts and the selection of parameters that affect the decay ratios, without special adjustments, in a wide range of parameters (e.g. $v_R > 15$ TeV, theoretically favoured range in the `MLRSM` model) to predict that the `HTM` model would give a signal with four muons below the standard background from known processes. In contrast, this signal could be substantial in the `MLRSM` model. This differentiation analysis between non-standard models is precious for planning research directions in future CLIC, HL-LHC or FCC-hh accelerators. The great effort of the work done is the consistent combination of different areas of high and low-energy physics to see how experimental constraints affect predictions about future outcomes.

The analysis given here can be extended, especially in the region of potentially positive signals, to a larger spectrum of models, especially supersymmetric models with scalar triplets, also matching the results to the general framework, including higher-dimensional operators of effective theories.

A Appendix

In the link https://jgluza.us.edu.pl/mkord/index.html talks given and posters prepared by the author and connected with the subject of this thesis can be found, as well as a description of the used software.

Major calculations were performed using the MadGraph program [213] and the PYTHIA program [214] where cuts were implemented. The HTM model was created using the FeynRules Mathematica package [215]. This model's files can be found on the above website. The low energy processes and models constraints were calculated in Mathematica [216] and Fortran [217].

A.1 Cuts

To optimize the detection of non-standard particles, I am using the following cuts and selection criteria.

C1. Lepton identification criteria: transverse momentum $p_T \geq 10$ GeV, pseudorapidity $|\eta| < 2.5$.

C2. Detector efficiency for electron (muon): 70% (90%).

C3. Lepton-lepton separation: $\Delta R_{ll} \geq 0.2$.

C4. Lepton-photon separation $\Delta R_{l\gamma} \geq 0.2$ with $p_{T_\gamma} > 10$ GeV.

C5. Lepton-jet separation $\Delta R_{lj} \geq 0.4$.

C6. Hadronic activity cut - within the cone of radius 0.2 around the lepton the hadronic activity should fulfill the inequality: $\sum p_{T_{hadron}} \geq 0.2 \times p_{T_l}$.

C7. Z-veto - the invariant mass of any same flavour and opposite charge lepton should satisfy the condition: $|m_{l_1 l_2} - M_{Z_1}| \geq 6\,\Gamma_{Z_1}$.

C8. Hard p_T cuts: $p_T(l_1) > 30$ GeV, $p_T(l_2) > 30$ GeV, $p_T(l_3) > 20$ GeV, $p_T(l_4) > 20$ GeV.

C9. Parton Distribution Functions (PDFs): CTEQ6L1 [218] [219].

A.2 SM background for four leptons production at e^+e^- and pp colliders

In this section the SM background for $4l$ production at lepton and hadron colliders are presented. For lepton collider I consider scattering and annihilation with photon radiation and lepton pair emission, $(Z/\gamma^*)(Z/\gamma^*)$ production and multiperipheral processes (Fig. 33). For centre-of-mass energy $\sqrt{s} = 1500$ GeV the cross section for the above processes is $\sigma = 4.465$ fb and $\sigma = 0.415$ fb, before and after cuts defined in the section A.1.

For the pp collision, the main processes contributing to the SM background for $4l$ signal are presented in the Table 19. For both e^+e^- and pp colliders cuts used are defined in the previous section.

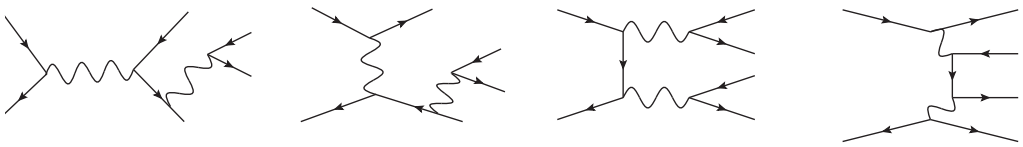

(a) (b) (c) (d)

Figure 33: Four lepton background diagrams at electron-positron colliders.

Process	Energy	$t\bar{t}(Z/\gamma^*)$	$(Z/\gamma^*)(Z/\gamma^*)$	TOTAL
$\sigma(pp \to 4l)$ [fb]	14 TeV	0.082	0.036	0.118
	100 TeV	0.79	0.13	0.92

Table 19: Dominant Standard Model background contributions to $4l$ signal at hadron colliders. The cross section are given in fb and are calculated using cuts from section A.1, for energies $\sqrt{s} = 14$ TeV and $\sqrt{s} = 100$ TeV. For the $t\bar{t}$ process the k-factor is set to 2.2 [220].

A.3 Dilepton distributions for $e^+e^- \to 4l$

In Figs. 34 - 41, I am presenting a complete distribution for $e^+e^- \to 4e$ and $e^+e^- \to 4\mu$ processes, with both `HTM` and `LRSM`, as well as the `SM` background, using cuts from the section A.1. The number of events is given as a function of lepton invariant mass $m_{l_1 l_2} = \sqrt{(E_1 + E_2)^2 - (\vec{P}_1 + \vec{P}_2)^2}$ and the lepton separation $\Delta_{R_{l_1 l_2}}$, defined in Eq. (4.20). As discussed in section 4.6, I consider two options, for the same sign lepton pair (`SSDL` - two electrons, positrons, muons or antimuons), or the opposite sign lepton pair (`OSDL` - e^+e^- or $\mu^+\mu^-$).

- The `SM` background:

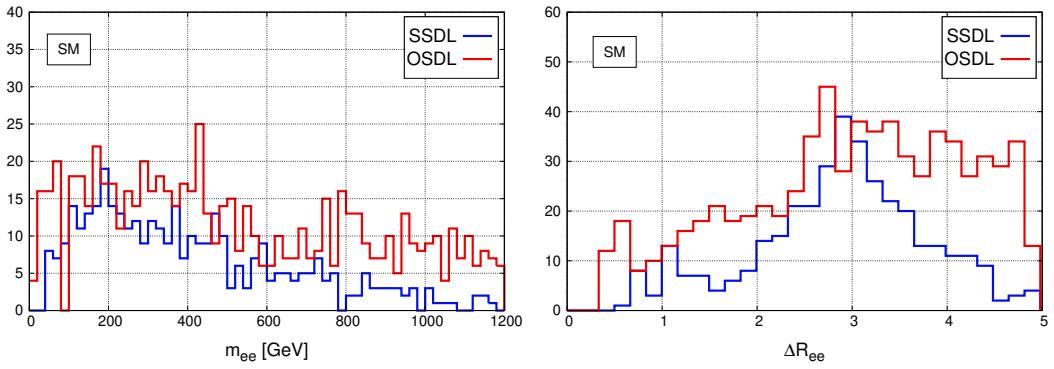

Figure 34: Dilepton distributions for $e^+e^- \to 4e$, the `SM` background.

- The `LRSM` signal.

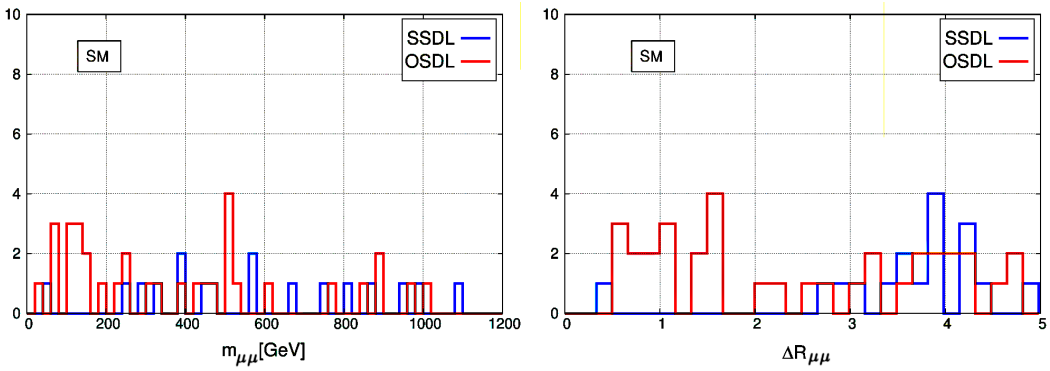

Figure 35: Dilepton distributions for $e^+e^- \to 4\mu$, the SM background.

Here I am presenting results for the 4μ signal. Dilepton distributions for $e^+e^- \to 4e$ were present in Fig. 32. The benchmark parameters as given in Tab.16 were applied.

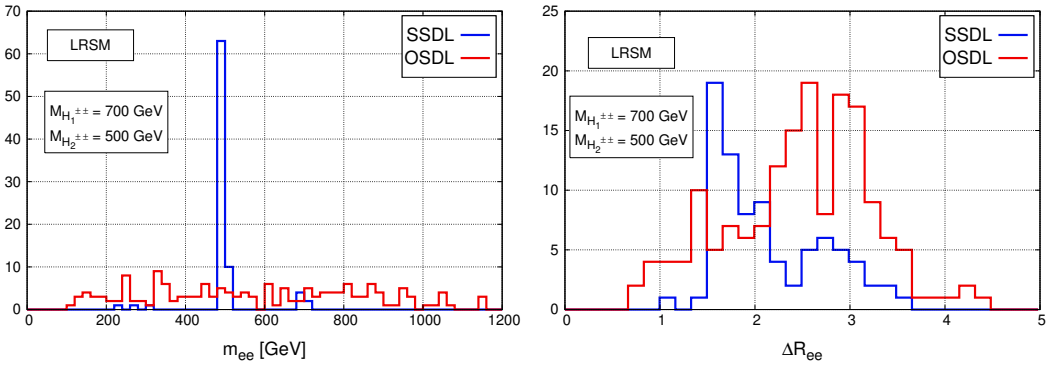

Figure 36: Dilepton distributions for $e^+e^- \to 4e$. On left m_{ee} distributions are shown for MLRSM with benchmark parameters for $v_R = 6$ TeV, $m_{H_1^{\pm\pm}} = 700$ GeV and $m_{H_2^{\pm\pm}} = 500$ GeV. On right, analogous plot for the $e - e$ separation observable ΔR_{ee} is given.

- The HTM signal for the normal and inverted hierarchies of neutrino masses.

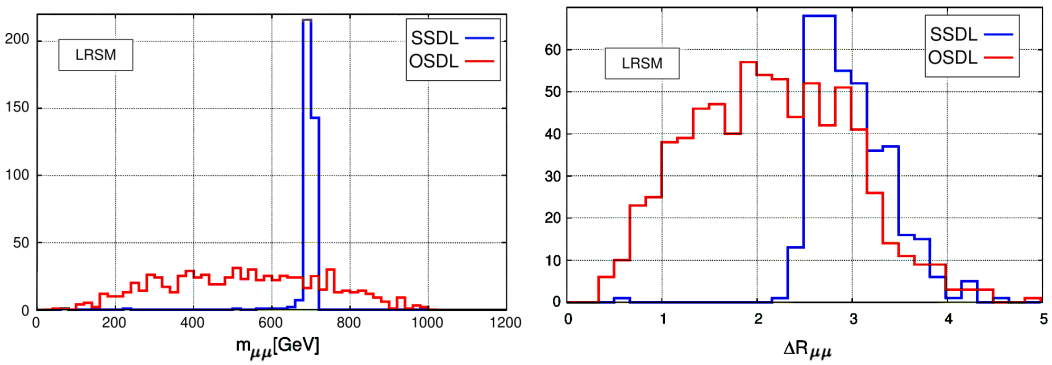

Figure 37: Dilepton distributions for $e^+e^- \to 4\mu$ in the LRSM. Benchmark parameters are given in Tab. 16 (for $M_{H^{\pm\pm}_{1,2}} = 700$ GeV).

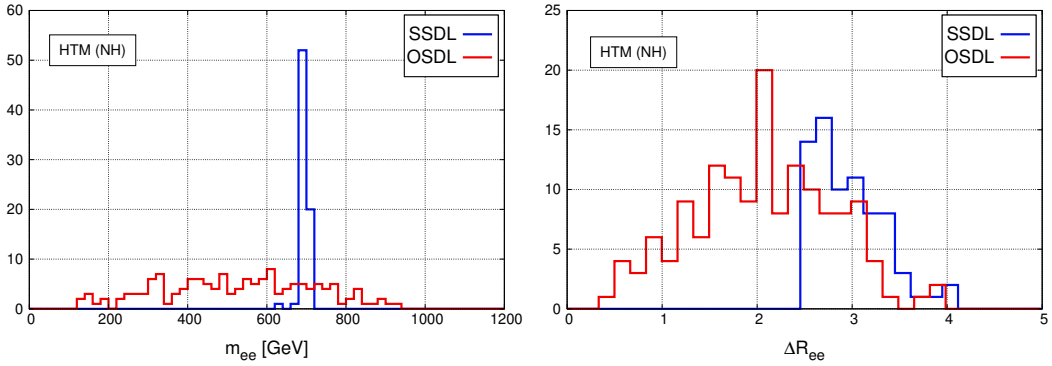

Figure 38: Dilepton distributions for $e^+e^- \to 4e$ for the HTM model with the NH scenario. Benchmark parameters as given in Tab. 15 for $M_{H^{\pm\pm}} = 700$ GeV.

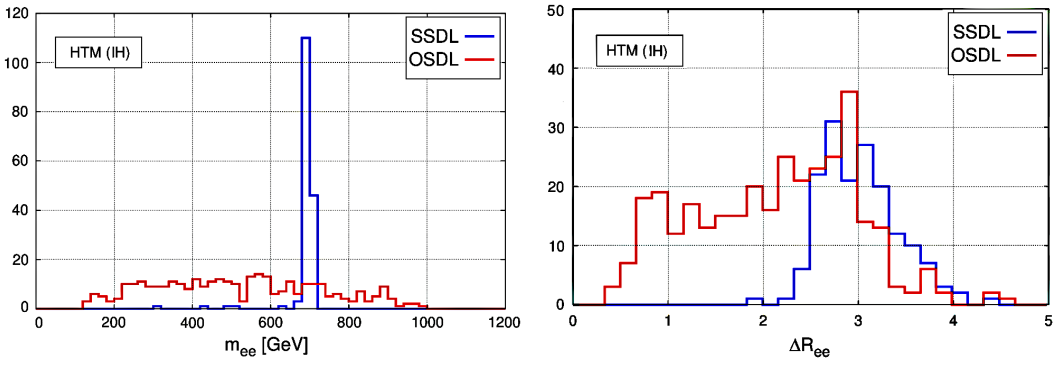

Figure 39: Dilepton distributions for $e^+e^- \to 4e$ for the HTM model with the IH scenario. Benchmark parameters as given in Tab. 15 for $M_{H^{\pm\pm}} = 700$ GeV.

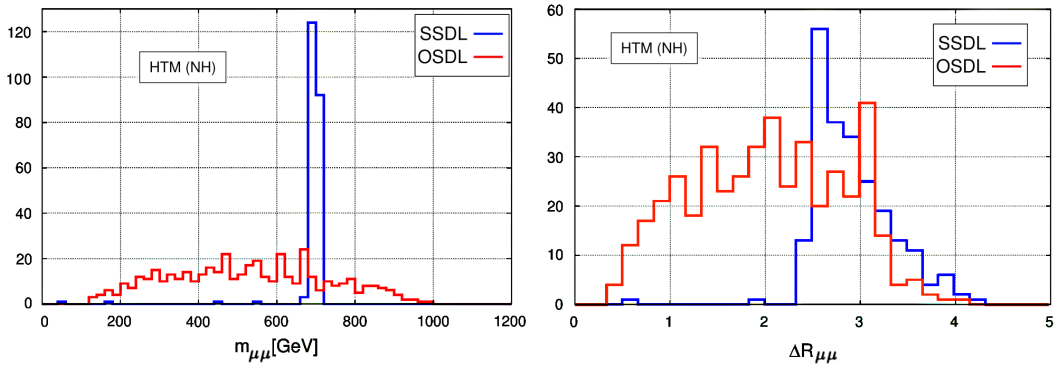

Figure 40: Dilepton distributions for $e^+e^- \to 4\mu$ for the HTM model with the NH scenario. Benchmark parameters as given in Tab. 15 for $M_{H^{\pm\pm}} = 700$ GeV.

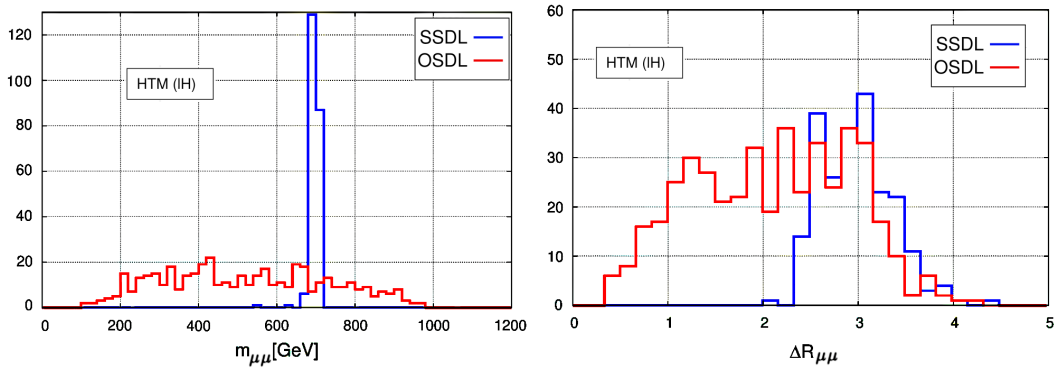

Figure 41: Dilepton distributions for $e^+e^- \to 4\mu$ for the HTM model with the IH scenario. Benchmark parameters as given in Tab. 15 for $M_{H^{\pm\pm}} = 700$ GeV.

A.4 Feynman diagrams for production of the doubly charged Higgs boson in association with the SM gauge bosons and/or other HTM scalars at hadron colliders

Below, we list the most relevant diagrams which contribute to the processes considered in section 4.6 in which one doubly charged Higgs boson is present, for simplicity within HTM. We keep the same numeration as in Tab. 12 for dominating processes denoted in blue, so the processes b), d), g), h) and i).

b) $pp \to H^{\pm\pm}H^{\mp}$

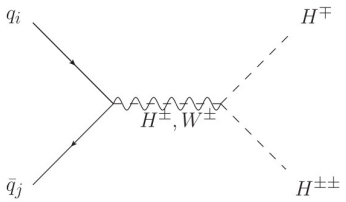

a)

d) $pp \to H^{\pm\pm}ZH^{\mp}$

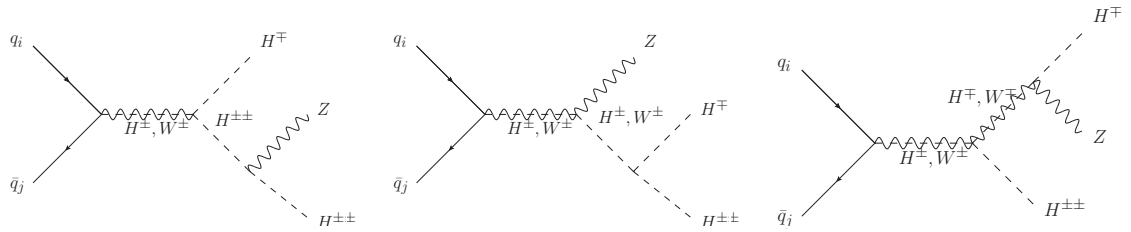

b) c) d)

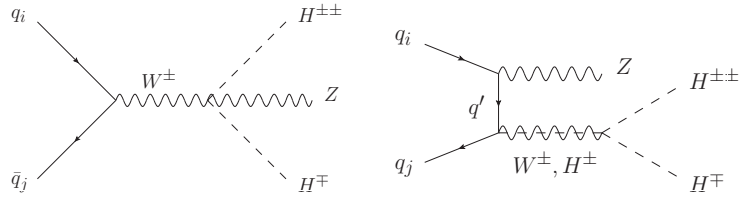

e) f)

g) $pp \to H^{\pm\pm}W^{\mp}H$

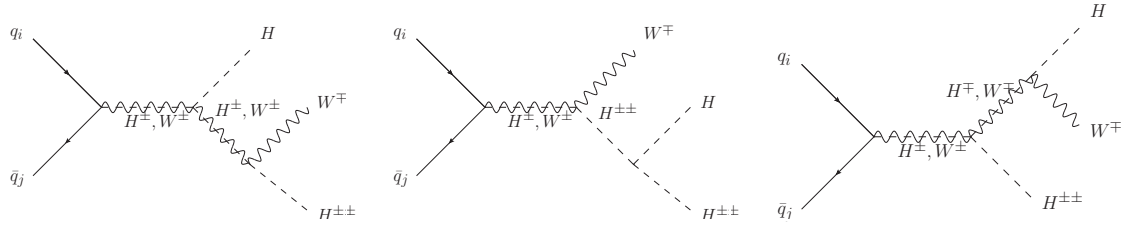

g) h) i)

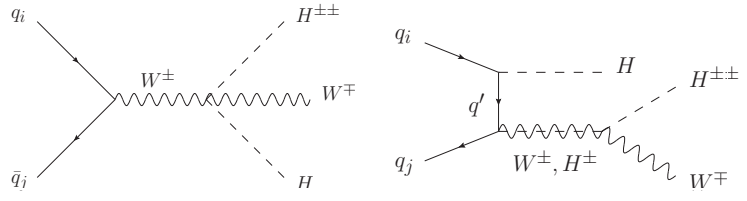

j) k)

h) $pp \to H^{\pm\pm}W^{\mp}H^{\mp}$

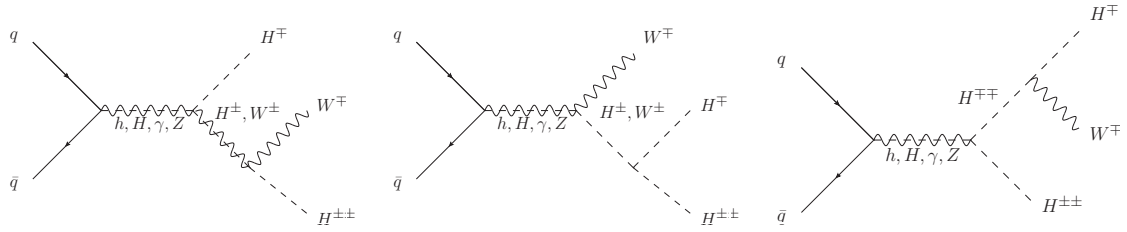

l) m) n)

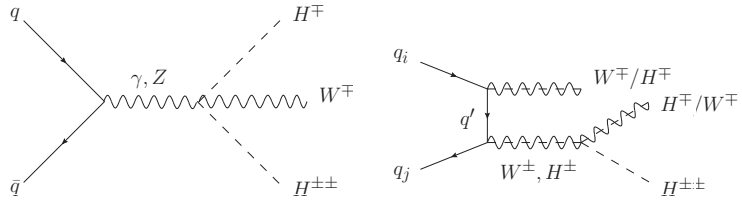

o) p)

i) $pp \to H^{\pm\pm}hH^{\mp}$

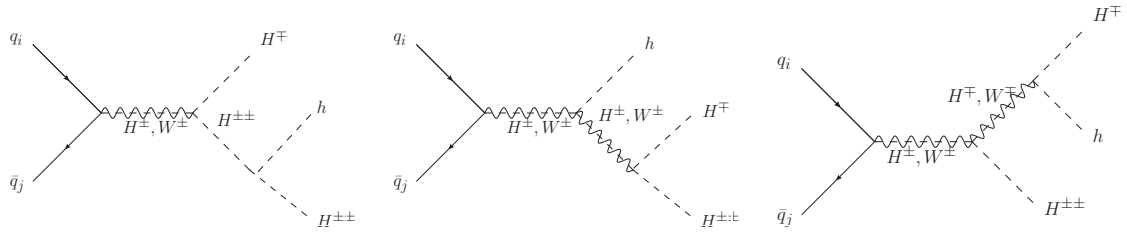

r) s) t)

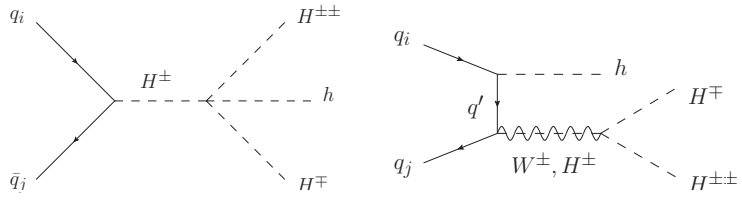

u) w)

$k)\quad pp \to H^{\pm\pm}H^{\mp}H^{\mp}$

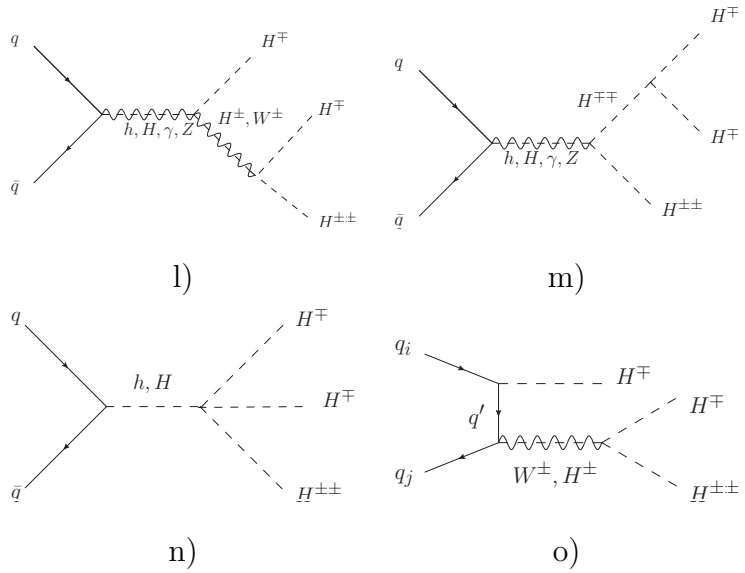

A.5 Unitarity, scalar potential's stability bound and T-parameter

The potential stability conditions guarantee that the potential has a stable vacuum value. In the case of the htm, that condition implicates the following dependence of the potential parameters [144, 145]

$$\begin{aligned} &\lambda \geq 0\,,\ \lambda_2 + \tfrac{\lambda_3}{2} \geq 0\,,\ \lambda_1 + \sqrt{\lambda(\lambda_2+\lambda_3)} \geq 0\,,\ \lambda_1 + \lambda_4 + \sqrt{\lambda(\lambda_2+\lambda_3)} \geq 0\,, \\ &|\lambda_4|\sqrt{\lambda_2+\lambda_3} - \lambda_3\sqrt{\lambda} \geq 0 \qquad \text{or} \qquad 2\lambda_1 + \lambda_4 + \sqrt{(2\lambda\lambda_3 - \lambda_4^2)(\tfrac{2\lambda_2}{\lambda_3}+1)} \geq 0. \end{aligned} \tag{A.1}$$

The BSM models need to fulfil the perturbative unitarity conditions, that means that in case of $2 \to 2$ processes the scattering matrix is limited and that involve some constrains on the potential parameter to bound the diagrams with propagators. I apply two conventions, with the scattering matrix element $\mathcal{M}$ less than 8π (what corresponds with the 0th partial wave amplitude $|\,\mathrm{Re}(a_0)| \leq \frac{1}{2}$, $a_0 \sim \int_{-1}^{1} d(\cos\theta)\mathcal{M}\cos\theta$). Those conditions are connected with the following bounds on the potential parameters [144, 146, 147]

$$\begin{aligned}\text{Max}\Big\{&\Big|\tfrac{\lambda}{2}\Big|\ ,\ \ |\lambda_1|\ ,\ \tfrac{1}{2}\,|2\lambda_1+3\lambda_4|\ ,\ \ |\lambda_1+\lambda_4|\ ,\ \tfrac{1}{2}\,|2\lambda_1-\lambda_4|\ ,\ \ |\lambda_3-2\lambda_2|\ ,\ \ |2\lambda_2|\ ,\\ &|2(\lambda_3+\lambda_2)|\ ,\ \tfrac{1}{4}\Big|3\lambda+16\lambda_2+12\lambda_3\pm\sqrt{(3\lambda-16\lambda_2-12\lambda_3)^2+24(\lambda_4+2\lambda_1)^2}\Big|\ ,\\ &\tfrac{1}{4}\Big|\lambda+4\lambda_2+8\lambda_3\pm\sqrt{(\lambda-4\lambda_2-8\lambda_3)^2+16\lambda_4^2}\Big|\Big\}\quad\leq\quad 8\pi.\end{aligned}\tag{A.2}$$

The new physics contribution to the T-parameter are given by the relation [172]:

$$\Delta T=\frac{1}{4\pi\sin^2\theta_W}\Big[F(M^2_{H^\pm},M^2_A)+F(M^2_{H^{\pm\pm}},M^2_{H^\pm})\Big]\tag{A.3}$$

where F function is

$$F(x,y)=\frac{x+y}{2}-\frac{xy}{x-y}\ln\frac{x}{y}.$$

Approximately, for $\delta\equiv|M_{H^\pm}-M_{H^{\pm\pm}}|\ll M_W$, the F function is proportional to the charged scalar mass difference squared $F\sim\delta^2$ [173]. I used the following bound on the new physics contribution to the T parameter $\Delta T<0.2$ [221].

The potential stability within the `MLRSM` is guaranteed by the following bounds [149, 222]

$$\lambda_1\geq 0\ ,\quad \rho_1\geq 0\ ,\quad \rho_1+\rho_2\geq 0\ ,\quad \rho_1+2\rho_2\geq 0.\tag{A.4}$$

The unitarity constrains lead to the following inequalities (assuming that the scattering matrix $\mathcal{M}<8\pi$)

$$\begin{aligned}&\lambda_1<\tfrac{4\pi}{3}\ ,\quad (\lambda_1+4\lambda_2+2\lambda_3)<4\pi\ ,\quad (\lambda_1-4\lambda_2+2\lambda_3)<4\pi\ ,\quad \lambda_4<\tfrac{4\pi}{3}\ ,\\ &\alpha_1<8\pi\ ,\quad \alpha_2<4\pi\ ,\quad (\alpha_1+\alpha_3)<8\pi\ ,\\ &\rho_1<\tfrac{4\pi}{3}\ ,\quad (\rho_1+\rho_2)<2\pi\ ,\quad \rho_2<2\sqrt{2}\pi\ ,\quad \rho_3<8\pi\ ,\quad \rho_4<2\sqrt{2}\pi.\end{aligned}\tag{A.5}$$

List of abbreviations

BSC	Bardeen–Cooper–Schrieffer Theory of Superconductivity
BR	Branching Ratio
CEPC	Circular Electron Positron Collider
CLIC	Compact Linear Collider
FCC	Future Circular Collider
FCNC	Flavour Changing Neutral Currents
GUT	Grand Unified Theories
HTM	Higgs Triplet Model
ILC	International Linear Collider
LEP	Large Electron-Positron Collider
LHC	Large Hadron Collider
LLP	Long-Lived Particle
MLRSM	Manifest Left-Right Symmetric Model
OSDL	Opposite-sign Dileptons
SM	Standard Model
SSB	Spontaneous Symmetry Breaking
SSDL	Same-sign Dileptons
VEV	Vacuum Expectation Value
QCD	Quantum Chromodynamics

References

[1] A. Djouadi, M. Spira, P. M. Zerwas, Two photon decay widths of Higgs particles, Phys. Lett. B311 (1993) 255–260. arXiv:hep-ph/9305335, doi:10.1016/0370-2693(93)90564-X.

[2] G. Aad, et al., Measurements of the Higgs boson production and decay rates and coupling strengths using pp collision data at $\sqrt{s} = 7$ and 8 TeV in the ATLAS experiment, Eur. Phys. J. C76 (1) (2016) 6. arXiv:1507.04548, doi:10.1140/epjc/s10052-015-3769-y.

[3] S. Chatrchyan, et al., Study of the Mass and Spin-Parity of the Higgs Boson Candidate Via Its Decays to Z Boson Pairs, Phys. Rev. Lett. 110 (8) (2013) 081803. arXiv:1212.6639, doi:10.1103/PhysRevLett.110.081803.

[4] G. Aad, et al., Evidence for the spin-0 nature of the Higgs boson using ATLAS data, Phys. Lett. B726 (2013) 120–144. arXiv:1307.1432, doi:10.1016/j.physletb.2013.08.026.

[5] G. Aad, et al., Study of the spin and parity of the Higgs boson in diboson decays with the ATLAS detector, Eur. Phys. J. C 75 (10) (2015) 476, [Erratum: Eur.Phys.J.C 76, 152 (2016)]. arXiv:1506.05669, doi:10.1140/epjc/s10052-015-3685-1.

[6] G. Aad, et al., Determination of spin and parity of the Higgs boson in the $WW^* \to e\nu\mu\nu$ decay channel with the ATLAS detector, Eur. Phys. J. C75 (5) (2015) 231. arXiv:1503.03643, doi:10.1140/epjc/s10052-015-3436-3.

[7] E. Di Marco, Studies of the Higgs boson spin and parity using the $\gamma\gamma$, ZZ, and WW decay channels with the CMS detector, Nucl. Part. Phys. Proc. 273-275 (2016) 746–752. doi:10.1016/j.nuclphysbps.2015.09.114.

[8] V. Khachatryan, et al., Constraints on the spin-parity and anomalous HVV couplings of the Higgs boson in proton collisions at 7 and 8 TeV, Phys. Rev. D 92 (1) (2015) 012004. arXiv:1411.3441, doi:10.1103/PhysRevD.92.012004.

[9] R. L. Workman, Review of Particle Physics, PTEP 2022 (2022) 083C01. doi:10.1093/ptep/ptac097.

[10] E. Torrente-Lujan, The Higgs and top masses: why the higgs mass is $m_H^2 = m_Z m_t$?, Eur. Phys. J. C 74 (2) (2014) 2744. arXiv:1209.0474, doi:10.1140/epjc/s10052-014-2744-3.

[11] I. Dubovyk, A. Freitas, J. Gluza, T. Riemann, J. Usovitsch, Electroweak pseudo-observables and Z-boson form factors at two-loop accuracy, JHEP 08 (2019) 113. arXiv:1906.08815, doi:10.1007/JHEP08(2019)113.

[12] F. Englert, Nobel Lecture: The BEH mechanism and its scalar boson, Rev. Mod. Phys. 86 (3) (2014) 843. doi:10.1103/RevModPhys.86.843.

[13] G. Aad, et al., Observation of a new particle in the search for the Standard Model Higgs boson with the ATLAS detector at the LHC, Phys. Lett. B716 (2012) 1–29. arXiv:1207.7214, doi:10.1016/j.physletb.2012.08.020.

[14] S. Chatrchyan, et al., Observation of a new boson at a mass of 125 GeV with the CMS experiment at the LHC, Phys. Lett. B716 (2012) 30–61. arXiv:1207.7235, doi:10.1016/j.physletb.2012.08.021.

[15] G. Aad, et al., A Particle Consistent with the Higgs Boson Observed with the ATLAS Detector at the Large Hadron Collider, Science 338 (6114) (2012) 1576–1582. doi:10.1126/science.1232005.

[16] S. Chatrchyan, et al., Measurement of W^+W^- production and search for the Higgs boson in pp collisions at $\sqrt{s} = 7$ TeV, Phys. Lett. B699 (2011) 25–47. arXiv:1102.5429, doi:10.1016/j.physletb.2011.03.056.

[17] V. Khachatryan, et al., Search for the associated production of the Higgs boson with a top-quark pair, JHEP 09 (2014) 087, [Erratum: JHEP 10, 106 (2014)]. arXiv:1408.1682, doi:10.1007/JHEP09(2014)087.

[18] G. Aad, et al., Search for $H \to \gamma\gamma$ produced in association with top quarks and constraints on the Yukawa coupling between the top quark and the Higgs boson using data taken at 7 TeV and 8 TeV with the ATLAS detector, Phys. Lett. B740 (2015) 222–242. arXiv:1409.3122, doi:10.1016/j.physletb.2014.11.049.

[19] G. Aad, et al., Measurements of the Higgs boson production and decay rates and constraints on its couplings from a combined ATLAS and CMS analysis of the LHC pp collision data at $\sqrt{s} = 7$ and 8 TeV, JHEP 08 (2016) 045. arXiv:1606.02266, doi:10.1007/JHEP08(2016)045.

[20] G. Aad, et al., Search for the associated production of the Higgs boson with a top quark pair in multilepton final states with the ATLAS detector, Phys. Lett. B749 (2015) 519–541. arXiv:1506.05988, doi:10.1016/j.physletb.2015.07.079.

[21] C. Quigg, Particle Physics after the Higgs-Boson Discovery: Opportunities for the Large Hadron Collider, Contemp. Phys. 57 (2) (2016) 177–187. arXiv:1507.02977, doi:10.1080/00107514.2015.1078076.

[22] J. Ellis, Discrete Glimpses of the Physics Landscape after the Higgs Discovery, J. Phys. Conf. Ser. 631 (1) (2015) 012001. arXiv:1501.05418, doi:10.1088/1742-6596/631/1/012001.

[23] M. E. Peskin, On the Trail of the Higgs Boson, Annalen Phys. 528 (1-2) (2016) 20–34. arXiv:1506.08185, doi:10.1002/andp.201500225.

[24] J. Bardeen, L. N. Cooper, J. R. Schrieffer, Microscopic theory of superconductivity, Phys. Rev. 106 (1957) 162. doi:10.1103/PhysRev.106.162.

[25] M. D. Schwartz, Quantum Field Theory and the Standard Model, Cambridge University Press, 2014.

[26] F. Englert, R. Brout, Broken Symmetry and the Mass of Gauge Vector Mesons, Phys. Rev. Lett. 13 (1964) 321–323. doi:10.1103/PhysRevLett.13.321.

[27] P. W. Higgs, Broken symmetries, massless particles and gauge fields, Phys. Lett. 12 (1964) 132–133. doi:10.1016/0031-9163(64)91136-9.

[28] P. W. Higgs, Broken Symmetries and the Masses of Gauge Bosons, Phys. Rev. Lett. 13 (1964) 508–509. doi:10.1103/PhysRevLett.13.508.

[29] G. S. Guralnik, C. R. Hagen, T. W. B. Kibble, Global Conservation Laws and Massless Particles, Phys. Rev. Lett. 13 (1964) 585–587. doi:10.1103/PhysRevLett.13.585.

[30] P. W. Higgs, Spontaneous Symmetry Breakdown without Massless Bosons, Phys. Rev. 145 (1966) 1156–1163. doi:10.1103/PhysRev.145.1156.

[31] T. W. B. Kibble, Symmetry breaking in nonAbelian gauge theories, Phys. Rev. 155 (1967) 1554–1561. doi:10.1103/PhysRev.155.1554.

[32] T. Williams, C. Kelley et al. , Gnuplot 5.5 An Interactive Plotting Program , http://http://gnuplot.info// (April 2022).

[33] M. Kordiaczyńska, Basic processes involving the top quark and Higgs particle at the LHC (*in Polish*) , https://apd.us.edu.pl/diplomas/65656/.

[34] M. J. G. Veltman, Reflections on the Higgs system, doi:10.5170/CERN-1997-005.

[35] J. S. Schwinger, A Theory of the Fundamental Interactions, Annals Phys. 2 (1957) 407–434. doi:10.1016/0003-4916(57)90015-5.

[36] M. Gell-Mann, M. Levy, The axial vector current in beta decay, Nuovo Cim. 16 (1960) 705. doi:10.1007/BF02859738.

[37] J. Goldstone, A. Salam, S. Weinberg, Broken Symmetries, Phys. Rev. 127 (1962) 965–970. doi:10.1103/PhysRev.127.965.

[38] P. W. Anderson, Plasmons, Gauge Invariance, and Mass, Phys. Rev. 130 (1963) 439–442. doi:10.1103/PhysRev.130.439.

[39] S. L. Glashow, Partial Symmetries of Weak Interactions, Nucl. Phys. 22 (1961) 579–588. doi:10.1016/0029-5582(61)90469-2.

[40] A. Salam, J. C. Ward, Electromagnetic and weak interactions, Phys. Lett. 13 (1964) 168–171. doi:10.1016/0031-9163(64)90711-5.

[41] S. Weinberg, A Model of Leptons, Phys. Rev. Lett. 19 (1967) 1264–1266. doi:10.1103/PhysRevLett.19.1264.

[42] G. 't Hooft, Renormalizable Lagrangians for Massive Yang-Mills Fields, Nucl. Phys. B 35 (1971) 167–188. doi:10.1016/0550-3213(71)90139-8.

[43] D. J. Gross, F. Wilczek, Ultraviolet Behavior of Nonabelian Gauge Theories, Phys. Rev. Lett. 30 (1973) 1343–1346. doi:10.1103/PhysRevLett.30.1343.

[44] D. J. Gross, F. Wilczek, Asymptotically Free Gauge Theories - I, Phys. Rev. D 8 (1973) 3633–3652. doi:10.1103/PhysRevD.8.3633.

[45] H. David Politzer, Asymptotic freedom: An approach to strong interactions, Physics Reports 14 (4) (1974) 129–180. doi:https://doi.org/10.1016/0370-1573(74)90014-3.
URL https://www.sciencedirect.com/science/article/pii/0370157374900143

[46] M. Gell-Mann, A Schematic Model of Baryons and Mesons, Phys. Lett. 8 (1964) 214–215. doi:10.1016/S0031-9163(64)92001-3.

[47] G. Zweig, An SU_3 model for strong interaction symmetry and its breaking; Version 2, doi:10.17181/CERN-TH-412.
URL https://cds.cern.ch/record/570209

[48] W. Pauli, Dear radioactive ladies and gentlemen, Phys. Today 31N9 (1978) 27.

[49] C. L. Cowan, F. Reines, F. B. Harrison, H. W. Kruse, A. D. McGuire, Detection of the free neutrino: A Confirmation, Science 124 (1956) 103–104. doi:10.1126/science.124.3212.103.

[50] G. Danby, J. M. Gaillard, K. A. Goulianos, L. M. Lederman, N. B. Mistry, M. Schwartz, J. Steinberger, Observation of High-Energy Neutrino Reactions and the Existence of Two Kinds of Neutrinos, Phys. Rev. Lett. 9 (1962) 36–44. doi:10.1103/PhysRevLett.9.36.

[51] C. S. Wu, E. Ambler, R. W. Hayward, D. D. Hoppes, R. P. Hudson, Experimental Test of Parity Conservation in β Decay, Phys. Rev. 105 (1957) 1413–1414. doi:10.1103/PhysRev.105.1413.

[52] T. D. Lee, C.-N. Yang, Question of Parity Conservation in Weak Interactions, Phys. Rev. 104 (1956) 254–258. doi:10.1103/PhysRev.104.254.

[53] G. Arnison, et al., Experimental Observation of Isolated Large Transverse Energy Electrons with Associated Missing Energy at $\sqrt{s} = 540$ GeV, Phys. Lett. B 122 (1983) 103–116. doi:10.1016/0370-2693(83)91177-2.

[54] G. Arnison, et al., Experimental Observation of Lepton Pairs of Invariant Mass Around 95-GeV/c**2 at the CERN SPS Collider, Phys. Lett. B 126 (1983) 398–410. doi:10.1016/0370-2693(83)90188-0.

[55] M. L. Perl, et al., Evidence for Anomalous Lepton Production in $e^+ - e^-$ Annihilation, Phys. Rev. Lett. 35 (1975) 1489–1492. doi:10.1103/PhysRevLett.35.1489.

[56] K. Kodama, et al., Observation of tau neutrino interactions, Phys. Lett. B 504 (2001) 218–224. arXiv:hep-ex/0012035, doi:10.1016/S0370-2693(01)00307-0.

[57] C. Berger, et al., Observation of a Narrow Resonance Formed in e^+e^- Annihilation at 9.46-GeV, Phys. Lett. B 76 (1978) 243–245. doi:10.1016/0370-2693(78)90287-3.

[58] M. Breidenbach, J. I. Friedman, H. W. Kendall, E. D. Bloom, D. H. Coward, H. C. DeStaebler, J. Drees, L. W. Mo, R. E. Taylor, Observed behavior of highly inelastic electron-proton scattering, Phys. Rev. Lett. 23 (1969) 935–939. doi:10.1103/PhysRevLett.23.935.

[59] E. D. Bloom, et al., High-Energy Inelastic e p Scattering at 6-Degrees and 10-Degrees, Phys. Rev. Lett. 23 (1969) 930–934. doi:10.1103/PhysRevLett.23.930.

[60] S. Abachi, et al., Observation of the top quark, Phys. Rev. Lett. 74 (1995) 2632–2637. arXiv:hep-ex/9503003, doi:10.1103/PhysRevLett.74.2632.

[61] F. Abe, et al., Observation of top quark production in $\bar{p}p$ collisions, Phys. Rev. Lett. 74 (1995) 2626–2631. arXiv:hep-ex/9503002, doi:10.1103/PhysRevLett.74.2626.

[62] J. Ellis, M. K. Gaillard, D. V. Nanopoulos, A Historical Profile of the Higgs BosonarXiv:1201.6045.

[63] R. Barate, et al., Observation of an excess in the search for the standard model Higgs boson at ALEPH, Phys. Lett. B 495 (2000) 1–17. arXiv:hep-ex/0011045, doi:10.1016/S0370-2693(00)01269-7.

[64] R. Barate, et al., Search for the standard model Higgs boson at LEP, Phys. Lett. B 565 (2003) 61–75. arXiv:hep-ex/0306033, doi:10.1016/S0370-2693(03)00614-2.

[65] Updated Combination of CDF and D0 Searches for Standard Model Higgs Boson Production with up to 10.0 fb^{-1} of Data, 2012. arXiv:1207.0449.

[66] A. Djouadi, The Anatomy of electro-weak symmetry breaking. I: The Higgs boson in the standard model, Phys. Rept. 457 (2008) 1–216. arXiv:hep-ph/0503172, doi:10.1016/j.physrep.2007.10.004.

[67] P. D. Group, Review of Particle Physics, Progress of Theoretical and Experimental Physics 2022 (8), 083C01. arXiv:https://academic.oup.com/ptep/article-pdf/2022/8/083C01/45434166/ptac097.pdf, doi:10.1093/ptep/ptac097.
URL https://doi.org/10.1093/ptep/ptac097

[68] M. Aaboud, et al., Observation of $H \to b\bar{b}$ decays and VH production with the ATLAS detector, Physics Letters B 786 (2018) 59 – 86. doi:https://doi.org/10.1016/j.physletb.2018.09.013.

[69] S. Chatrchyan, et al., Observation of a New Boson at a Mass of 125 GeV with the CMS Experiment at the LHC, Phys. Lett. B 716 (2012) 30–61. arXiv:1207.7235, doi:10.1016/j.physletb.2012.08.021.

[70] G. Aad, et al., Observation of a new particle in the search for the Standard Model Higgs boson with the ATLAS detector at the LHC, Phys. Lett. B 716 (2012) 1–29. arXiv:1207.7214, doi:10.1016/j.physletb.2012.08.020.

[71] S. Chatrchyan, et al., Observation of a New Boson at a Mass of 125 GeV with the CMS Experiment at the LHC, Phys. Lett. B 716 (2012) 30–61. arXiv:1207.7235, doi:10.1016/j.physletb.2012.08.021.

[72] Higgs boson property measurements at the ATLAS and CMS experiments by L. Brenner, Corfu SM and Beyond 2022, https://indico.cern.ch/event/1166991.

[73] Recent results from ATLAS by M. Cristinziani, Corfu SM and Beyond 2022, https://indico.cern.ch/event/1166991.

[74] HL-LHC project by M. Zerlauth, Corfu SM and Beyond 2022, https://indico.cern.ch/event/1166991.

[75] R. K. Ellis, et al., Physics Briefing Book: Input for the European Strategy for Particle Physics Update 2020. arXiv:1910.11775.

[76] S. Ashanujjaman, K. Ghosh, R. Sahu, Low-mass doubly-charged Higgs bosons at LHC arXiv:2211.00632.

[77] J. Butterworth, J. Heeck, S. H. Jeon, O. Mattelaer, R. Ruiz, Testing the Scalar Triplet Solution to CDF's Fat W Problem at the LHC arXiv:2210.13496.

[78] Y. Kuno, A search for muon-to-electron conversion at J-PARC: The COMET experiment, PTEP 2013 (2013) 022C01. doi:10.1093/ptep/pts089.

[79] D. Brown, The Mu2e Experiment: Searching for Muon to Electron Conversion, Nucl. Part. Phys. Proc. 260 (2015) 151–154. doi:10.1016/j.nuclphysbps.2015.02.032.

[80] N. Abgrall, et al., The Majorana Demonstrator Neutrinoless Double-Beta Decay Experiment, Adv. High Energy Phys. 2014 (2014) 365432. arXiv:1308.1633, doi:10.1155/2014/365432.

[81] L. Calibbi, G. Signorelli, Charged Lepton Flavour Violation: An Experimental and Theoretical Introduction, Riv. Nuovo Cim. 41 (2) (2018) 1. arXiv:1709.00294, doi:10.1393/ncr/i2018-10144-0.

[82] A. M. Baldini, et al., MEG Upgrade Proposal. arXiv:1301.7225.

[83] A. Blondel, et al., Research Proposal for an Experiment to Search for the Decay $\mu \to eee$. arXiv:1301.6113.

[84] L. Bartoszek, et al., Mu2e Technical Design Report arXiv:1501.05241, doi:10.2172/1172555.

[85] T. M. Nguyen, Search for μ − e conversion with DeeMe experiment at J-PARC MLF, PoS FPCP2015 (2015) 060. doi:10.22323/1.248.0060.

[86] T. Aushev, et al., Physics at Super B Factory. arXiv:1002.5012.

[87] M. Moulson, Forbidden Kaon and Pion Decays in NA62, PoS KAON13 (2013) 013. arXiv:1306.3361, doi:10.22323/1.181.0013.

[88] S. Banerjee, B. Bhattacherjee, M. Mitra, M. Spannowsky, The Lepton Flavour Violating Higgs Decays at the HL-LHC and the ILC, JHEP 07 (2016) 059. arXiv:1603.05952, doi:10.1007/JHEP07(2016)059.

[89] A. Blondel, P. Janot, Future strategies for the discovery and the precise measurement of the Higgs self coupling, arXiv:1809.10041.

[90] V. Shiltsev, F. Zimmermann, Modern and Future Colliders, Rev. Mod. Phys. 93 (2021) 015006. arXiv:2003.09084, doi:10.1103/RevModPhys.93.015006.

[91] The Electron-Ion Collider (EIC), https://www.bnl.gov/eic/.

[92] M. Benedikt, A. Blondel, P. Janot, M. Mangano, F. Zimmermann, Future Circular Colliders succeeding the LHC, Nature Phys. 16 (4) (2020) 402–407. doi:10.1038/s41567-020-0856-2.

[93] I. Zurbano Fernandez, et al., High-Luminosity Large Hadron Collider (HL-LHC): Technical design report 10/2020. doi:10.23731/CYRM-2020-0010.

[94] R. Steerenberg, et al., Operation and performance of the CERN Large Hadron Collider during proton Run 2, in: 10th International Particle Accelerator Conference, 2019, p. MOPMP031. doi:10.18429/JACoW-IPAC2019-MOPMP031.

[95] A. Abada, et al., FCC Physics Opportunities: Future Circular Collider Conceptual Design Report Volume 1, Eur. Phys. J. C 79 (6) (2019) 474. doi:10.1140/epjc/s10052-019-6904-3.

[96] N. Alipour Tehrani, et al., FCC-ee: Your Questions Answered, in: A. Blondel, P. Janot (Eds.), CERN Council Open Symposium on the Update of European Strategy for Particle Physics, 2019. arXiv:1906.02693.

[97] A. Abada, et al., FCC-hh: The Hadron Collider: Future Circular Collider Conceptual Design Report Volume 3, Eur. Phys. J. ST 228 (4) (2019) 755–1107. doi:10.1140/epjst/e2019-900087-0.

[98] The FCC Feasibility Study and Global Collaboration by Tsesmelis, Corfu SM and Beyond 2022, https://indico.cern.ch/event/1166991.

[99] A. Abada, et al., FCC-ee: The Lepton Collider: Future Circular Collider Conceptual Design Report Volume 2, Eur. Phys. J. ST 228 (2) (2019) 261–623. doi:10.1140/epjst/e2019-900045-4.

[100] A. Blondel, P. Janot, FCC-ee overview: new opportunities create new challenges, Eur. Phys. J. Plus 137 (1) (2022) 92. arXiv:2106.13885, doi:10.1140/epjp/s13360-021-02154-9.

[101] J. de Blas, M. Ciuchini, E. Franco, A. Goncalves, S. Mishima, M. Pierini, L. Reina, L. Silvestrini, Global analysis of electroweak data in the Standard Model, Phys. Rev. D 106 (3) (2022) 033003. arXiv:2112.07274, doi:10.1103/PhysRevD.106.033003.

[102] A. David, A. Denner, M. Duehrssen, M. Grazzini, C. Grojean, G. Passarino, M. Schumacher, M. Spira, G. Weiglein, M. Zanetti, LHC HXSWG interim recommendations to explore the coupling structure of a Higgs-like particle, arXiv:1209.0040.

[103] J. de Blas, et al., Higgs Boson Studies at Future Particle Colliders, JHEP 01 (2020) 139. arXiv:1905.03764, doi:10.1007/JHEP01(2020)139.

[104] A. Blondel, P. Janot, Circular and Linear e^+e^- Colliders: Another Story of Complementarity, arXiv:1912.11871.

[105] F. Zimmermann, et al., High-Energy LHC Design, J. Phys. Conf. Ser. 1067 (2) (2018) 022009. doi:10.18429/JACoW-IPAC2018-MOPMF064.

[106] A. Abada, et al., HE-LHC: The High-Energy Large Hadron Collider: Future Circular Collider Conceptual Design Report Volume 4, Eur. Phys. J. ST 228 (5) (2019) 1109–1382. doi:10.1140/epjst/e2019-900088-6.

[107] A. Blondel, et al., LEP3: A High Luminosity e^+e^- Collider to Study the Higgs Boson arXiv:1208.0504.

[108] C. Yu, et al., Status of Circular Electron-Positron Collider and Super Proton-Proton Collider, in: 10th International Particle Accelerator Conference, 2019, p. WEYPLM1. doi:10.18429/JACoW-IPAC2019-WEYPLM1.

[109] M. Dong, et al., CEPC Conceptual Design Report: Volume 2 - Physics & Detector arXiv:1811.10545.

[110] CEPC Conceptual Design Report: Volume 1 - AcceleratorarXiv:1809.00285.

[111] A. Abada, et al., FCC-ee: The Lepton Collider: Future Circular Collider Conceptual Design Report Volume 2, Eur. Phys. J. ST 228 (2) (2019) 261–623. doi:10.1140/epjst/e2019-900045-4.

[112] Physics and Detectors at CLIC: CLIC Conceptual Design ReportarXiv:1202.5940, doi:10.5170/CERN-2012-003.

[113] The International Linear Collider Technical Design Report - Volume 1: Executive Summary arXiv:1306.6327.

[114] Gamma Factory – New physics opportunities for CERN by D. M. Krasny, Corfu SM and Beyond 2022, https://indico.cern.ch/event/1166991.

[115] S. Dasu, et al., Strategy for Understanding the Higgs Physics: The Cool Copper Collider, , in: 2022 Snowmass Summer Study, 2022. arXiv:2203.07646.

[116] E. Adli, Plasma Wakefield Linear Colliders - Opportunities and Challenges. arXiv:1905.01879, doi:10.1098/rsta.2018.0419.

[117] Talks on muon colliders by D. Marzocca and J. Reuter, Corfu SM and Beyond 2022, https://indico.cern.ch/event/1166991.

[118] P. S. B. Dev, S. Khan, M. Mitra, S. K. Rai, Doubly-charged Higgs boson at a future electron-proton collider, Phys. Rev. D 99 (11) (2019) 115015. arXiv:1903.01431, doi:10.1103/PhysRevD.99.115015.

[119] D. Buttazzo, G. Degrassi, P. P. Giardino, G. F. Giudice, F. Sala, A. Salvio, A. Strumia, Investigating the near-criticality of the Higgs boson, JHEP 12 (2013) 089. arXiv:1307.3536, doi:10.1007/JHEP12(2013)089.

[120] J. R. Ellis, D. Ross, A Light Higgs boson would invite supersymmetry, Phys. Lett. B 506 (2001) 331–336. arXiv:hep-ph/0012067, doi:10.1016/S0370-2693(01)00156-3.

[121] A. Andreassen, W. Frost, M. D. Schwartz, Scale Invariant Instantons and the Complete Lifetime of the Standard Model, Phys. Rev. D 97 (5) (2018) 056006. arXiv:1707.08124, doi:10.1103/PhysRevD.97.056006.

[122] F. Jegerlehner, The Standard Model of Particle Physics as a Conspiracy Theory and the Possible Role of the Higgs Boson in the Evolution of the Early Universe, Acta Phys. Polon. B 52 (6-7) (2021) 575–605. arXiv:2106.00862, doi:10.5506/APhysPolB.52.575.

[123] J. Lesgourgues, S. Pastor, Massive neutrinos and cosmology, Phys. Rept. 429 (2006) 307–379. arXiv:astro-ph/0603494, doi:10.1016/j.physrep.2006.04.001.

[124] C. Jaramillo, Reviving keV sterile neutrino dark matter, JCAP 10 (2022) 093. arXiv:2207.11269, doi:10.1088/1475-7516/2022/10/093.

[125] D. A. Ross, M. J. G. Veltman, Neutral Currents in Neutrino Experiments, Nucl. Phys. B 95 (1975) 135–147. doi:10.1016/0550-3213(75)90485-X.

[126] J. C. Taylor, Gauge Theories of Weak Interactions, Cambridge Monographs on Mathematical Physics, Cambridge Univ. Press, Cambridge, UK, 1979.

[127] T. G. Rizzo, Tests of the fermion and Higgs multiplet structure of the $SU(2)\times U(1)$ model, Phys. Rev. D 21 (1980) 1404–1409. doi:10.1103/PhysRevD.21.1404.

[128] M. J. G. Veltman, The Screening theorem and the Higgs system, Acta Phys. Polon. B 25 (1994) 1627–1636.

[129] M. E. Peskin, T. Takeuchi, Estimation of oblique electroweak corrections, Phys. Rev. D 46 (1992) 381–409. doi:10.1103/PhysRevD.46.381.

[130] P. Q. Hung, Constraints from the S-parameter on models with scalar triplets arXiv:1810.04234.

[131] Z. U. Khandker, D. Li, W. Skiba, Electroweak Corrections from Triplet Scalars, Phys. Rev. D 86 (2012) 015006. arXiv:1201.4383, doi:10.1103/PhysRevD.86.015006.

[132] Anisha, S. Das Bakshi, J. Chakrabortty, S. Prakash, Hilbert Series and Plethystics: Paving the path towards 2HDM- and MLRSM-EFT, JHEP 09 (2019) 035. arXiv:1905.11047, doi:10.1007/JHEP09(2019)035.

[133] U. Banerjee, J. Chakrabortty, J. Gluza, S. Prakash, S. U. Rahaman, The Effective MLRSM Model and Low-energy Observables, Acta Phys. Polon. Supp. 15 (2) (2022) A9. doi:10.5506/APhysPolBSupp.15.2-A9.

[134] M. J. G. Veltman, Limit on Mass Differences in the Weinberg Model, Nucl. Phys. B 123 (1977) 89–99. doi:10.1016/0550-3213(77)90342-X.

[135] J. Gluza, M. Kordiaczynska, T. Srivastava, Discriminating the HTM and MLRSM models in collider studies via doubly charged Higgs boson pair production and the subsequent leptonic decays, Chin. Phys. C 45 (7) (2021) 073113. arXiv:2006.04610, doi:10.1088/1674-1137/abfe51.

[136] M. Aoki, S. Kanemura, Unitarity bounds in the Higgs model including triplet fields with custodial symmetry, Phys. Rev. D 77 (9) (2008) 095009, [Erratum: Phys.Rev.D 89, 059902 (2014)]. arXiv:0712.4053, doi:10.1103/PhysRevD.77.095009.

[137] H. Georgi, M. Machacek, Doubly charged Higgs bosons, Nucl. Phys. B262 (1985) 463–477. doi:10.1016/0550-3213(85)90325-6.

[138] C.-W. Chiang, K. Yagyu, Testing the custodial symmetry in the Higgs sector of the Georgi-Machacek model, JHEP 01 (2013) 026. arXiv:1211.2658, doi:10.1007/JHEP01(2013)026.

[139] M. Lindner, M. Sher, H. W. Zaglauer, Probing Vacuum Stability Bounds at the Fermilab Collider, Phys. Lett. B 228 (1989) 139–143. doi:10.1016/0370-2693(89)90540-6.

[140] M. Sher, Electroweak Higgs Potentials and Vacuum Stability, Phys. Rept. 179 (1989) 273–418. doi:10.1016/0370-1573(89)90061-6.

[141] C. H. Llewellyn Smith, High-Energy Behavior and Gauge Symmetry, Phys. Lett. B 46 (1973) 233–236. doi:10.1016/0370-2693(73)90692-8.

[142] J. S. Bell, High energy behaviour of tree diagrams in gauge theories , Nucl. Phys. B 60 (1973) 427–436. doi:10.1016/0550-3213(73)90191-0.

[143] A. Kobakhidze, A. Spencer-Smith, Neutrino Masses and Higgs Vacuum Stability, JHEP 08 (2013) 036. arXiv:1305.7283, doi:10.1007/JHEP08(2013)036.

[144] D. Das, A. Santamaria, Updated scalar sector constraints in higgs triplet model, Phys. Rev. D94 (2016) 015015. arXiv:1604.08099, doi:10.1103/PhysRevD.94.015015.

[145] C. Bonilla, R. M. Fonseca, J. W. F. Valle, Consistency of the triplet seesaw model revisited, Phys. Rev. D92 (7) (2015) 075028. arXiv:1508.02323, doi:10.1103/PhysRevD.92.075028.

[146] A. Arhrib, R. Benbrik, M. Chabab, G. Moultaka, M. C. Peyranere, L. Rahili, J. Ramadan, The Higgs Potential in the Type II Seesaw Model, Phys. Rev. D84 (2011) 095005. arXiv:1105.1925, doi:10.1103/PhysRevD.84.095005.

[147] M. E. Krauss, F. Staub, Unitarity constraints in triplet extensions beyond the large s limit, Phys. Rev. D 98 (1) (2018) 015041. arXiv:1805.07309, doi:10.1103/PhysRevD.98.015041.

[148] G. Chauhan, Vacuum Stability and Symmetry Breaking in Left-Right Symmetric Model, JHEP 12 (2019) 137. arXiv:1907.07153, doi:10.1007/JHEP12(2019)137.

[149] J. Chakrabortty, J. Gluza, T. Jelinski, T. Srivastava, Theoretical constraints on masses of heavy particles in Left-Right Symmetric Models, Phys. Lett. B 759 (2016) 361–368. arXiv:1604.06987, doi:10.1016/j.physletb.2016.05.092.

[150] T. Mondal, U. K. Dey, P. Konar, Implications of unitarity and charge breaking minima in a left-right symmetric model, Phys. Rev. D 92 (9) (2015) 096005. arXiv:1508.04960, doi:10.1103/PhysRevD.92.096005.

[151] T. Fukuyama, H. Sugiyama, K. Tsumura, Constraints from muon g-2 and LFV processes in the Higgs Triplet Model, JHEP 03 (2010) 044. arXiv:0909.4943, doi:10.1007/JHEP03(2010)044.

[152] J. C. Pati, A. Salam, Unified Lepton-Hadron Symmetry and a Gauge Theory of the Basic Interactions, Phys. Rev. D 8 (1973) 1240–1251. doi:10.1103/PhysRevD.8.1240.

[153] G. Senjanovic, R. N. Mohapatra, Exact Left-Right Symmetry and Spontaneous Violation of Parity, Phys. Rev. D 12 (1975) 1502. doi:10.1103/PhysRevD.12.1502.

[154] R. N. Mohapatra, J. C. Pati, A Natural Left-Right Symmetry, Phys. Rev. D 11 (1975) 2558. doi:10.1103/PhysRevD.11.2558.

[155] R. E. Marshak, R. N. Mohapatra, Quark - Lepton Symmetry and B-L as the U(1) Generator of the Electroweak Symmetry Group, Phys. Lett. B 91 (1980) 222–224. doi:10.1016/0370-2693(80)90436-0.

[156] P. Duka, J. Gluza, M. Zralek, Quantization and renormalization of the manifest left-right symmetric model of electroweak interactions, Annals Phys. 280 (2000) 336–408. arXiv:hep-ph/9910279, doi:10.1006/aphy.1999.5988.

[157] N. G. Deshpande, J. F. Gunion, B. Kayser, F. Olness, Left-right-symmetric electroweak models with triplet higgs field, Phys. Rev. D 44 (1991) 837–858. doi:10.1103/PhysRevD.44.837.
URL https://link.aps.org/doi/10.1103/PhysRevD.44.837

[158] N. Deshpande, J. Gunion, B. Kayser, F. I. Olness, Left-right symmetric electroweak models with triplet Higgs, Phys. Rev. D 44 (1991) 837–858. doi:10.1103/PhysRevD.44.837.

[159] J. Gluza, M. Zralek, Neutrino production in e^+e^- collisions in a left-right symmetric model, Phys. Rev. D48 (1993) 5093–5105. doi:10.1103/PhysRevD.48.5093.

[160] Search for doubly charged Higgs boson production in multi-lepton final states using 139 fb^{-1} of proton–proton collisions at $\sqrt{s} = 13$ TeV with the ATLAS detector, Tech. rep., CERN, Geneva, all figures including auxiliary figures are available at https://atlas.web.cern.ch/Atlas/GROUPS/PHYSICS/CONFNOTES/ATLAS-CONF-2022-010 (2022).
URL http://cds.cern.ch/record/2805214

[161] E. J. Chun, K. Y. Lee, S. C. Park, Testing Higgs triplet model and neutrino mass patterns, Phys. Lett. B 566 (2003) 142–151. arXiv:hep-ph/0304069, doi:10.1016/S0370-2693(03)00770-6.

[162] P. Achard, et al., Search for doubly charged Higgs bosons at LEP, Phys. Lett. B 576 (2003) 18–28. arXiv:hep-ex/0309076, doi:10.1016/j.physletb.2003.09.082.

[163] J. Abdallah, et al., Search for doubly charged Higgs bosons at LEP-2, Phys. Lett. B 552 (2003) 127–137. arXiv:hep-ex/0303026, doi:10.1016/S0370-2693(02)03125-8.

[164] D. Acosta, et al., Search for doubly-charged Higgs bosons decaying to dileptons in $p\bar{p}$ collisions at $\sqrt{s} = 1.96$ TeV, Phys. Rev. Lett. 93 (2004) 221802. arXiv:hep-ex/0406073, doi:10.1103/PhysRevLett.93.221802.

[165] T. Aaltonen, et al., Search for Doubly Charged Higgs Bosons with Lepton-Flavor-Violating Decays involving Tau Leptons, Phys. Rev. Lett. 101 (2008) 121801. arXiv:0808.2161, doi:10.1103/PhysRevLett.101.121801.

[166] V. M. Abazov, et al., Search for doubly-charged Higgs boson pair production in $p\bar{p}$ collisions at $\sqrt{s} = 1.96$ TeV, Phys. Rev. Lett. 108 (2012) 021801. arXiv:1106.4250, doi:10.1103/PhysRevLett.108.021801.

[167] V. M. Abazov, et al., Search for pair production of doubly-charged Higgs bosons in the $H^{++}H^{--} \to \mu^+\mu^+\mu^-\mu^-$ final state at D0, Phys. Rev. Lett. 101 (2008) 071803. arXiv:0803.1534, doi:10.1103/PhysRevLett.101.071803.

[168] C.-W. Chiang, T. Nomura, K. Tsumura, Search for doubly charged Higgs bosons using the same-sign diboson mode at the LHC, Phys. Rev. D 85 (2012) 095023. arXiv:1202.2014, doi:10.1103/PhysRevD.85.095023.

[169] Z. Kang, J. Li, T. Li, Y. Liu, G.-Z. Ning, Light Doubly Charged Higgs Boson via the WW^* Channel at LHC, Eur. Phys. J. C 75 (12) (2015) 574. arXiv:1404.5207, doi:10.1140/epjc/s10052-015-3774-1.

[170] S. Kanemura, M. Kikuchi, K. Yagyu, H. Yokoya, Bounds on the mass of doubly-charged Higgs bosons in the same-sign diboson decay scenario, Phys. Rev. D 90 (11) (2014) 115018. arXiv:1407.6547, doi:10.1103/PhysRevD.90.115018.

[171] B. Dziewit, M. Kordiaczyńska, T. Srivastava, Production of the Doubly Charged Higgs Boson in Association with the SM Gauge Bosons and/or Other HTM Scalars at Hadron Colliders, Symmetry 13 (7) (2021) 1240. doi:10.3390/sym13071240.

[172] E. J. Chun, H. M. Lee, P. Sharma, Vacuum Stability, Perturbativity, EWPD and Higgs-to-diphoton rate in Type II Seesaw Models, JHEP 11 (2012) 106. arXiv:1209.1303, doi:10.1007/JHEP11(2012)106.

[173] D. Das, A. Santamaria, Updated scalar sector constraints in the Higgs triplet model, Phys. Rev. D 94 (1) (2016) 015015. arXiv:1604.08099, doi:10.1103/PhysRevD.94.015015.

[174] J. Gluza, M. Kordiaczyńska, T. Srivastava, Doubly Charged Higgs Bosons and Spontaneous Symmetry Breaking at eV and TeV Scales, Symmetry 12 (1) (2020) 153. doi:10.3390/sym12010153.

[175] M. B. Einhorn, D. R. T. Jones, M. J. G. Veltman, Heavy Particles and the rho Parameter in the Standard Model, Nucl. Phys. B 191 (1981) 146–172. doi:10.1016/0550-3213(81)90292-3.

[176] L. Lavoura, L.-F. Li, Making the small oblique parameters large, Phys. Rev. D 49 (1994) 1409–1416. arXiv:hep-ph/9309262, doi:10.1103/PhysRevD.49.1409.

[177] T. G. Rizzo, Tests of the fermion and higgs multiplet structure of the su(2)×u(1) model, Phys. Rev. D 21 (1980) 1404–1409. doi:10.1103/PhysRevD.21.1404.

[178] A. G. Akeroyd, S. Moretti, Enhancement of H to gamma gamma from doubly charged scalars in the Higgs Triplet Model, Phys. Rev. D86 (2012) 035015. arXiv:1206.0535, doi:10.1103/PhysRevD.86.035015.

[179] J.-F. Shen, Y.-P. Bi, Z.-X. Li, Pair production of scalars at the ILC in the Higgs triplet model under the non-degenerate case, EPL 112 (3) (2015) 31002. doi:10.1209/0295-5075/112/31002.

[180] G. Bambhaniya, J. Chakrabortty, J. Gluza, T. Jeliński, M. Kordiaczynska, Lowest limits on the doubly charged Higgs boson masses in the minimal left-right symmetric model, Phys. Rev. D 90 (9) (2014) 095003. arXiv:1408.0774, doi:10.1103/PhysRevD.90.095003.

[181] A. Datta, A. Raychaudhuri, Mass bounds for triplet scalars of the left-right symmetric model and their future detection prospects, Phys. Rev. D 62 (2000) 055002. arXiv:hep-ph/9905421, doi:10.1103/PhysRevD.62.055002.

[182] D. Guadagnoli, R. N. Mohapatra, TeV Scale Left Right Symmetry and Flavor Changing Neutral Higgs Effects, Phys. Lett. B694 (2011) 386–392. arXiv:1008.1074, doi:10.1016/j.physletb.2010.10.027.

[183] E. Ma, M. Raidal, U. Sarkar, Phenomenology of the neutrino mass giving Higgs triplet and the low-energy seesaw violation of lepton number, Nucl. Phys. B615 (2001) 313–330. arXiv:hep-ph/0012101, doi:10.1016/S0550-3213(01)00416-3.

[184] A. G. Akeroyd, M. Aoki, H. Sugiyama, Lepton Flavour Violating Decays $\tau \to \bar{l}ll$ and $\mu \to e\gamma$ in the Higgs Triplet Model, Phys. Rev. D79 (2009) 113010. arXiv:0904.3640, doi:10.1103/PhysRevD.79.113010.

[185] D. Dinh, A. Ibarra, E. Molinaro, S. Petcov, The $\mu - e$ Conversion in Nuclei, $\mu \to e\gamma, \mu \to 3e$ Decays and TeV Scale See-Saw Scenarios of Neutrino Mass Generation, JHEP 08 (2012) 125, [Erratum: JHEP 09, 023 (2013)]. arXiv:1205.4671, doi:10.1007/JHEP08(2012)125.

[186] J. Chakrabortty, P. Ghosh, W. Rodejohann, Lower Limits on $\mu \to e\gamma$ from New Measurements on U_{e3}, Phys. Rev. D86 (2012) 075020. arXiv:1204.1000, doi:10.1103/PhysRevD.86.075020.

[187] A. Crivellin, M. Ghezzi, L. Panizzi, G. M. Pruna, A. Signer, Low- and high-energy phenomenology of a doubly charged scalar, Phys. Rev. D 99 (3) (2019) 035004. arXiv:1807.10224, doi:10.1103/PhysRevD.99.035004.

[188] N. Chakrabarty, C.-W. Chiang, T. Ohata, K. Tsumura, Charged scalars confronting neutrino mass and muon $g - 2$ anomaly, JHEP 12 (2018) 104. arXiv:1807.08167, doi:10.1007/JHEP12(2018)104.

[189] J. Chakrabortty, P. Ghosh, S. Mondal, T. Srivastava, Reconciling $(g-2)_\mu$ and charged lepton flavor violating processes through a doubly charged scalar, Phys. Rev. D93 (11) (2016) 115004. arXiv:1512.03581, doi:10.1103/PhysRevD.93.115004.

[190] A. M. Baldini, et al., Search for the lepton flavour violating decay $\mu^+ \to e^+\gamma$ with the full dataset of the MEG experiment, Eur. Phys. J. C76 (8) (2016) 434. arXiv:1605.05081, doi:10.1140/epjc/s10052-016-4271-x.

[191] B. Aubert, et al., Searches for Lepton Flavor Violation in the Decays $\tau^\pm \to e^\pm\gamma$ and $\tau^\pm \to \mu^\pm\gamma$, Phys. Rev. Lett. 104 (2010) 021802. arXiv:0908.2381, doi:10.1103/PhysRevLett.104.021802.

[192] U. Bellgardt, et al., Search for the Decay $\mu^+ \to e^+e^+e^-$, Nucl. Phys. B299 (1988) 1–6. doi:10.1016/0550-3213(88)90462-2.

[193] K. Hayasaka, et al., Search for Lepton Flavor Violating Tau Decays into Three Leptons with 719 Million Produced Tau+Tau- Pairs, Phys. Lett. B687 (2010) 139–143. arXiv:1001.3221, doi:10.1016/j.physletb.2010.03.037.

[194] W. H. Bertl, et al., A Search for muon to electron conversion in muonic gold, Eur.Phys.J. C47 (2006) 337–346. doi:10.1140/epjc/s2006-02582-x.

[195] J. Maalampi, N. Romanenko, Single production of doubly charged Higgs bosons at hadron colliders, Phys. Lett. B532 (2002) 202–208. arXiv:hep-ph/0201196, doi:10.1016/S0370-2693(02)01549-6.

[196] Y. Cai, T. Han, T. Li, R. Ruiz, Lepton Number Violation: Seesaw Models and Their Collider Tests, Front. in Phys. 6 (2018) 40. arXiv:1711.02180, doi:10.3389/fphy.2018.00040.

[197] B. Fuks, M. Nemevsek, R. Ruiz, Doubly Charged Higgs Boson Production at Hadron Colliders, Phys. Rev. D 101 (7) (2020) 075022. arXiv:1912.08975, doi:10.1103/PhysRevD.101.075022.

[198] Nufit 4.1, http://www.nu-fit.org/ (2019).

[199] G. Ucchielli, Searches for doubly charged Higgs bosons with the ATLAS detector, PoS CHARGED2018 (2019) 008. doi:10.22323/1.339.0008.

[200] T. Nomura, H. Okada, H. Yokoya, Discriminating leptonic Yukawa interactions with doubly charged scalar at the ILC, Nucl. Phys. B 929 (2018) 193–206. arXiv:1702.03396, doi:10.1016/j.nuclphysb.2018.02.011.

[201] P. B. Dev, M. J. Ramsey-Musolf, Y. Zhang, Doubly-Charged Scalars in the Type-II Seesaw Mechanism: Fundamental Symmetry Tests and High-Energy Searches, Phys. Rev. D 98 (5) (2018) 055013. arXiv:1806.08499, doi:10.1103/PhysRevD.98.055013.

[202] M. Czakon, J. Gluza, M. Zralek, Low-energy physics and left-right symmetry: Bounds on the model parameters, Phys. Lett. B458 (1999) 355–360. arXiv:hep-ph/9904216, doi:10.1016/S0370-2693(99)00567-5.

[203] M. Tanabashi, et al., Review of Particle Physics, Phys. Rev. D98 (3) (2018) 030001. doi:10.1103/PhysRevD.98.030001.

[204] P. A. R. Ade, et al., Planck 2013 results. XVI. Cosmological parameters, Astron. Astrophys. 571 (2014) A16. arXiv:1303.5076, doi:10.1051/0004-6361/201321591.

[205] M. Aaboud, et al., Search for doubly charged Higgs boson production in multi-lepton final states with the ATLAS detector using proton–proton collisions at $\sqrt{s} = 13\,\text{TeV}$, Eur. Phys. J. C 78 (3) (2018) 199. arXiv:1710.09748, doi:10.1140/epjc/s10052-018-5661-z.

[206] K. Bondarenko, A. Boyarsky, M. Ovchynnikov, O. Ruchayskiy, L. Shchutska, Probing new physics with displaced vertices: muon tracker at CMS, Phys. Rev. D 100 (7) (2019) 075015. arXiv:1903.11918, doi:10.1103/PhysRevD.100.075015.

[207] A. M. Sirunyan, et al., Search for a heavy right-handed W boson and a heavy neutrino in events with two same-flavor leptons and two jets at $\sqrt{s} = 13$ TeV, JHEP 05 (2018) 148. arXiv:1803.11116, doi:10.1007/JHEP05(2018)148.

[208] A. M. Sirunyan, et al., Search for a heavy right-handed W boson and a heavy neutrino in events with two same-flavor leptons and two jets at $\sqrt{s} = 13$ TeV, JHEP 05 (05) (2018) 148. arXiv:1803.11116, doi:10.1007/JHEP05(2018)148.

[209] G. Bambhaniya, J. Chakrabortty, J. Gluza, M. Kordiaczyńska, R. Szafron, Left-Right Symmetry and the Charged Higgs Bosons at the LHC, JHEP 05 (2014) 033. arXiv:1311.4144, doi:10.1007/JHEP05(2014)033.

[210] A. M. Sirunyan, et al., Search for heavy neutrinos and third-generation leptoquarks in hadronic states of two τ leptons and two jets in proton-proton collisions at $\sqrt{s} =$ 13 TeV, JHEP 03 (2019) 170. arXiv:1811.00806, doi:10.1007/JHEP03(2019)170.

[211] J. Gluza, T. Jelinski, R. Szafron, Lepton number violation and 'Diracness' of massive neutrinos composed of Majorana states, Phys. Rev. D93 (11) (2016) 113017. arXiv:1604.01388, doi:10.1103/PhysRevD.93.113017.

[212] P. Bhupal Dev, R. N. Mohapatra, Y. Zhang, CP Violating Effects in Heavy Neutrino Oscillations: Implications for Colliders and Leptogenesis, JHEP 11 (2019) 137. arXiv:1904.04787, doi:10.1007/JHEP11(2019)137.

[213] J. Alwall, R. Frederix, S. Frixione, V. Hirschi, F. Maltoni, O. Mattelaer, H. S. Shao, T. Stelzer, P. Torrielli, M. Zaro, The automated computation of tree-level and next-to-leading order differential cross sections, and their matching to parton shower simulations, JHEP 07 (2014) 079. arXiv:1405.0301, doi:10.1007/JHEP07(2014)079.

[214] C. Bierlich, et al., A comprehensive guide to the physics and usage of PYTHIA 8.3arXiv:2203.11601, doi:10.21468/SciPostPhysCodeb.8.

[215] A. Alloul, N. D. Christensen, C. Degrande, C. Duhr, B. Fuks, FeynRules 2.0 - A complete toolbox for tree-level phenomenology, Comput. Phys. Commun. 185 (2014) 2250–2300. arXiv:1310.1921, doi:10.1016/j.cpc.2014.04.012.

[216] [link].
URL https://www.wolfram.com/mathematica/

[217] [link].
URL https://gcc.gnu.org/wiki/GFortranStandards

[218] J. Pumplin, D. Stump, J. Huston, H. Lai, P. M. Nadolsky, W. Tung, New generation of parton distributions with uncertainties from global QCD analysis, JHEP 07 (2002) 012. arXiv:hep-ph/0201195, doi:10.1088/1126-6708/2002/07/012.

[219] T.-J. Hou, et al., New CTEQ global analysis of quantum chromodynamics with high-precision data from the LHC. arXiv:1912.10053.

[220] M. Cacciari, S. Frixione, M. L. Mangano, P. Nason, G. Ridolfi, Updated predictions for the total production cross sections of top and of heavier quark pairs at the Tevatron and at the LHC, JHEP 09 (2008) 127. arXiv:0804.2800, doi:10.1088/1126-6708/2008/09/127.

[221] K. A. Olive, et al., Review of Particle Physics, Chin. Phys. C 38 (2014) 090001. doi:10.1088/1674-1137/38/9/090001.

[222] J. Chakrabortty, P. Konar, T. Mondal, Constraining a class of B−L extended models from vacuum stability and perturbativity, Phys. Rev. D 89 (5) (2014) 056014. arXiv:1308.1291, doi:10.1103/PhysRevD.89.056014.